NUMERICAL AND ANALYTICAL ASSESSMENT OF RADON DIFFUSION IN VARIOUS MEDIA AND POTENTIAL OF CHARCOAL AS RADON DETECTOR

by

Andrey Rybalkin

A thesis submitted to the faculty of
The University of Utah
in partial fulfillment of the requirements for the degree of

Master of Science

in

Nuclear Engineering

Department of Civil and Environmental Engineering

The University of Utah

December 2012

The University of Utah Graduate School

STATEMENT OF THESIS APPROVAL

The thesis of Andrey Rybalkin

has been approved by the following supervisory committee members:

Tatjana Jevremovic	, Chair	**10/25/2012** Date Approved
Dong-Ok Choe	, Member	**10/19/2012** Date Approved
Haori Yang	, Member	**10/19/2012** Date Approved

and by **Chris Pantelides** , Chair of

the Department of **Civil and Environmental Engineering**

and by Charles A. Wight, Dean of The Graduate School.

ABSTRACT

Numerical assessments of radon diffusion together with analytical estimates for short-time and long-time exposure were the first objective of this thesis with the goal to demonstrate how radon propagates in various media. Theoretical predictions were compared to numerical simulations, and obtained values of total radon activities inside each material match quite well with the analytical estimates. These estimates, for activated and nonactivated charcoal, were then used to evaluate the possibility of designing a charcoal system to be used as a radon detector.

Another objective was to use nonactivated charcoal samples and measure the level of radon accumulation, and use these data to estimate radon diffusion and adsorption coefficients. The analytical approach was developed to estimate these values. Radon adsorption coefficient in nonactivated charcoal was found to be from 0.2 to 0.4 m^3/kg. Radon diffusion coefficient for nonactivated charcoal is in the range of 1.2×10^{-11} to 5.1×10^{-10} m^2/s in comparison to activated charcoal with adsorption coefficient of 4 m^3/kg and diffusion coefficient of 1.43×10^{-9} m^2/s.

The third objective was to use GEANT4 numerical code to simulate decay of ^{238}U series and ^{222}Rn in an arbitrary soil sample. Based on that model, the goal was to provide a guideline for merging GEANT4 radioactive decay modeling with the diffusion of radon in a soil sample.

It is known that radon can be used as an earthquake predictor by measuring its concentration in groundwater, or if possible, along the faults. Numerical simulations of radon migration by diffusion only were made to estimate how fast and how far radon can move along the fault strands.

Among the known cases of successful correlations between radon concentration anomalies and earthquake are the 1966 Tashkent and 1976 Songpan-Pingwu earthquakes. Thus, an idea of radon monitoring along the Wasatch Fault, using system of activated/nonactivated charcoals together with solid state radon detectors is suggested in the thesis. Also, the use of neutron activation analysis for soil samples, collected along and away from Wasatch Fault, and looking for the trace elements can result in correlation with earthquakes, occurred in the past. This approach can be used for earthquake prediction in future.

This thesis is dedicated to my wife

CONTENTS

LIST OF FIGURES

LIST OF TABLES

ACKNOWLEDGEMENTS

First and foremost my sincerest gratitude goes to my thesis advisor and committee chairperson, Professor Tatjana Jevremovic, who guided me through this thesis and read my numerous revisions. I acknowledge Professor Dong-Ok Choe and Professor Haori Yang for their helpful remarks. I also thank all my school friends at the University of Utah and especially at UNEP for their encouragement. Last, but by no means least, I thank my wife who has dealt with my absence and supported me with great patience at all times.

CHAPTER 1

ABOUT THIS THESIS

1.1 Motivation

The problem of radon diffusion, detection and measurement has been studied widely since the middle of the last century. Since then radon measurements have played important role in many fields, such as but not limited to health physics, mining and milling industries, public water supplies, real estate transactions, and geophysical studies.

Studying and simulating radon diffusion in various media can help in understanding how radon propagates in different structures. Therefore, the results can be useful for applications in radon detection and measurements as well as in correlating to the earthquake activities.

1.2 Thesis Objectives

Radon is omnipresent radioactive gas. This creates a lot of possibilities for studies of its propagation. Migration of radon depends on structure and properties of the material in which the transportation of atoms occurs. Numerical assessments of radon diffusion together with analytical estimates were chosen to demonstrate how radon propagates in various media: air, water, soil, and charcoal. The estimates for activated and non-

activated charcoal are used for evaluation of charcoal potential as radon detector. Besides, understanding of how radon propagates in groundwater can be used for earthquake prediction. Thereby, the objectives of this thesis are:

1. Simulate radon diffusion in a various media including activated charcoal canister used for radon measurements according to the Environmental Protection Agency (EPA) Standard and Protocol. Compare simulation results with analytical estimates of radon diffusion.
2. Develop the experiment with nonactivated charcoal samples to measure radon absorption and calculate diffusion and adsorption coefficients for radon in nonactivated charcoal using two analytical approaches with disregarding and considering radon decay.
3. Based on the analytical and experimental data discuss potential of activated and nonactivated charcoals as radon detector.
4. Use GEANT4 numerical code to simulate ^{238}U series decay and decay of ^{222}Rn alone in soil.
5. Outline how radon gas can be used as an earthquake predictor, and show the existing examples of yet successful radon measured data in correlation to the earthquakes occurred in the past.

1.3 Organization of the Thesis

Characteristics of radon gas and its properties, isotopes of radon and decay chains involved are described in the first section of Chapter 2. This section also explains radon origin and propagation in nature. The second section delineates basic principles of radon detection, measurement techniques and methods used for detection, and particularities of

radon detection in water. The third section describes different types of detectors and assemblies used for radon measurements with their accuracies.

Chapter 3 starts with introducing general diffusion theory and particularities of diffusion in porous medium. The second section delineates analytical approach to short-time and long-time radon diffusion. Chapter 3 continues with analytical and numerical estimates of radon diffusion in various media.

Characteristics of charcoal, its ability to absorb radon are given in Chapter 4. This chapter also reports the experiment with radon absorption by nonactivated charcoal samples. Experimental data is analyzed with theoretical findings to obtain diffusion and adsorption coefficient for radon in nonactivated charcoal. Potential of charcoal as radon detector is summarized.

GEANT4 simulations for ^{238}U decay chain and ^{222}Rn decay alone in soil are shown in Chapter 5.

Chapter 6 describes the role of radon as earthquake predictor, gives an overview of radon emanation during earthquake stages, its propagation in soil, and illustrates correlations of anomalies in radon concentrations before and after earthquakes that occurred in the past. Numerical simulations of radon migration along the fault strands are shown as well.

The last chapter concludes the thesis findings and suggests ideas for future work for analytical estimates and numerical simulations. Chapter 7 also describes how radon can be used as earthquake predictor in the Wasatch Fault region and how charcoal detectors can be used as a replacement of expensive equipment in monitoring tectonic movements.

CHAPTER 2

ORIGIN OF RADON GAS IN NATURE AND METHODS OF ITS DETECTION

2.1 Radon Gas Characteristics

2.1.1 Radon Gas and Its Properties

Radon is a naturally occurring noble gas, i.e., it is almost chemically inert or is not prone to combine with other atoms to create molecules. Radon has no color, odor or taste. It is soluble in water, and its solubility decreases with increasing temperature [*1*]. Density of radon is 9.73 g/l under standard conditions making it the heaviest gas in nature [*2*]. When cooled below its freezing point, radon has a brilliant phosphorescence which becomes yellow at lower temperatures and orange-red at the temperature of liquid air [*3*]. Radon is sometimes referred to as a *metalloid* element which lies on a diagonal between the true metals and nonmetals in the periodic table. It has some of the characteristics of both groups behaving similarly to boron, germanium, antimony and polonium [*4*].

Some physical properties of radon are given in Table 2-1. Radon is absorbed in charcoal, silica-gel and similar substances. This allows to separate it from other gases. Radon can be effectively removed from a sample air stream by collecting it on activated charcoal cooled to the temeperature of solid CO_2 (-78.5 °C) [*5*]. Radon is desorbed from charcoal by heating it up to 350 °C [*2*].

The most importaint feature of radon is its radioactivity. With atomic number of 86, radon has no stable isotopes. It is produced by the alpha decay of radium and by migrating in soil and water, can reach outdoor or indoor air.

Typically, outdoor radon concentration near the ground level is about 0.13 pCi/l (approx. 4.8 Bq/m^3) [*1*]. In the United States, the average outdoor radon concentration is about 0.4 pCi/l (approx. 15 Bq/m^3) and the mean indoor concenteration is 1.5 pCi/l (approx. 55 Bq/m^3) [*6*]. For indoor radon concentrations the EPA recommends 4 pCi/l (148 Bq/m^3) as a safe level. The concerns are explained by the fact that high concentrations of radon can cause lung cancer.

Once radon or its daughters are inhaled, they can decay in the lungs. That results in emitting alpha particles, which produce intense ionizing radiation, and therefore, possess high relative biological effectivness (RBE). It is especially improrant for mining and milling workers to monitor the radon exposure.

The first recorded awareness of unusually high mortality from respiratory disease that turned out to be lung cancer was reported by Agricola for miners in the Erz Mountains of eastern Europe in 1556. However, the first association of lung cancer with miners was determined only in 1879. Finally, it was not until the 1950s that it was found that radon was the primary cause of lung cancer in miners [*2*]. It was reported by Saccomanno et al. [*7*] that radon and its daughters' levels in United States uranium mines were measured from 1950 to 1968 and ranged from 100 to 10,000 pCi/l (3,700 to 370,000 Bq/m^3). These radon concentrations led to increased mortality among workers reported by Lundin et al. [*8*]. Uranium miners, exposed to lower radon levels of 50 to 150 pCi/l of air for about 10 years have shown an increased frequency of lung cancer [*9*].

2.1.2 Isotopes of Radon and Decay Chains

There are 39 known isotopes of radon with atomic mass numbers ranging from 193 to 231. The first discovered isotope was ^{222}Rn. In 1899, when P. Curie and M. Curie were studying radium samples, they reported a presence of unknown radioactive gas. It was identified by Friedrich Ernst Dorn in 1900 and named radium emanation. Radon was isolated as an element by M. Curie in 1908 [*10*]. The most recently identified isotopes, ^{230}Rn and ^{231}Rn, were discovered by H. Alvarez-Pol in 2010 [*11*]. Four isotopes, ^{218}Rn, ^{219}Rn, ^{220}Rn, ^{222}Rn are naturally occurring in decay chains of ^{238}U, ^{235}U and ^{232}Th, as shown in Figure 2-1, Figure 2-2 and Figure 2-3, respectively. ^{218}Rn is a daughter isotope of ^{218}At, which is produced from ^{218}Po. Both branches have low probabilities and are not shown in Figure 2-1. The most long-lived isotope is ^{222}Rn with a half-life of 3.8235(3) days [*11*]. It produces a series of short-lived radioactive products called progeny, or daughters.

For instance, when some amount of ^{222}Rn decays to ^{218}Po, which is also radioactive and has half-life of 3.10 minutes [*12*], half of polonium atoms will decay in 3.10 minutes. Thus, ^{218}Po cannot accumulate, but it will reach an equilibrium amount. Since ^{218}Po half-life is much shorter than the one of ^{222}Rn, this example demonstrates a case of secular equilibrium. This means that after a period of time, quantity of polonium will remain constant (will decrease only due to decrease of radon amount). In this case, polonium production rate is equal to its decay rate. While moving down the decay chain, it is obvious, that the amount of each next isotope produced, depends on the activity of its parent. When the half-live of progeny is not short enough, compared to the parent's half-life, only transient equilibrium can be achieved. Finally, when the half-life of the

daughter isotope is longer, than the one of the parent, no equilibrium can occur.

2.1.3 Radon Gas Origin

Naturally occurring radon originates from radium that is present in soil or rock. Radon seeps out of the ground from the ubiquitous uranium and thorium series. For example, ^{222}Rn is a progeny of ^{226}Ra, which is finally characterized by the level of ^{238}U in soil. This way, the rate of radon production in soil is influenced by the distribution of uranium in the earth's upper crust. The average concentration of uranium and thorium in the top 0.3 meter of soil is 1 ton and 3 tons, respectively, per square mile [*6*]. However, concentrations of uranium in the earth's crust vary widely as shown in Table 2-1.

Radioactivity in soils is related to radioactivity in rocks from which the soil is formed. Since uranium and radium can be found throughout the earth's crust and radium is also soluble in water, radon is found virtually everywhere [*13*].

Due to a ^{222}Rn half-lafe of almost 4 days, it can migrate from its place of origin either by pores in soil or groundwater, being dissolved in it. Table 2-2 shows relatively high solubility of radon in water (230 cm^3/kg) that accounts for its presence in substantial amounts in certain spring waters. Eventually, some atoms of radon escape into the atmosphere.

Due to its wide distribution in the atmosphere, radon makes up a unique set of tracers for a variety of transport and mixing processes. Measured profiles of ^{222}Rn and ^{220}Rn above the earth's surface are in general agreement with those predicted by turbulent diffusion theory [*2*]. Details on radon propagation are described in the following section.

2.1.4 Radon Propagation in Nature

Originated in the earth crust, radon can propagate in soil. Some of the radon atoms, while formed from radium, become trapped within the grain of rock or soil and are not able to escape into pore spaces for further propagation. The atoms that are not trapped can be absorbed in groundwater or diffuse through the soil and migrate.

Fracturing and faulting of rocks can contribute to the radon migration. Cracks and ruptures can be freeway to soil gas molecules [*14*]. More detailed discussion on radon propagation in soil is given in section 6.2.

The atoms of ^{218}Rn, ^{219}Rn, ^{220}Rn, ^{222}Rn can emanate from soil, uraniferous rocks and water and become dispersed in the air. As it was described in section 2.1.1, radon is a noble gas; this fact allows it to migrate by diffusion and convection without significant interaction with nitrogen, oxygen and other atoms in air. In the process of airborne radon decay, free atoms of polonium, lead, bismuth, astatine, thallium and mercury are produced. They are either positive or negative ions, depending on decay mode of the parent isotope: beta or alpha decay, respectively. The presence of charge allows the ions to be electrostatically attached to dust particles or aerosols. As it was described in section 2.1.1, once such substance is inhaled, it can increase a radiation dose to lung tissue. This is the main reason of why radon and its daughters account for half of the total radiation dose to human from all natural sources [*15*], [*13*].

The fact that radon is radioactive, and does not chemically react with other gases, makes it unique as a tracer for the studying various processes in the indoor and outdoor air [*2*]. The main mechanisms of transport in the atmosphere are horizontal winds, convection and eddy diffusion as used in tracer studies. Relatively high levels of radon

encountered in caves have also been the target of studies as well as natural radon transport from earth to the atmosphere by volcanoes. The sharp contrast that occurs between ^{222}Rn flux from the oceans compared with land areas has led to the identification of significant differences in radon concentration over those parts of the continents where marine air masses are common [*16*]. Another radon application was described by Israel [*17*]; the rate at which ions are produced in the air, their electrical conductivity and mobility spectra are all affected by the concentration of ^{222}Rn, ^{220}Rn and their decay products. The ions created by decay of the radon daughters have been used to investigate the atmospheric electrical environments under fair weather and thunderstorm conditions [*18*], [*19*].

Radon concentrations in soil gas exceed those of the ambient atmosphere by a factor of about 1,000. As a result, radon emanates from soil by escaping from the surfaces of mineral grains to the soil at the air-earth interface by transport in a porous medium [*20*]. One of the early applications of the use of radon in soil was for uranium exploration. Changes in soil radon concentrations have been used to study stress-strain relations in rock formations and have been proposed for prediction earthquakes [*2*]. Such studies of measuring radon prior to the Tashkent earthquake were reported by Ulomov and Mavashev [*21*]. They observed increase of radon concentration in a hot mineral water aquifer in the Tashkent artesian basin, USSR before the Tashkent earthquake of M = 5.3 in 1966. This is described in detail in section 6.3.

2.2 Basic Principles of Radon Gas Detection

2.2.1 Measurement Techniques and Methods

Radon cannot be detected by human senses, but nuclear signatures that come from alpha and gamma radiation, produced by radon and its progeny, are the main key for measuring its presence.

Generally, measurement techniques can be divided into three categories: grab sampling, continuous and active sampling, and integrative sampling [*22*]. The main reasons for choosing between these categories are costs, time, type of information required, and desired accuracy.

Grab sampling technique implies short sampling time, usually a few minutes. It is useful for indoor radon measurements, as it provides a quick screening of a residence to determine if there is extremely high radon concentration [*14*]. The radon grab sampling is based on a very slow drawing of small air volume into the counter chamber through a millipore filter. During the filtering most of the airborne radioactive particulates are removed, including radon progeny that are attached to dust and aerosols. When radon decays in the chamber, it produces daughters, and the alpha particles, emitted in the decay of radon and its progeny, are counted by an alpha scintillation counter or an ionization chamber [*14*]. Grab sampling technique is illustrated in [*23*].

Continuous sampling is based on the automatic measurements that are taken at closely spaced time intervals over a long period of time. This results in a series of measurements which can give information on how the concentration varied during the experiment [*1*]. An example of continuous radon measurements is shown by Kávási et al. [*24*] as a function of time in the tunnel of Hungarian manganese mine.

The method can be explained in more detail by describing the operation of a continuous radon monitor (CRM). The work of this monitor is based on continuously sampling the ambient air by pumping it into a scintillation cell. The filtering process is involved, and it is similar to the one that is used in grab sampling technique. This way, the air in the cell is filtered from radioactive particulates that exist in the ambient air. As radon in the cell decays, the charged progeny is attracted and becomes attached to the interior surface of the scintillation cell. The decay events are counted by a photomultiplier tube (PMT) [*14*]. Schematic diagram of the CRM is shown in [*25*]. Continuous sampling is useful for the scientific studies of the radon and its progeny. It is used to measure the real-time changes in the concentrations [*14*].

Integrating devices collect information on the total number of radiation events which occur throughout some long period of time, usually from several days to months. The result from the integrating devices is an estimate of the approximate average concentration through the measurements interval [*1*].

All of the methods discussed are based on detecting the radionuclides through a measurement of the various type of radiation emitted. Gamma rays, beta and alpha particles may be measured and used for evaluation of the activity levels. Some of the measurement methods count only alpha particles, since the background for alpha counting usually is much less than for gamma rays and beta particles. However, the very short range of the alpha particles (a few centimeters in air) requires the detector to be placed very close to the source [*1*].

The radon can be measured using active or passive technique. Active technique implies that air is pumped through the filter, while passive technique is based on unaided

radon entry inside the detector. Examples of passive techniques are given in sections 2.3.6 and 2.3.7.

2.2.2 Measurement of Radon in Water

The evaluation of radon level in water is relatively simple compared to measurements in air. There are fewer sampling problems, and the rate and magnitude of variations are much lower. However, all methods require correction for radon decay during the delay between sampling and analysis. A serious sampling problem is associated with the actual transfer of a water sample into a container. Because radon is a gas, special care is required to collect a sample without significant radon outgassing.

There are two primary methods for the radon measurements in water. The standard technique for many years was the radon bubbler and alpha scintillation method [*26*]. In this method, a carrier gas is passed through the sample in a bubbler flask to purge out the dissolved radon. Either a once-through or a recirculating system may be used for purging. The released radon is then transferred either directly or after a concentrating step into an evacuated scintillation cell, referred to as a Lucas cell in honor of its inventor, Henry Lucas [*1*]. The cell is coated with a ZnS:Ag phosphor and has a quartz window. After radon is concentrated in Lucas cell, the sample is stored for about three hours to allow equilibrium to be reached between radon and its short-lived progeny.

Plotting relative activities as a function of time for radon and its daughters is good illustration for understanding how and when the equilibrium is reached. Assuming non-zero radon concentration in terms of the number of atoms $N_1(0) \neq 0$, and zero

concentrations of its decay products $N_i(0) = 0$ when $i > 1$, the concentration of n^{th} nuclide after time t can be calculated using Bateman equation [*27*]:

$$N_n(t) = \frac{N_1(0)}{\lambda_n} \sum_{i=1}^{n} \lambda_i \alpha_i e^{-\lambda_i t} \tag{2.1}$$

where λ represents decay constant, and

$$\alpha_i = \prod_{\substack{j=1 \\ j \neq i}}^{n} \frac{\lambda_j}{(\lambda_j - \lambda_i)} \tag{2.2}$$

Therefore, $N_2(t)$ or the number of ^{218}Po atoms as a function of time can be calculated as follows:

$$N_2(t) = N_1(0)\lambda_1 \left(\frac{e^{-\lambda_1 t}}{(\lambda_2 - \lambda_1)} + \frac{e^{-\lambda_2 t}}{(\lambda_1 - \lambda_2)} \right) \tag{2.3}$$

The same way, $N_3(t)$ and $N_4(t)$are the concentrations of ^{214}Pb and ^{214}Bi, respectively:

$$N_3(t) = N_1(0)\lambda_1\lambda_2 \left(\frac{e^{-\lambda_1 t}}{(\lambda_2 - \lambda_1)(\lambda_3 - \lambda_1)} + \frac{e^{-\lambda_2 t}}{(\lambda_1 - \lambda_2)(\lambda_3 - \lambda_2)} + \frac{e^{-\lambda_3 t}}{(\lambda_1 - \lambda_3)(\lambda_2 - \lambda_3)} \right) \tag{2.4}$$

$$N_4(t) = N_1(0)\lambda_1\lambda_2\lambda_3\left(\frac{e^{-\lambda_1 t}}{(\lambda_2-\lambda_1)(\lambda_3-\lambda_1)(\lambda_4-\lambda_1)} + \frac{e^{-\lambda_2 t}}{(\lambda_1-\lambda_2)(\lambda_3-\lambda_2)(\lambda_4-\lambda_2)}\right.$$
$$\left. + \frac{e^{-\lambda_3 t}}{(\lambda_1-\lambda_3)(\lambda_2-\lambda_3)(\lambda_4-\lambda_3)} + \frac{e^{-\lambda_4 t}}{(\lambda_1-\lambda_4)(\lambda_2-\lambda_4)(\lambda_3-\lambda_4)}\right) \quad (2.5)$$

After multiplying these concentrations by decay constants and dividing by ^{222}Rn activity at time *t*, the relative activities for each daughter are obtained. Based on these calculations, Figure 2-4 represents the buildup of ^{222}Rn progeny relative activities. It can be noticed that after around 200 minutes, activities of the daughters reach the parent's activity. As soon as equilibrium is reached, the cell is placed in a photomultiplier tube for detection of the pulses generated by alpha particles striking the phosphor. Counting time is usually less than 10 minutes at the concentrations frequently found in groundwater [*1*].

The bubbler method has low background and low detection limit, which is about 50 Bq/m^3. The analytical precision of this technique is reported in the literature to be about ±10% [*1*]. The disadvantage of this method is that the sample should be collected in the same bubbler flask used during measurement. Only glass can be used because most of plastics are permeable to radon. Besides, handling and transport of glass flasks that are traditionally round-bottomed is awkward. Loss of sample integrity is a frequent problem too.

These problems led to the development of a faster analytical technique for radon measurements in water: liquid scintillation counting [*28*]. In this method, 10 mL of sample are injected into a glass vial containing 5 – 10 mL of liquid scintillation solution. The vial is tightly capped and shaken vigorously. The samples are then returned to the laboratory and counted with a liquid scintillation counter. The detection limit is about 370

Bq/m^3 for a counting period of 40 minutes [*1*].

The precision in the analytical determination of radon in water is about 5%.

2.3 Detectors and Equipment for Radon Gas Measurements

2.3.1 Assemblies Used for Radon Gas Measurements

To measure the radon concentration in air or in water, special assemblies that count alpha and gamma radiation are used. They differ depending on the way of measuring. For example, the assembly, used for outdoor measuring of radon that comes from soil, can be constructed with two pipes made of polyvinyl chloride and a nuclear track etch detector film [*29*]. The assemblies for indoor radon measurements are usually as simple as charcoal canister or sealed plastic film track detector, which should be unsealed before the exposure and sealed again after [*14*].

2.3.2 Detection Systems' Accuracies

An important step in radon measurement is calibration of the instrument used. The accuracy of the measurement depends on the calibration of instrument that determines its response to a known concentration of radioactivity. This response allows a correlation to be made between the instrument reading and the actual concentration present.

Defined accuracies for radon measurements ranges from 70% to 95% [*30*]. Detection limit can be as low as 10^{-3} Bq/m^3. Accuracies and detection limits for some radon detection methods are summarized in Table 2-3.

2.3.3 Solid State Alpha Detectors

The solid state alpha detector consists of a semiconductor material that converts alpha radiation directly to an electric signal. The main advantage of solid state detectors is the ability to determine energy of each alpha particle. This makes it possible to tell exactly which isotope produced the radiation, and therefore allows immediately to distinguish ^{218}Po from ^{214}Po, ^{222}Rn from ^{220}Rn, and signal from noise. Very few instruments are able to do this, and one of the solid state alpha detectors that has this alpha spectrometry feature is DURRIDGE RAD7 detector [*31*]. It possesses an internal sample cell of 0.7 liter and has a hemispherical shape as can be observed in schematic of the RAD7 in [*32*].

The inside of the hemisphere is coated with an electrical conductor. High voltage power supply charges the inside of the conductor to a potential of 2,000 to 2,500 volts, relative to the detector. This creates an electric field throughout the cell volume. The electric field propels the positively charged particles onto the detector in the periodic-fill cell. A ^{222}Rn nucleus that decays within the cell leaves behind a positively charged ^{218}Po, which is driven by the electric field to the detector and sticks to it. The ^{218}Po nucleus has a relatively short half-life and when it decays upon the detector's active surface, its alpha particle has a 50% probability of entering the detector where it will produce an electrical signal, proportional in strength to the energy of the alpha particle.

Different isotopes have different alpha energies, and produce different strength signals in the detector. The RAD7 detector has an energy scale from 0 to 10 MeV. Of particular interest are energies in the range of 6 to 9 MeV, since ^{222}Rn and ^{220}Rn daughters produce alpha particles with such energies.

2.3.4 Alpha Track Detectors

An alpha track detector consists of a small piece of special plastic film enclosed in a container with a filter-covered opening. The filter serves as a barrier to radon progeny in the air but allows radon to enter container freely. In the container, some of the radon atoms disintegrate and produce daughters. The alpha particles emitted by radon and some of its short-lived progeny strike the plastic film and leave permanent submicroscopic tracks on it.

In the laboratory, the plastic film is etched by a solution of potassium hydroxide or sodium hydroxide. The damage tracks are enlarged and made visible by the etching process and can then be counted under a wide-screen microscope. The number of tracks per unit area is then correlated to the radon concentration in the air, using a conversion factor derived from data obtained at a calibration facility [*14*].

2.3.5 Scintillation Detectors

The main part of a scintillation detector is scintillator, the material which exhibits scintillation when exited by ionizing radiation. The detector is coupled to a PMT which absorbs the light emitted by the scintillator and reemits it in the form of electrons via the photoelectric effect. Dynodes multiply electrons that produce current which is then recorded as a signal. Figure 2-5 shows the typical components of a scintillation detector.

The radon is sampled with help of a pump through a filter. The purpose of the filter is to remove radon decay products as well as dust particles. The radon decay inside the scintillation cells, and the progeny plate out on the interior surface of the cells. The alpha radiation from the radon decay or that of the decay products, strike the coating of the scintillation cell. The subsequent scintillations are detected by a PMT, which

generates electrical pulses in turn, which are then processed by the detector electronics.

2.3.6 Electret Detectors

The principle of electret detectors is based on measuring the reduction of voltage caused by ions produced by alpha decay of radon inside the detector that strike an electrostatically charged disk. This disk is called an electret and mounted in a small canister isolated from particulates by a filter. Radon passes through the filter and induces a minor negative charge in the air near the positively charged electric. The negative ions are attracted to the electret surface and a voltage is imparted. This measured voltage is proportional to the radon concentration in air and can be corrected for length of exposure, background, and other factors. The method can be deployed for short or long periods, depending on the electret used. The same detector can be reused a number of times until the charged surface has been effectively neutralized, perhaps after some ten uses. Short- and long-term electrets manufactured by Rad Elec Inc. are illustrated in [*32*].

The electret detectors are not sensitive to humidity unlike charcoal canisters and may give results equal to those obtained from alpha track measurements over long-term deployment situations [*33*].

2.3.7 Activated Charcoal Detectors

Activated charcoal detectors are very popular for radon measurements. These consist of tightly sealed canisters of activated charcoal. This type of charcoal features higher absorption ability compared to the usual ones. Its porous structure results in a significantly larger surface. The air to be sampled diffuses through activated charcoal granules loosely packed in a canister that is open to the air, and the radon is adsorbed

onto the carbon. After about 4–7 days of exposure, the charcoal-containing canister is sealed shut and the gamma radiation from the radon and its daughters is counted using scintillation counter [*6*]. Because of the short half-lives of radon and its progeny, it is important to have the analysis done quickly after the deployment period so that enough radon daughter product is available for measurement [*34*]. The counts are then compared to a calibration curve to determine the mean radon concentration during the sampling period.

Table 2-1. Uranium in Rocks and Soils, adapted from [*35*]

Material	Micrograms per gram	Picocuries per gram
Igneous rocks		
Basalt (crustal average)	0.5-1	0.2-0.3
Mafic	0.5, 0.9	0.2, 0.3
Salic	3.9, 4.7	1.3, 1.6
Granite (crustal average)	3.0	1.0
Sedimentary rocks		
Shale	3.7	1.0
Sandstones		
Clean quartz	<1.0	<0.3
Dirty quartz	2-3	1.0
Arkose	1-2	0.3-0.7
Beach sands (unconsolidated)	3.0	1.0
Carbonate rocks	2.0	0.7
Soils	1.8	0.6

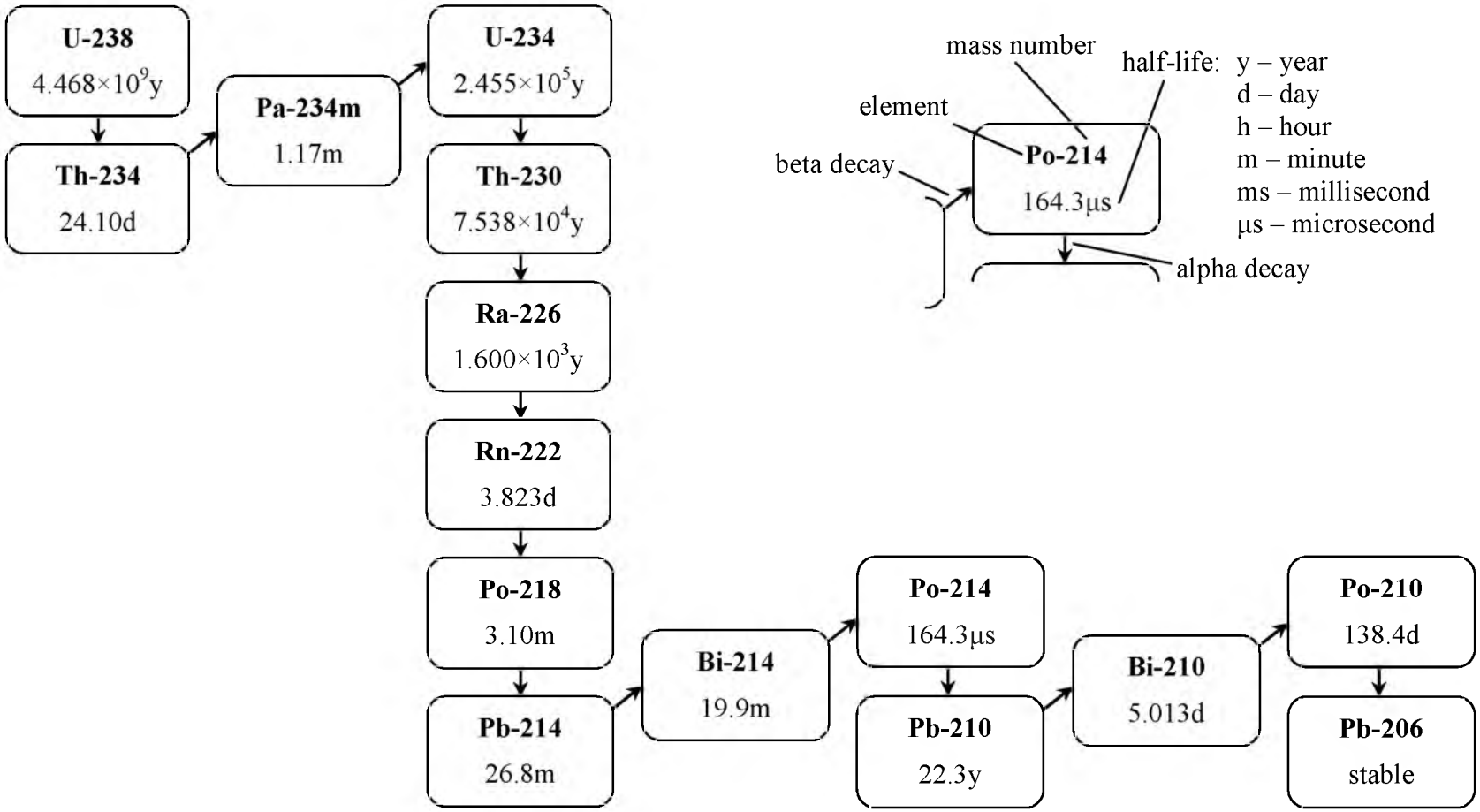

Figure 2-1. Uranium-238 decay chain

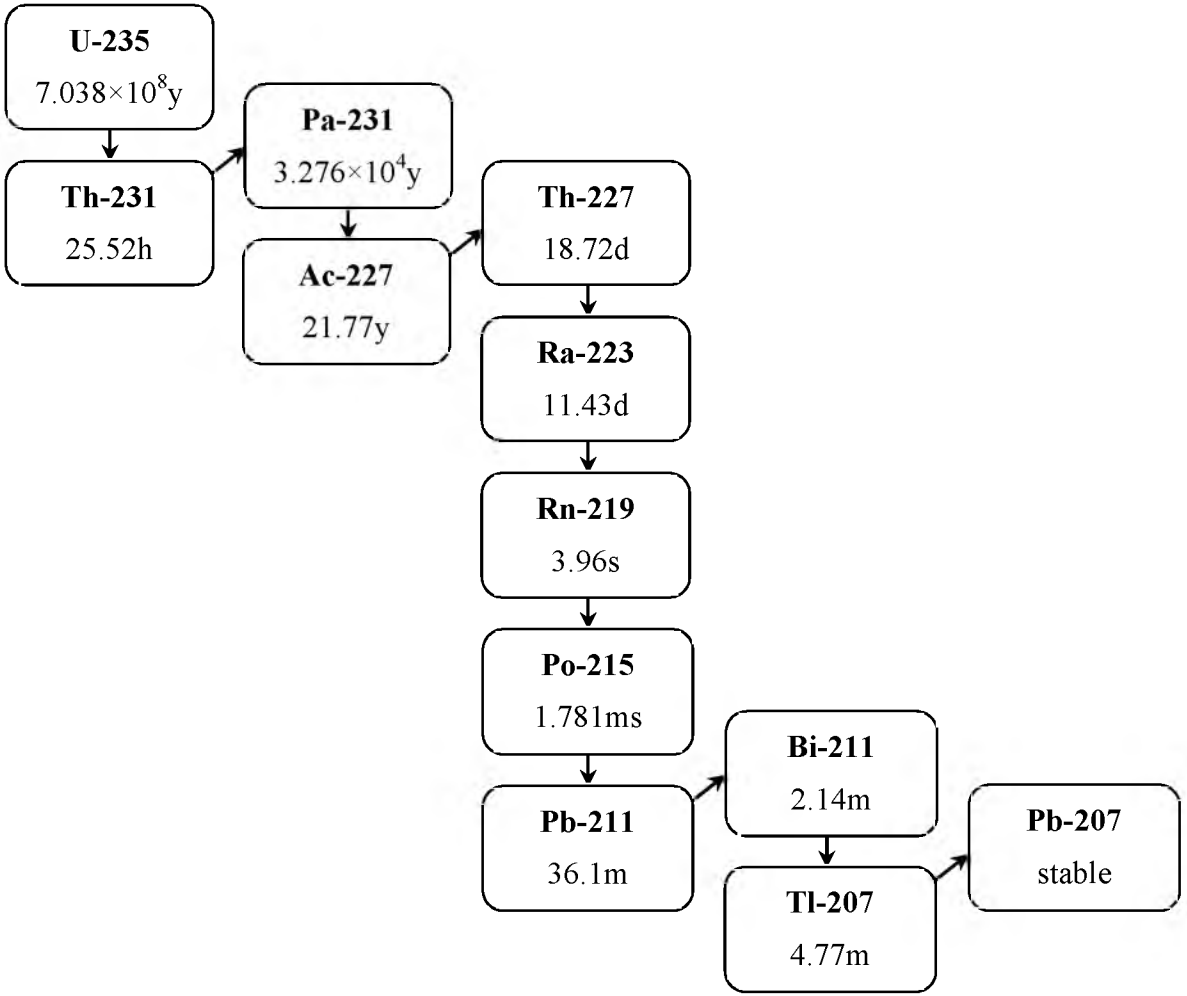

Figure 2-2. Uranium-235 decay chain

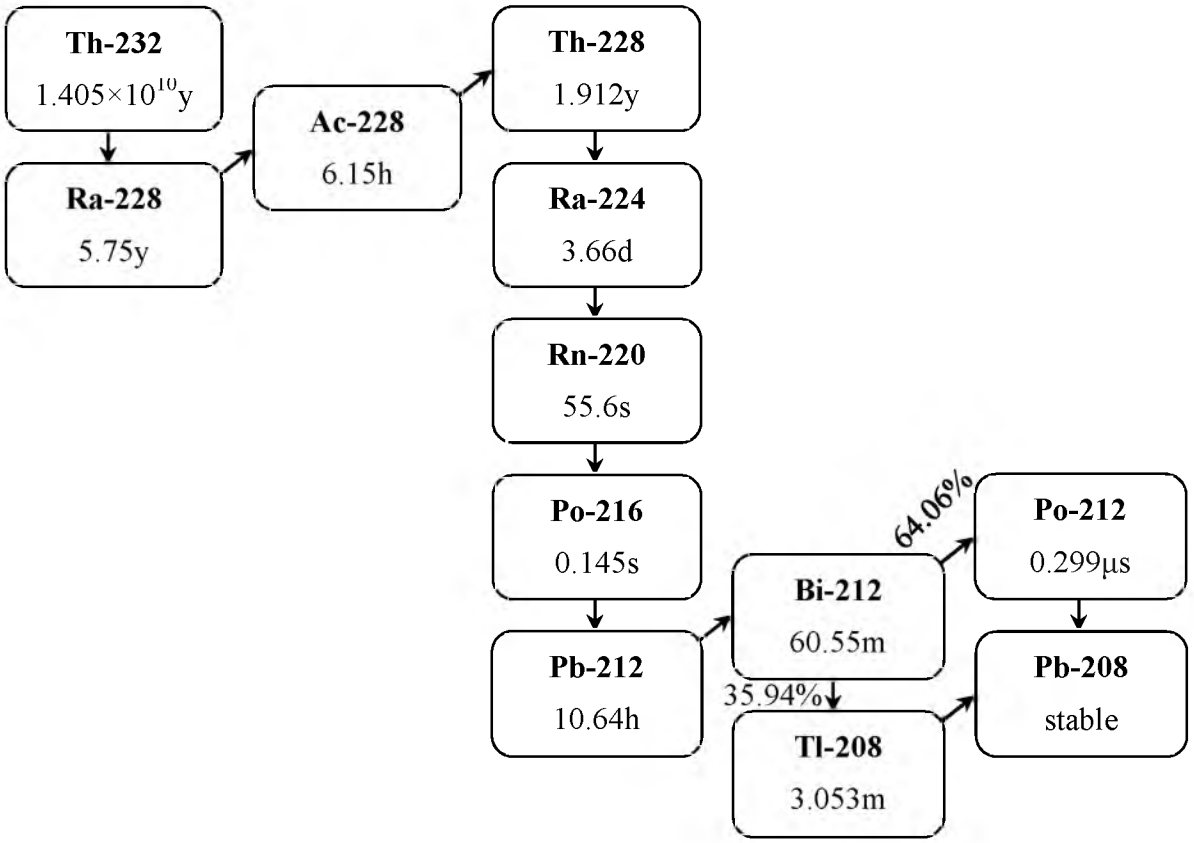

Figure 2-3. Thorium-232 decay chain

Table 2-2. Physical properties of ^{222}Rn. Reprinted with permission of **[***36***]**

Density at 0° C and 1 atm	9.73 g/l
Boiling point, normal (1 atm)	-62 °C
Density of liquid at normal boiling point	4.4 g/cm^3
Diffusion coefficient in free air	0.1 cm^3/sec
Viscosity at 1 atm pressure and 20 °C	229.0 micropoise
Critical pressure	62 atm
Critical temperatures	105 °C
Solubility in water at 1 atm partial pressure and 20 °C	230 cm^3 (STP)/ kg water
Solubility in various liquids at 1 atm pressure and 18 °C	
Glycerin	0.21 cm^3/kg liquid
Ethyl alcohol	7.4 cm^3/kg liquid
Petroleum (liquid paraffin)	9.2 cm^3/kg liquid
Toluene	13.2 cm^3/kg liquid
Carbon disulfide	23.1 cm^3/kg liquid
Olive oil	29.0 cm^3/kg liquid

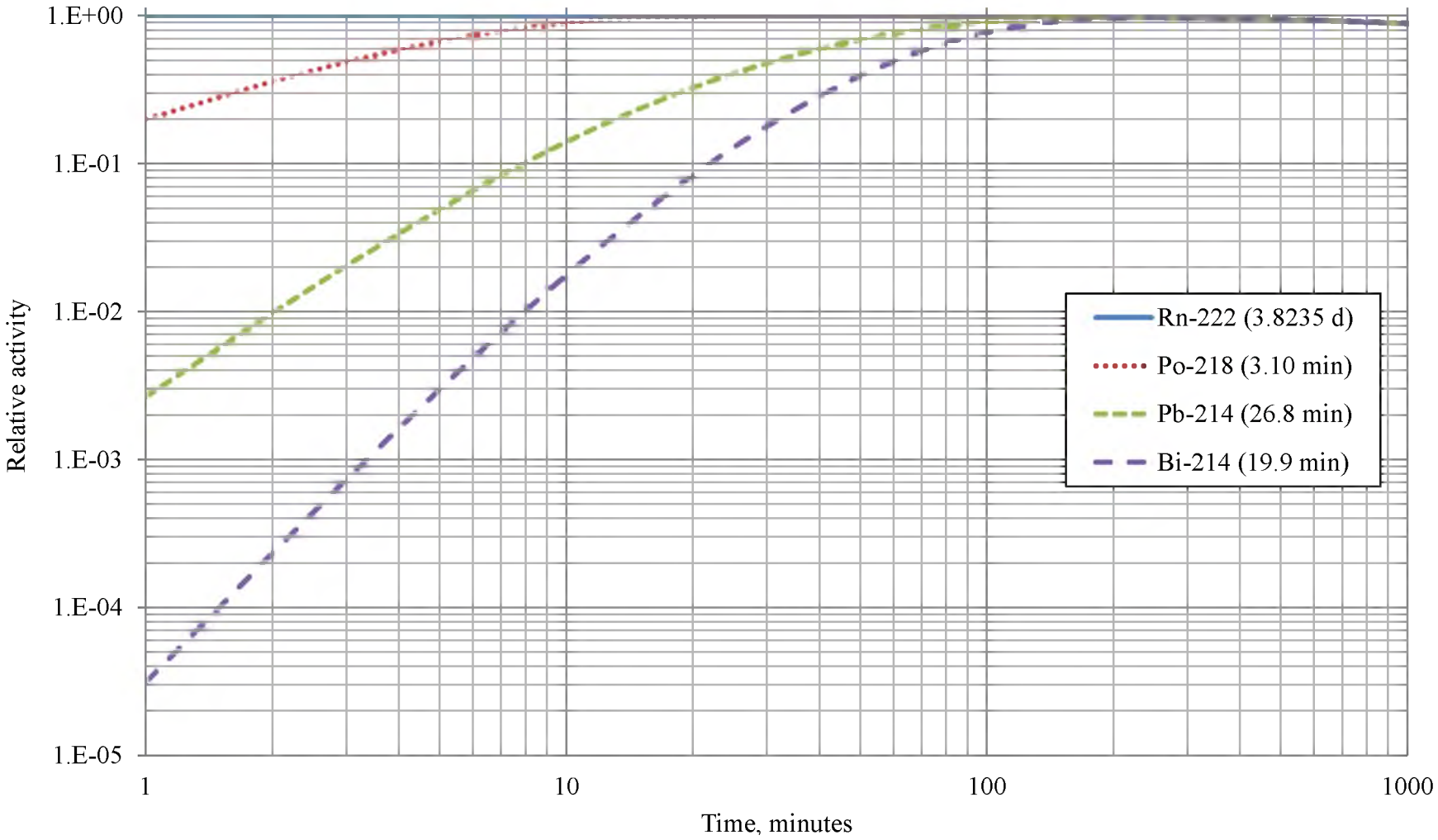

Figure 2-4. Relative activities of ^{222}Rn progeny vs. time

Table 2-3. Analytical methods for determining radon in environmental samples, detection limits and accuracies.
Reprinted with permission of [*30*]

Sample Matrix	Sample Preparation	Analytical Method	Sample Detection Limit	Accuracy
Air				
Radon				
	Adsorb onto activated charcoal, 2 to 7 days	Gamma spectroscopy	1.3 pCi/m^3 (0.048 Bq/m^3)	No data
	Adsorb onto activated charcoal; extract with toluene; gently shake	Liquid scintillation	0.21-0.37 pCi/m^3 (0.007-0.014 Bq/m^3)	0.094 of true concentration
	Scintillation Cell Allow air to enter detection chamber through Millipore filter until equilibrated, or collect sample in bag (Mylar or Tedlar), transfer to chamber ASAP	ZnS (Ag) scintillation/ photomultiplier tube	0.1 pCi/m^3 (0.004 Bq/m^3)	No data
	Diffuse through filter into detector housing; collections with electret	TLD chip	89 pCi/m^3 (3.30 Bq/m^3)	0.95-1.08 of true concentration
	Two-Filter Method Draw air into fixed length tube with entry and exit filters; monitor exit filter activity	ZnS (Ag) scintillation/ photomultiplier tube	0.011 pCi/m^3 (<0.001 Bq/m^3)	90%
	Solid State Nuclear Track Detector Diffuse through a filter into a cup containing alpha track material (cellulose nitrate film) for up to 1 year; etch in acidic or basic solution operated upon by an alternating electric field	Microscopic examination of damaged material	14 pCi/m^3 (<0.519 Bq/m^3)	No data

Table 2-3. (*Continued*)

Radon progeny	
	Draw air through filter for a sampling time of 5 to 10
	Draw air through filter at a known flow rate for specified time (10 m to 1 h) Charge surface electrostatically to attract aerosols
Soil	
	Dry in 55°C oven for 24 hours; place 5 grams in 20 ml borosilicate glass scintillation. Cover with 10 ml distilled water; allow soil to become wet; add 5 ml high-efficiency mineral oil; allow to age 30 days
	None
Water	
	Pass carrier gas through samples in a bubbler flask to purge out dissolved radon; transfer radon to evacuated scintillation cell
	Inject into glass vial containing liquid scintillation solution
	Direct measurement

Gross alpha counting	1.1 pCi/m^3 (<0.041 Bq/m^3)	No data
Alpha spectrometry	1.1 pCi/m^3 (<0.041 Bq/m^3)	70%
Alpha spectrometry	1.1 pCi/m^3 (<0.041 Bq/m^3)	70%
Scintillation counter	No data	No data
Track etch detector buried 30 cm deep	No data	No data
Scintillation counter	1.4 pCi/L (52 Bq/m^3)	90%
Liquid scintillation counter	10 pCi/L (370 Bq/m^3)	No data
Gamma ray spectroscopy	10 pCi/L for 1 L sample (370 Bq/m^3)	No data

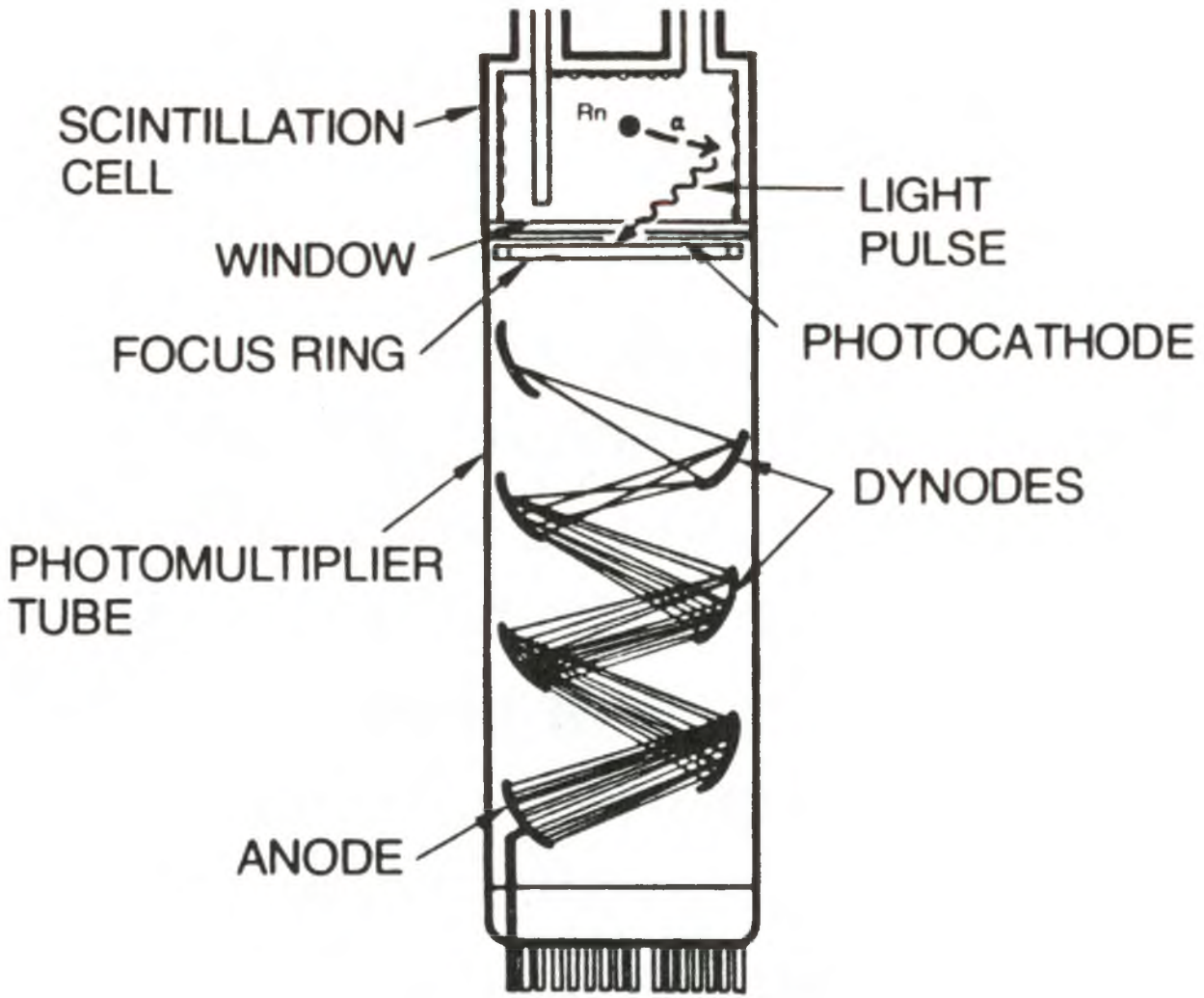

Figure 2-5. A typical counting system that uses a scintillation cell. Reprinted with permission of [*1*]

CHAPTER 3

DIFFUSION OF RADON IN VARIOUS MEDIA

3.1 Basic Principles of Diffusion Theory of Gases in Arbitrary Medium

3.1.1 Diffusion Theory

Diffusion is defined as spreading out one substance through another due to molecular motion, rather than flow. The rate of diffusion shows how fast the material can diffuse. In liquids the rate of diffusion is typically fractions of a millimeter per second. It can be observed with the naked eye when the colors of two liquid substances are different. It is more difficult to observe diffusion in solids. Even around the melting temperature of a solid substance, the diffusion rate is only on the order of nanometers per second. It decreases with decreasing temperature. Atomic-scale motion is rather rapid in gases – gas diffusion progresses at a rate of centimeters per second.

A major advance in diffusion theory came from the work of the German physiologist Adolf Eugen Fick. He postulated that the flux j [time^{-1} length^{-2}] in direction x [length] is proportional to the pertaining gradient of concentration C [length^{-3}]:

$$j(x,t) = -D\frac{\partial C(x,t)}{\partial x} \tag{3.1}$$

This relationship is called *Fick's First Law.* D is denoted as diffusion coefficient

or diffusivity and has a unit of [length^2 time^{-1}]. Considering the principle of conservation of matter:

$$\frac{\partial C(x,t)}{\partial t} = D\frac{\partial^2 C(x,t)}{\partial x^2} \tag{3.2}$$

This equation is called *Fick's Second Law*. It predicts how diffusion causes the concentration to change with time. For the case of diffusion in more than one dimension Fick's Second Law becomes:

$$\frac{\partial C(r,t)}{\partial t} = D\left(\frac{\partial^2 C(x,t)}{\partial x^2} + \frac{\partial^2 C(y,t)}{\partial y^2} + \frac{\partial^2 C(z,t)}{\partial z^2}\right) \tag{3.3}$$

or after introducing the Laplace operator:

$$\frac{\partial C(r,t)}{\partial t} = D\Delta C(r,t) \tag{3.4}$$

Solving this partial differential equation is a baseline for diffusion numerical simulations.

3.1.2 Diffusion of Gases in Porous Medium

Gas diffusion in another gas is rather fast as the distance between molecules is relatively large, compared to their size. Thus, they can cover significant distances. Slower gas diffusion rate is observed in water and the slowest in solids.

However if solid material has a porous structure, the gas can penetrate much deeper. This is explained by moving partially in gas, inside and between the pores. Figure

3-1 shows possible ways for gas that moves in porous material. Arrows indicate possible scenarios for gas to come out of the solid particle, to move between particles, enter pore spaces and leave the material.

Diffusion through dry porous granular materials is influenced by porosity, packing, and particle shape and size, in addition to the composition, temperature, and pressure of the pore-filling fluid. An empirical equation accounting for the solid properties is

$$\frac{D}{D_i} = \gamma \varepsilon^{\mu} \tag{3.5}$$

where D_i is the diffusion coefficient in the pore as a continuous medium; ε is the porosity; the constant γ ranges from 0.8 to 1.0; and μ is a constant ≥ 1 measuring pore shape. Every term on the right-hand side of the equation (3.5) is unitless [*37*].

Importance of the particle shape decreases if the medium is wet. The diffusion coefficient is less for porous media with wet pores than for those that are dry but have the same air-filled porosity. United States Geological Survey [*37*] reports that the reason for that is blocking of the interpore paths by water.

Another model that can be applied to gas propagation in porous medium is Knudsen diffusion. In large capillaries molecular diffusion prevails, as gas atoms collide mainly with other gas atoms. Knudsen diffusion is used to describe diffusion process when the scale length of a system is comparable to or smaller than the mean free path of the particles. In other words, atoms collide mainly with pore walls, not with other atoms.

The relative contributions of diffusion and transport of gases are difficult to

determine in practice. One of the early reports on gas diffusion in porous medium was written by Tanner [***38***]. This study analyzes one-dimensional migration of radon gas in homogeneous porous medium. Exponential argument includes both diffusion and transport parameters. Unless the diffusion coefficient or the transport velocity is accurately known, any combination of the two components will satisfy the diffusion model. Results of this work show that concentration of radon exponentially decreases in the direction of migration.

3.2 Diffusion Theory Applicable to Radon

3.2.1 Theory Describing Radon Diffusion During Short-time Exposures

In this and in the next section diffusion of radon in an activated charcoal canister is described. To take into account the radioactivity of radon, and therefore loss in its concentration with time, the diffusion equation (3.4) must be rewritten as follows:

$$\frac{\partial C(r,t)}{\partial t} = D\Delta C(r,t) - \lambda C(r,t) \tag{3.6}$$

where C [activity/length^3] denotes radon concentration in air; t is time; D [legth^2/time] is radon diffusion coefficient in activated charcoal; λ [time^{-1}] is the decay constant of radon.

Diffusion along the x and y axis can be ignored, because it does not change the concentration along canister depth. Considering diffusion only along z axis, the equation transforms into the following:

$$\frac{\partial C(z,t)}{\partial t} = D\frac{\partial^2 C(z,t)}{\partial z^2} - \lambda C(z,t) \tag{3.7}$$

To solve this partial differential equation, boundary and initial conditions must be defined. The initial condition is simply zero radon concentration in activated charcoal at time $t = 0$:

$$C(z, 0) = 0 \tag{3.8}$$

The first boundary condition can be stated as follows:

$$C(0, t) = k\rho C(t) \tag{3.9}$$

where k denotes adsorption coefficient [length^3/mass] and ρ [mass/length^3] is the charcoal density. It is assumed that radon concentration in air is constant and equal to C_0. In this case the first boundary condition becomes:

$$C(0, t) = k\rho C_0 \tag{3.10}$$

The initial and first boundary conditions for activated charcoal canister geometry are illustrated in Figure 3-2 at the top of the cylinder.

The second boundary condition is related to the other end of the canister, at $z = l$ and indicates that radon cannot enter the bottom of the canister, so radon gas flux there equals zero:

$$\left(\frac{\partial C(z, t)}{\partial z}\right)_{z=l} = 0 \tag{3.11}$$

To solve the diffusion equation (3.7) for the initial and boundary conditions (3.8),

(3.10), (3.11) for the case of short-term exposure of activated charcoal to radon, considering its constant concentration in air during exposure, it is necessary to define the range of short-term exposure.

As described by Nikezić and Urošević [*39*], short-term exposure of activated charcoal canister to radon lasts less than 3 days. In this case disintegration of radon can be ignored. Therefore, radon decay constant is equal to zero:

$$\frac{\partial C(z,t)}{\partial t} = D\frac{\partial^2 C(z,t)}{\partial z^2} \tag{3.12}$$

Fourier's method of separation of variables can be applied to solve this equation. The function $C(z,t)$ can be represented as a product of two functions: $Z(z)$ and $T(t)$ where $Z(z)$ depends only on coordinate *z*, and $T(t)$ depends only on time *t*.

$$C(z,t) = Z(z)T(t) \tag{3.13}$$

Equation (3.12) requires $C(z,t)$ to be differentiated once with respect to time *t* on the left-hand side, and twice with respect to coordinate *z* on the right-hand side:

$$\frac{dC(z,t)}{dt} = \frac{d\big(Z(z)T(t)\big)}{dt} = \frac{dZ(z)T(t) + Z(z)dT(t)}{dt} = \frac{Z(z)dT(t)}{dt} \tag{3.14}$$

$$\frac{d^2C(z,t)}{dz^2} = \frac{d^2\big(Z(z)T(t)\big)}{dz^2} = \frac{d\big(dZ(z)T(t) + Z(z)dT(t)\big)}{dz^2} = \frac{d^2Z(z)T(t)}{dz^2} \tag{3.15}$$

After substituting (3.14) and (3.15) in the equation (3.12):

$$\frac{Z(z)dT(t)}{dt} = D\frac{d^2Z(z)T(t)}{dz^2} \tag{3.16}$$

After dividing both sides of the equation (3.16) by $DZ(z)T(t)$:

$$\frac{1}{DT(t)}\frac{dT(t)}{dt} = \frac{1}{Z(z)}\frac{d^2Z(z)}{dz^2} \tag{3.17}$$

Assuming that both sides of the equation are equal to certain constant $-a^2$:

$$\frac{1}{DT(t)}\frac{dT(t)}{dt} = -a^2 \tag{3.18}$$

$$\frac{1}{Z(z)}\frac{d^2Z(z)}{dz^2} = -a^2 \tag{3.19}$$

Solution to the equation (3.18) is

$$T(t) = C'e^{-a^2Dt} \tag{3.20}$$

Solution to the equation (3.19) is

$$Z(z) = A\sin az + B\cos az \tag{3.21}$$

where C', A and B are constants of integration.

The final solution according to equation (3.13) is a product of solutions of equations (3.20) and (3.21):

$$C(z,t) = C'e^{-a^2Dt}(A\sin az + B\cos az) + C_1z + C_2 \tag{3.22}$$

The last two terms appear since equation (3.12) is a second order differential equation. These terms vanish after double derivation on z as well as after derivation on t:

$$\frac{d^2C(z,t)}{dz^2} = \frac{d^2\left(C'e^{-a^2Dt}(A\sin az + B\cos az) + C_1z + C_2\right)}{dz^2}$$

$$= \frac{d^2\left(C'e^{-a^2Dt}(A\sin az + B\cos az)\right)}{dz^2} + 0 + 0 \qquad (3.22a)$$

$$\frac{dC(z,t)}{dt} = \frac{d\left(C'e^{-a^2Dt}(A\sin az + B\cos az) + C_1z + C_2\right)}{dt}$$

$$= \frac{d\left(C'e^{-a^2Dt}(A\sin az + B\cos az)\right)}{dt} + 0 + 0 \qquad (3.22b)$$

After applying the first boundary condition, equation (3.10), to the equation (3.22):

$$C(0,t) = k\rho C_0 = BC'e^{-a^2Dt} + C_2 \qquad (3.23)$$

Since the right-hand side of the equation depends on time and the left-hand side is constant, then $B = 0$. The equation can be rewritten as follows:

$$C_2 = k\rho C_0 \qquad (3.24)$$

In this case solution becomes:

$$C(z,t) = k\rho C_0 + AC'e^{-a^2Dt}\sin az + C_1z \qquad (3.25)$$

After applying the second boundary condition (3.11):

$$\left(\frac{\partial C(z,t)}{\partial z}\right)_{z=l} = \left(\frac{\partial\left(k\rho C_0 + AC'e^{-a^2Dt}\sin az + C_1 z\right)}{\partial z}\right)_{z=l} = a\,AC'e^{-a^2Dt}\cos al + C_1$$

$$= 0 \tag{3.26}$$

This expression is true when $\cos al = 0$ and $C_1 = 0$. Therefore, $al = \pi n + \frac{\pi}{2} = (2n+1)\frac{\pi}{2}$ where $n = 0, 1, 2, ...$, hence the solution is

$$C(z,t) = k\rho C_0 + AC'e^{-\frac{(2n+1)^2}{4l^2}\pi^2 Dt}\sin\frac{(2n+1)\pi z}{2l} \tag{3.27}$$

This is a partial solution of equation (3.12) for conditions (3.8), (3.10), (3.11). According to the theory of linear differential equations, the general solution is the sum of all partial solutions:

$$C(z,t) = k\rho C_0 + \sum_{n=0}^{\infty} C_n' e^{-\frac{(2n+1)^2}{4l^2}\pi^2 Dt}\sin\frac{(2n+1)\pi z}{2l} \tag{3.28}$$

After applying initial condition (3.8):

$$C(z,0) = k\rho C_0 + \sum_{n=0}^{\infty} C_n' \sin\frac{(2n+1)\pi z}{2l} = 0 \tag{3.29}$$

Constants C_n' are Fourier development of the function $-k\rho C_0$:

$$C_n' = \frac{2}{l}\int_0^l -k\rho C_0 \sin\frac{(2n+1)\pi z}{2l}\,dz$$

$$= -\frac{2k\rho C_0}{l}\left(-\frac{2l}{(2n+1)\pi}\cos\frac{(2n+1)\pi l}{2l} + \frac{2l}{(2n+1)\pi}\cos 0\right)$$

$$= -\frac{4k\rho C_0}{(2n+1)\pi} \tag{3.30}$$

In this case, substitution of (3.30) to equation (3.28) yields in:

$$C(z,t) = k\rho C_0\left(1 - \frac{4}{\pi}\sum_{n=0}^{\infty}\frac{1}{(2n+1)}e^{-(2n+1)^2\pi^2\frac{Dt}{4l^2}}\sin\frac{(2n+1)\pi z}{2l}\right) \tag{3.31}$$

This equation gives spatial nd time-dependent distribution of radon absorbed in activated charcoal with the assumption that there is no decay of radon and its concentration in air is constant.

After introducing S as a cross section surface [length^2] of charcoal canister, $SC(z,t)dz$ is radon activity in layer *z+dz* at the moment *t*.

The total radon activity $A(t)$ [Bq] in activated charcoal can be obtained by integrating $SC(z,t)dz$ along the canister length:

$$A(t) = S\int_0^l C(z,t)dz \tag{3.32}$$

The result of integration is:

$$A(t) = S\int_0^l k\rho C_0\left(1 - \frac{4}{\pi}\sum_{n=0}^{\infty}\frac{1}{(2n+1)}e^{-(2n+1)^2\pi^2\frac{Dt}{4l^2}}\sin\frac{(2n+1)\pi z}{2l}\right)dz$$

$$= Sk\rho C_0\left(l - 0 + \frac{4}{\pi}\sum_{n=0}^{\infty}\frac{2l}{(2n+1)^2\pi}e^{-(2n+1)^2\pi^2\frac{Dt}{4l^2}}\cos\frac{(2n+1)\pi l}{2l}\right.$$

$$\left. - \frac{4}{\pi}\sum_{n=0}^{\infty}\frac{2l}{(2n+1)^2\pi}e^{-(2n+1)^2\pi^2\frac{Dt}{4l^2}}\cos 0\right)$$

$$= Slk\rho C_0\left(1 - \frac{8}{\pi^2}\sum_{n=0}^{\infty}\frac{e^{-(2n+1)^2\pi^2\frac{Dt}{4l^2}}}{(2n+1)^2}\right) \tag{3.33}$$

This result represents the total radon activity absorbed in a layer of activated charcoal of the depth *l* and surface area *S*, in time *t*.

This approach shows how diffusion theory can be used to determine the activity of radon in activated charcoal during short-time exposure. The next section describes the case of long-time exposure.

3.2.2 Theory Describing Radon Diffusion During Long-time Exposures

According to Nikezić and Urošević [***39***] the long-term exposure of activated charcoal canister to radon lasts for more than half-life of ^{222}Rn (approx. 3.8 days). Radon decay inside the charcoal cannot be ignored in this case and the diffusion equation (3.7) should be solved taking into account radon decay constant. Boundary and initial conditions are the same as for the short-time exposure case.

Equation (3.7) can be reduced to equation (3.12) by introducing the substitution

$$C(z,t) = u(z,t)e^{-\lambda t} \tag{3.34}$$

Solving equation (3.7) using the function $u(z,t)$ is analogous to the previous case and is not be described in detail. The result for the concentration is:

$$C(z,t) = k\rho C_0 \left[\frac{\cosh\sqrt{\frac{\lambda}{D}}(l-z)}{\cosh\sqrt{\frac{\lambda}{D}}l} - \frac{D\pi}{l^2}\sum_{n=0}^{\infty} \frac{(2n+1)e^{-\left(\frac{(2n+1)^2\pi^2 D}{4l^2}+\lambda\right)t}}{\left(\frac{(2n+1)^2\pi^2 D}{4l^2}+\lambda\right)} \sin\frac{(2n+1)\pi z}{2l} \right] \tag{3.35}$$

which gives a spatial and temporal distribution of radon concentration in activated charcoal canister for the exposure time much longer than half-life of ^{222}Rn.

The total activity can be obtained as for the short-time case by integrating the previous equation along the canister length and multiplying by the result by its surface area. Integration gives:

$$A(t) = Sk\rho C_0 \left[\sqrt{\frac{D}{\lambda}} \frac{\sinh\sqrt{\frac{\lambda}{D}}l}{\cosh\sqrt{\frac{\lambda}{D}}l} - \frac{2D}{l}\sum_{n=0}^{\infty} \frac{e^{-\left(\frac{(2n+1)^2\pi^2 D}{4l^2}+\lambda\right)t}}{\left(\frac{(2n+1)^2\pi^2 D}{4l^2}+\lambda\right)} \right] \tag{3.36}$$

In the case of very long exposure $t \to \infty$ and the second term on the right-hand side of the equation vanishes:

$$A_\infty = Sk\rho C_0 \sqrt{\frac{D}{\lambda}} \frac{\sinh\sqrt{\frac{\lambda}{D}}l}{\cosh\sqrt{\frac{\lambda}{D}}l} \tag{3.37}$$

This equation gives the maximum possible activity of radon absorbed in the activated charcoal canister with depth l and surface area S.

3.3 Analytical Estimates of Radon Diffusion in Various Media

3.3.1 Analytical Estimates of Radon Diffusion in Charcoal

Parameters of activated charcoal canister described in the EPA Standard and Protocol [***40***] are used for analytical estimates of radon diffusion in activated charcoal:

$l = 1.7278$ cm – canister depth;
$S = 81$ cm^2 – surface of the cross section of the canister;
$\rho = 0.5$ g/cm^3 – charcoal density.

Other parameters and conditions for the estimates are:

$k = 4$ m^3/kg – activated charcoal adsorption coefficient;
$D = 1.43\ 10^{-9}$ m^2/s – radon diffusion coefficient in activated charcoal;
$C_0 = 200$ Bq/m^3 – constant radon concentration in air.

Calculations are made using equations (3.33) and (3.36) for the case when radon decay is disregarded and considered, respectively. Total radon activities for some exposure intervals are listed in Table 3-1.

The obtained values of total radon activity in activated charcoal canister are plotted against exposure intervals in Figure 3-3. The solid line corresponds to radon activity in case when decay in disregarded; the dashed line shows the activity for the case when radon decay is not omitted. Figure 3-3 shows that radon activity saturation in charcoal canister occurs after exposure of about 150 hours. The maximum possible radon activity, absorbed in the canister, can be obtained by substituting $t \to \infty$ in equations (3.33) and (3.36).

This yields 55.98 Bq or 28% of initial activity in 1 m^3 of air for the case when radon decay is disregarded and 48.99 Bq or 24% of initial activity in 1 m^3 of air for the

case when decay is considered.

3.3.2 Analytical Estimates of Radon Diffusion in Air

Equations (3.33) and (3.36) are used for calculation of radon concentration in the air. It was reported by the National Council on Radiation Protection and Measurements [***36***] that diffusion coefficient of radon in air is $D_a = 1 \times 10^{-5}$ m^2/s. The geometry adopted for the analytical estimates is a 1 m^3 cylinder of 1 m length with radius of $\frac{1}{\sqrt{\pi}}$ m. Radon concentration in ambient air is assumed to be constant and equals C_0 = 200 Bq/m^3.

Since adsorption coefficients for air, water and soil are unknown constants in equation (3.33), the k and ρ terms, responsible for material adsorption characteristic, are omitted ($k = \rho = 1$). Radon adsorption coefficient can be estimated experimentally for any material, including air, however, this could be complicated.

Table 3-2 shows total radon activities in 1 m length cylinder of volume 1 m^3 obtained with equation (3.33) for some exposure time intervals. Calculations were extended to 72 hours to check when radon activity in air cylinder reaches saturation. Figure 3-4 illustrates these data.

Analyzing this figure leads to a finding that the saturation in water canister is reached after exposure of about 3 days. Substituting infinite time in equations (3.33) and (3.36) gives 200 Bq or 100% of initial activity in 1 m^3 of air for the case when radon decay is disregarded and 187.0 Bq or 93% of initial activity in 1 m^3 of air for the case when decay is considered. This example demonstrates that the approach of omitting adsorption coefficient and density (to make them equal 1 in equations (3.33) and (3.36)) gives the correct results, since the maximum possible total activity in a cylinder of 1 m^3

equals 200 Bq, in other words, radon concentration equals to initial constant concentration $C_0 = 200$ Bq/m^3.

3.3.3 Analytical Estimates of Radon Diffusion in Water

The same method of calculation as described in previous section is used for analytical estimates for radon diffusion in water. The geometry adopted is the same as for charcoal canister:

$l = 1.7278$ cm – cylinder depth;
$S = 81$ cm^2 – cross sectional surface of the cylinder.

Radon concentration in ambient air is assumed to be constant and equals $C_0 = 200$ Bq/m^3. Radon diffusion coefficient in water reported by the Committee on Risk Assessment of Exposure to Radon in Drinking Water [*41*] to have a value of $D_w = 1 \times 10^{-9}$ m^2/s.

Calculations using equations (3.33) and (3.36) give the total radon activities in water cylinder for some exposure intervals. They are listed in Table 3-3.

Calculations were extended to 300 hours to check when radon activity in water cylinder reaches saturation. Figure 3-5 illustrates these data.

The figure shows that radon activity saturation for the water geometry is reached after about 200 hours. Substituting infinite time in equations (3.33) and (3.36) gives 2.80×10^{-2} Bq or 0.014% of initial activity in 1 m^3 of air for the case when radon decay is disregarded and 2.33×10^{-2} Bq or 0.012% of initial activity in 1 m^3 of air for the case when decay is considered.

3.3.4 Analytical Estimates of Radon Diffusion in Soil

The same method of calculation as described in previous section is used for analytical estimates of radon diffusion in soil. The geometry adopted is the same as for charcoal canister:

l = 1.7278 cm – cylinder depth;
S = 81 cm^2 – cross sectional surface of the cylinder.

Radon concentration in ambient air is assumed to be constant and equals C_0 = 200 Bq/m^3. Diffusion coefficient for soil is determined by C. Papachristodoulou et al. [*42*] and equals $D_s = 4.1 \times 10^{-7}$ m^2/s.

Calculations using equations (3.33) and (3.36) give the next total radon activities in soil cylinder for some exposure intervals.

It can be understood from the table that saturation of total radon activity in soil cylinder is reached after about 40 minutes. Figure 3-6 illustrates these data.

The figure illustrates the statement made, when analyzing Table 3-4, that radon activity saturation for the soil geometry is reached after about 40 minutes exposure. Substituting infinite time in equations (3.33) and (3.36) gives 2.80×10^{-2} Bq or 0.014% of initial activity in 1 m^3 of air for the case when radon decay is disregarded and also 2.80×10^{-2} Bq or 0.014% of initial activity in 1 m^3 of air for the case when decay is considered. The same activity is explained by very quick saturation. Insignificant number of radon atoms that are absorbed in soil are decayed during that time.

In order to show how diffusion and adsorption coefficients influence saturation time and activity values, total absorbed activities against time are plotted for each medium for the same geometry, canister, described in the EPA Standard and Protocol. Figure 3-7 illustrates these dependencies. Radon decay is neglected due to its short decay

time. The plots show that for higher diffusion coefficient values saturation is reached faster. For example, the value of radon diffusion coefficient in air is $D_a = 10^{-5}$ m^2/s and saturation is reached in approximately 1 minute. For soil with $D_s = 4.1\times10^{-7}$ m^2/s saturation is reached after about half an hour. It takes much longer to reach saturation of radon activity in water and activated charcoal, since these media have diffusion coefficient values of order of 10^{-9} m^2/s.

3.4 Numerical Simulations of Radon Diffusion in Various Media

3.4.1 COMSOL Multiphysics

COMSOL Multiphysics numerical code was used for radon diffusion simulations in various media. The code uses finite element method (FEM) to solve partial differential equations of diffusion. One of the most important features of FEM is that it is based on unstructured grids. This means that it is more flexible with respect to geometry compared to codes that use finite difference method, where submeshing is strictly structured.

Simulation accuracy can be controlled through the size of the elements. COMSOL Multiphysics suggests two types of submeshing: physics-controlled mesh and user-controlled mesh. The first type includes nine built-in options that range from extremely coarse to extremely fine. User-controlled mesh allows selecting maximum and minimum element sizes in length units, maximum element growth rate, resolution of curvature and resolution of narrow regions. Figure 3-8 illustrates the list of available physics-controlled mesh element sizes.

After the element size is applied, the submeshed geometry can be displayed. Figure 3-9 shows the “normal” element size for activated charcoal canister cylindrical geometry.

Accuracy can be increased by creating more elements and decreasing their size. Figure 3-10 reflects "extremely fine" element size.

Equation (3.12) is used in COMSOL Multiphysics for simulations of time dependent diffusion. Initial concentration and boundary conditions are specified by user.

3.4.2 Numerical Simulations of Radon Diffusion in Air

It is described in section 3.3.2 that diffusion coefficient of radon in air is $D_a = 10^{-5}$ m^2/s. The geometry adopted for the numerical simulation of radon diffusion in air is the same as used for analytical estimates: 1 m^3 cylinder of 1 m length with radius of $\frac{1}{\sqrt{\pi}}$ m. Initial and boundary conditions used for the simulation are described in section 3.2.1.

Simulations were made for 5 time intervals: from 1 hour to 5 hours with a step of 1 hour. Radon concentration in ambient air is assumed to be constant and has the same value as for analytical estimates, C_0 = 200 Bq/m^3. Figure 3-11 shows relative radon concentration in the air cylinder after 5 hours exposure time.

More detailed descriptions of radon concentration at different depths of air cylinder for all time intervals can be obtained from Figure 3-12.

Integration method was used to calculate total radon concentration in air cylinder to obtain activities that can be compared to values obtained with equation (3.33). The values of total radon activity obtained from the simulation are listed in Table 3-5.

Comparison of these data with the results obtained from analytical estimates is shown in Figure 3-13. The figure illustrates that values for total radon activity in air cylinder, obtained in simulation, match quite well with analytical estimates.

3.4.3 Numerical Simulations of Radon Diffusion in Water

Radon diffusion coefficient in water is defined in section 3.3.3 and has a value of $D_w = 10^{-9}$ m^2/s. The geometry adopted for the numerical simulation of radon diffusion in air is the same as used for analytical estimates:

l = 1.7278 cm – cylinder depth;
S = 81 cm^2 – cross sectional surface of the cylinder.

Initial and boundary conditions used for the simulation are described in section 3.2.1. Simulations were made for 6 time intervals: from 12 hours to 72 hours with step of 12 hours. Radon concentration in ambient air is assumed to be constant and has the same value as for analytical estimates, C_0 = 200 Bq/m^3. Figure 3-14 shows relative radon concentration in water cylinder after 72 hours exposure time.

Similar to the case with air cylinder, an integration method was used to calculate total radon concentration in water cylinder to obtain activities that can be compared to values obtained with equation (3.33). The values of integrated radon activities absorbed in water cylinder for exposure time intervals are listed in Table 3-6. Figure 3-15 illustrates how relative radon activity changes with depth of the water for different exposure time intervals. It can be noticed that the line for 12 hours exposure interval is not smooth. This is explained by the small geometry size and low value of water diffusion coefficient. In comparison, Figure 3-12, that reflects relative radon concentration vs. depth in 1 m^3 air cylinder, shows a very smooth line for 1 hour exposure interval.

Comparison of simulation data with the results obtained from analytical estimates for water cylinder is shown in Figure 3-16. Simulation results match theoretical

predictions quite well. A little difference for lower exposure times is explained by small geometry size.

3.4.4 Numerical Simulations of Radon Diffusion in Soil

Radon diffusion coefficient in soil is defined in section 3.3.4 and equals $D_S = 4.1 \times 10^{-7}$ m^2/s. The geometry adopted is the same as for analytical estimates of radon diffusion in soil:

l = 1.7278 cm – cylinder depth;
S = 81 cm^2 – cross sectional surface of the cylinder.

Initial and boundary conditions used for the simulation are described in section 3.2.1. Simulations were made for 6 time intervals: from 10 minutes to 60 minutes with a step of 10 minutes. Radon concentration in ambient air is assumed to be constant and has the same value as for analytical estimates, C_0 = 200 Bq/m^3. Figure 3-17 shows relative radon concentration in soil cylinder after 50 minutes exposure time.

Similar to the case with air and water cylinders, an integration method was used to calculate total radon concentration in soil geometry to obtain activities that can be compared to values obtained with equation (3.33). The values of integrated radon activities absorbed in soil cylinder for exposure time intervals are listed in Table 3-7. Figure 3-18 illustrates how relative radon activity changes with depth of the soil for different exposures. The figure shows that after about 40 minutes the radon concentration is equal to concentration in ambient air. This reflects very well Figure 3-6 that shows the same observations for analytical estimates. Comparison of simulation data with the results obtained from analytical estimates for soil cylinder is shown in Figure 3-19.

Simulation results match theoretical predictions quite well. A little difference for

lower exposure times is explained by small geometry size.

3.4.5 Numerical Simulations of Radon Diffusion in Charcoal

The same parameters as for section 3.3.1 are used for radon diffusion simulation in activated charcoal. Since COMSOL Multiphysics does not include adsorption coefficient, the obtained results were multiplied by density of charcoal and adsorption coefficient values given in section 3.3.1. Initial and boundary conditions used for the simulation are described in section 3.2.1. Results of the simulation with these corrections are listed in Table 3-8. Comparison of the analytical estimates obtained with the equation (3.33), and listed in Table 3-1, is reflected in Figure 3-20.

Simulation results match theoretical predictions quite well. A little difference for lower exposure times is explained by small geometry size. Figure 3-21 and Figure 3-22 show how relative radon concentration changes with canister depth.

A detailed description of radon concentration at different depths of activated charcoal canister for all time intervals can be obtained from Figure 3-23.

Summarizing the simulation results and comparing the values of total absorbed activities obtained with analytical estimates, show that COMSOL Multiphysics has a great potential for diffusion simulation. It can be extended to more complex geometries and cases for simulations of radon emanation from the bedrock and in the fault regions.

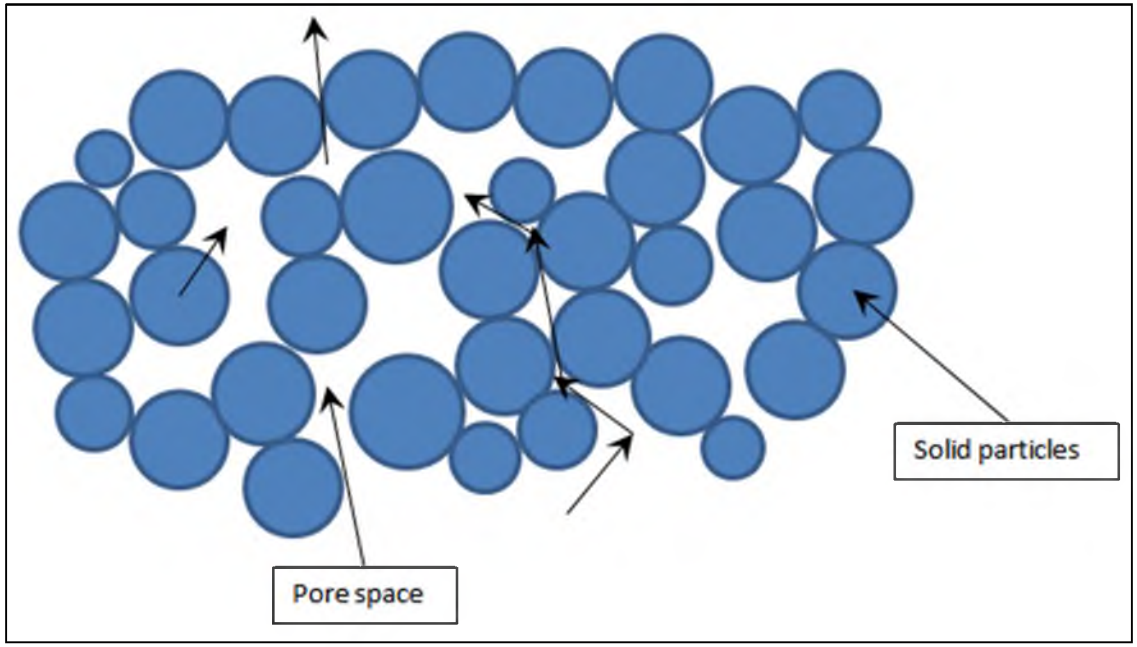

Figure 3-1. Gas diffusion in porous material

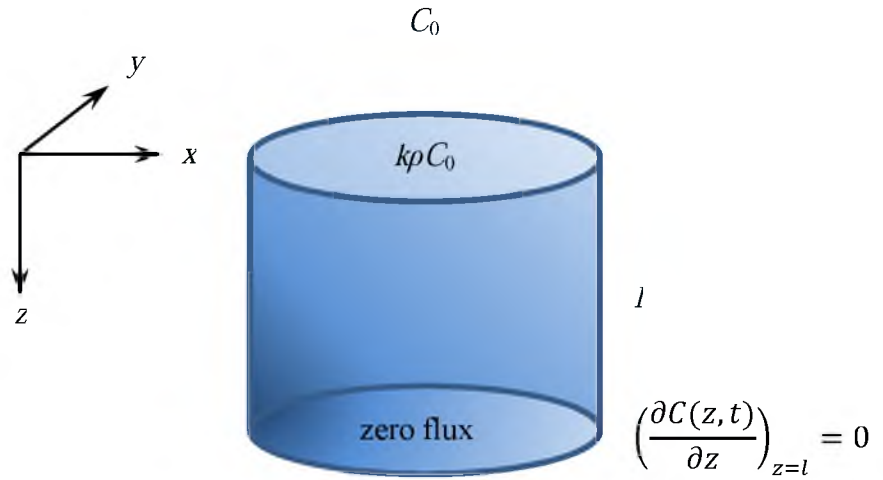

Figure 3-2. Adopted geometry with initial and boundary conditions for the diffusion equation

Table 3-1. Radon activities in activated charcoal canister during different exposure times, calculated considering and disregarding radioactive decay of radon

Time, hours	Radon activity, Bq (no decay, equation 3.33)	Radon activity, Bq (decay, equation 3.36)
12	28.70	27.85
24	39.64	37.43
36	46.17	42.66
48	50.09	45.52
60	52.45	47.18
72	53.86	47.95

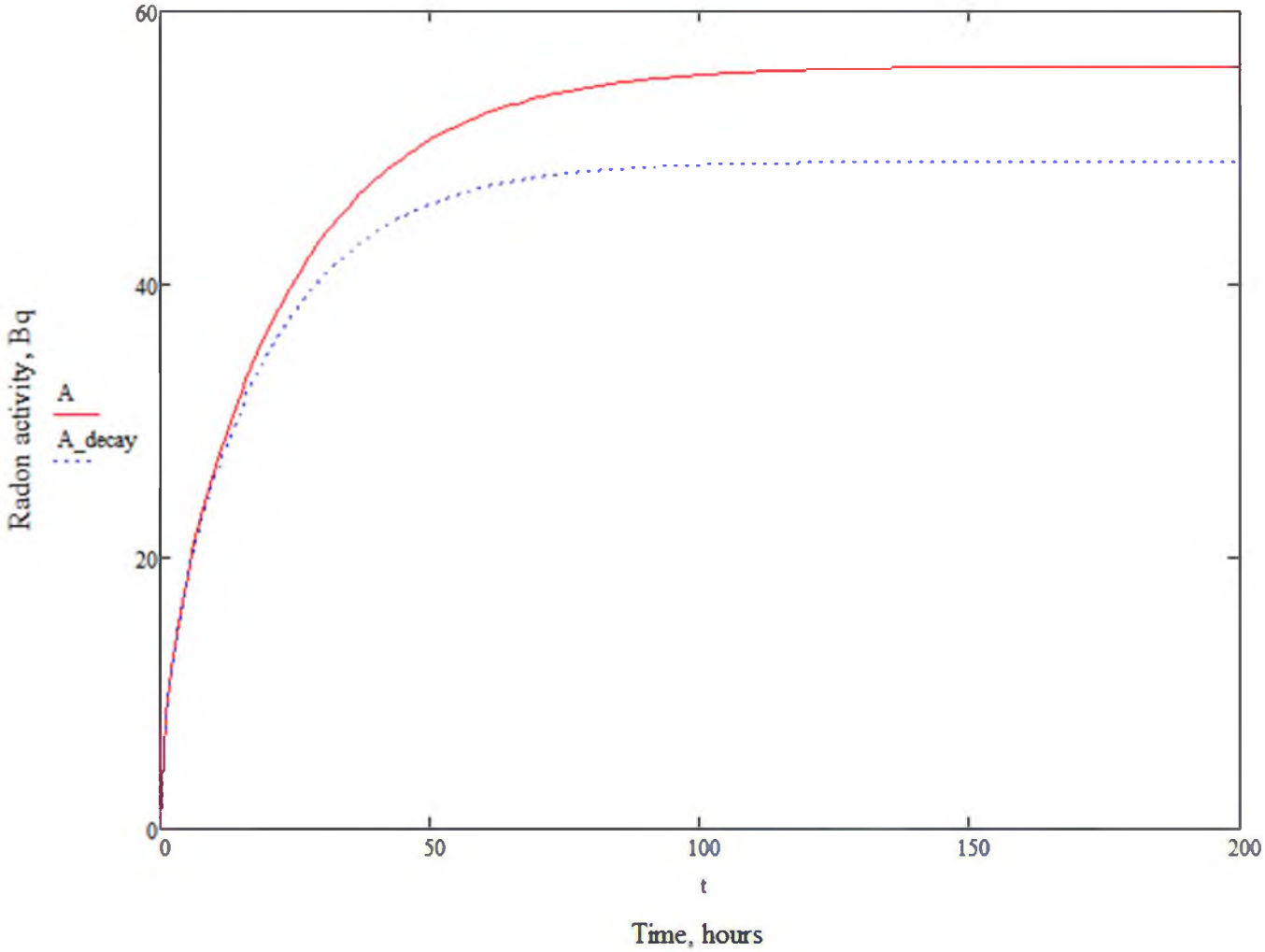

Figure 3-3. Total radon activity in activated charcoal canister vs. exposure time

Table 3-2. Total radon activities in air cylinder for different exposure time intervals

Time, hours	1	2	3	4	5
A, Bq	42.82	60.55	74.16	85.63	95.69

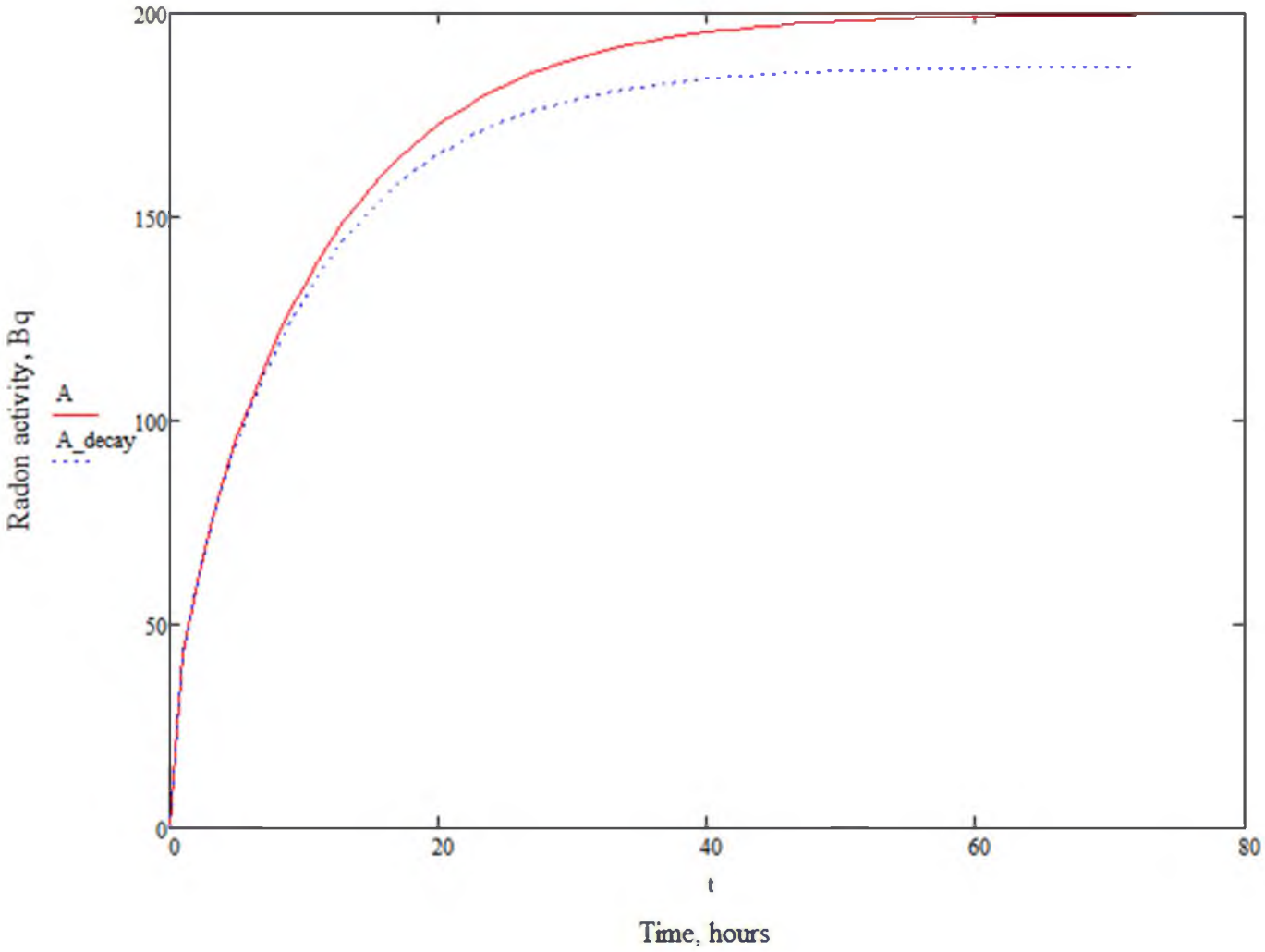

Figure 3-4. Total radon activity in air cylinder vs. exposure time

Table 3-3. Total radon activities in water cylinder for different exposure time intervals

Time, hours	12	24	36	48	60	72
A, 10^{-2} Bq	1.20	1.69	2.02	2.25	2.42	2.53

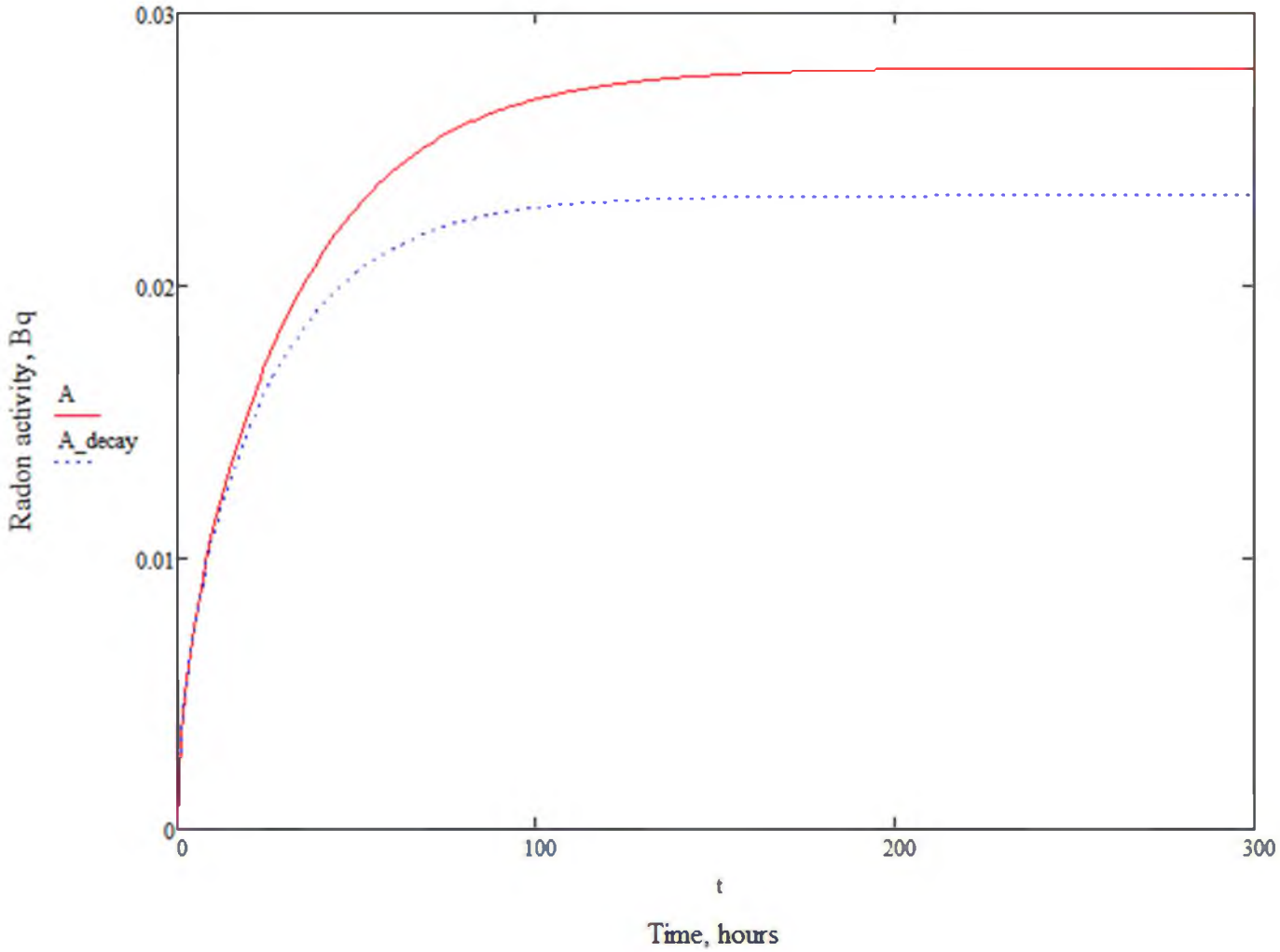

Figure 3-5. Total radon activity in water cylinder vs. exposure time

Table 3-4. Total radon activities in soil cylinder for different exposure time intervals

Time, minutes	10	20	30	40	50	60
A, 10^{-2} Bq	2.50	2.76	2.79	2.80	2.80	2.80

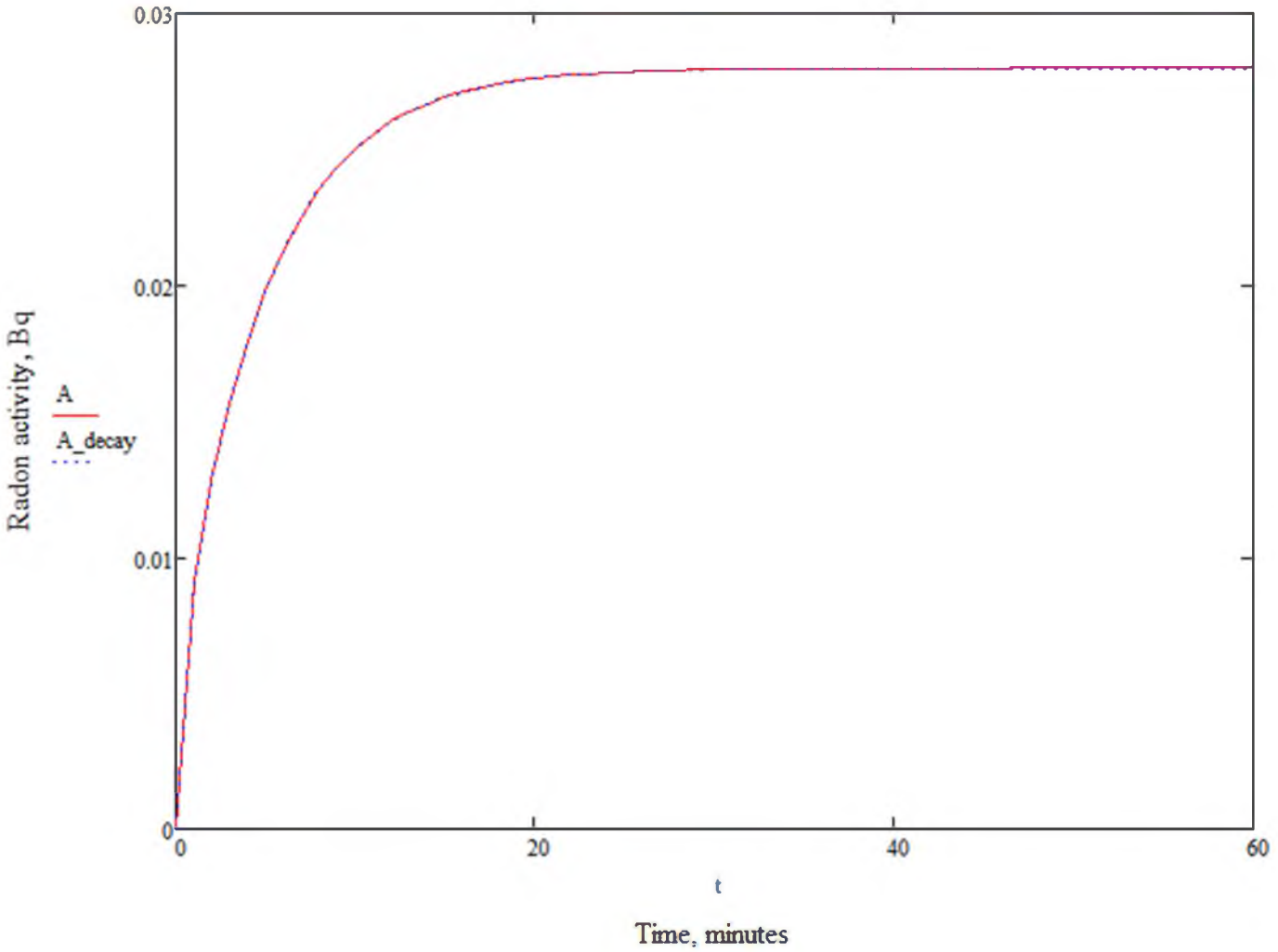

Figure 3-6. Total radon activity in soil cylinder vs. exposure time

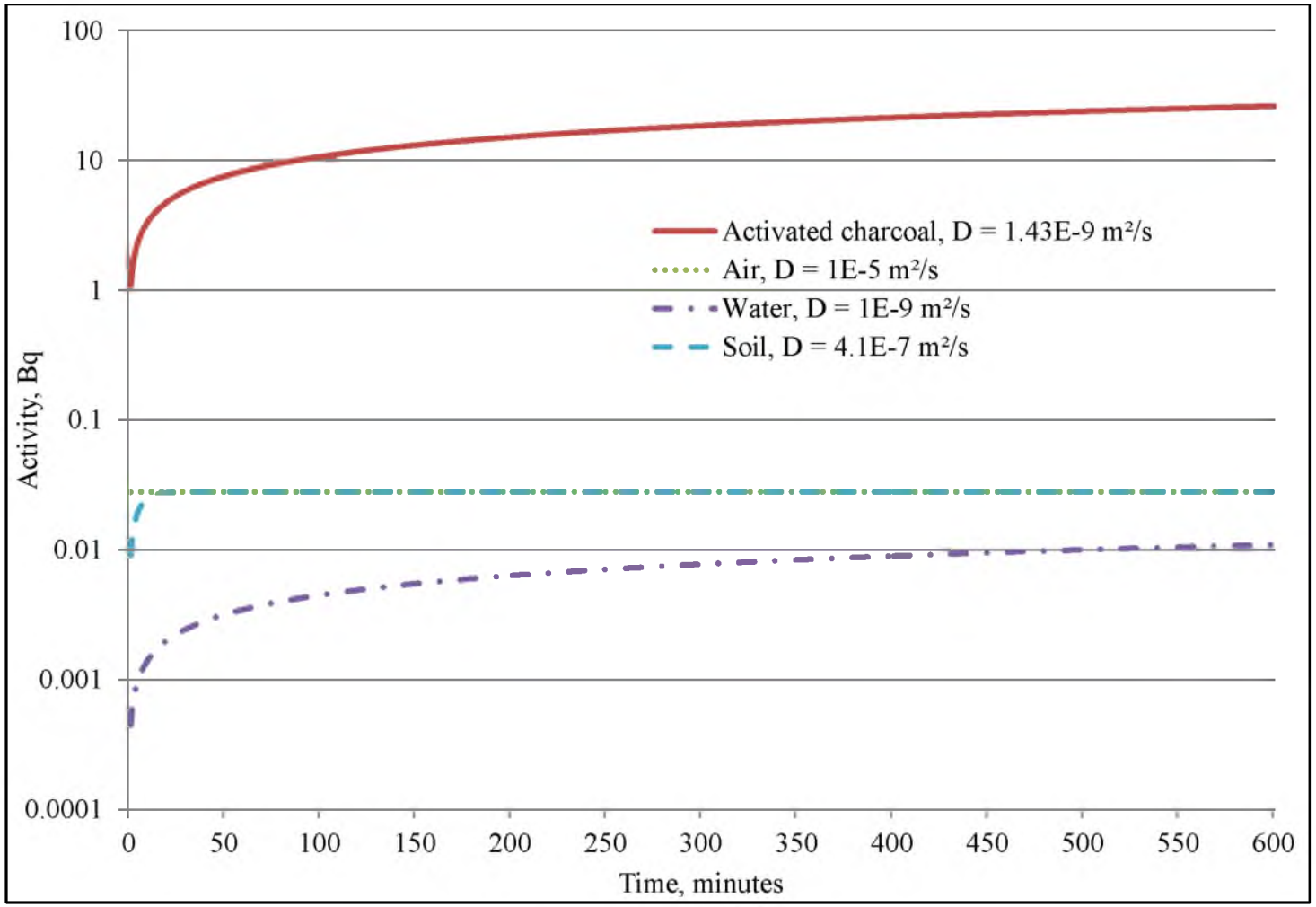

Figure 3-7. Total radon activities vs. time, absorbed in various media of the same EPA canister geometry

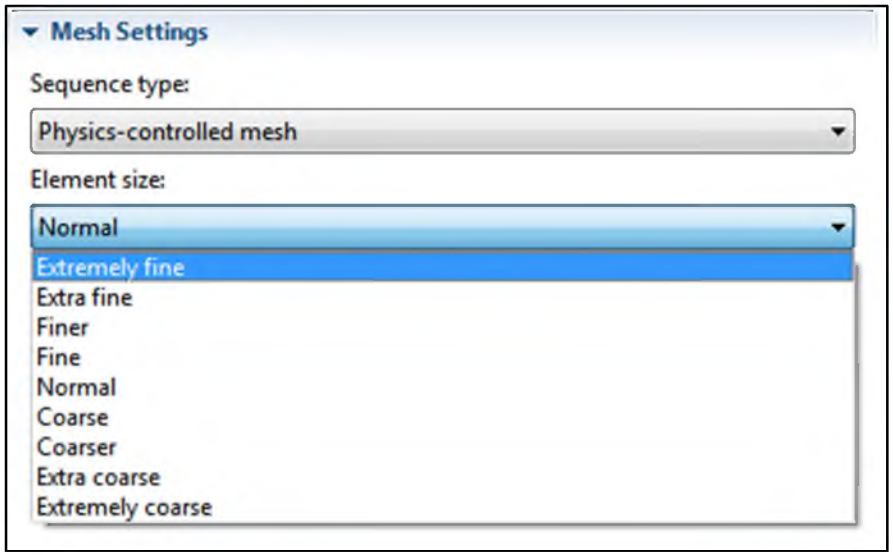

Figure 3-8. Submeshing options in COMSOL

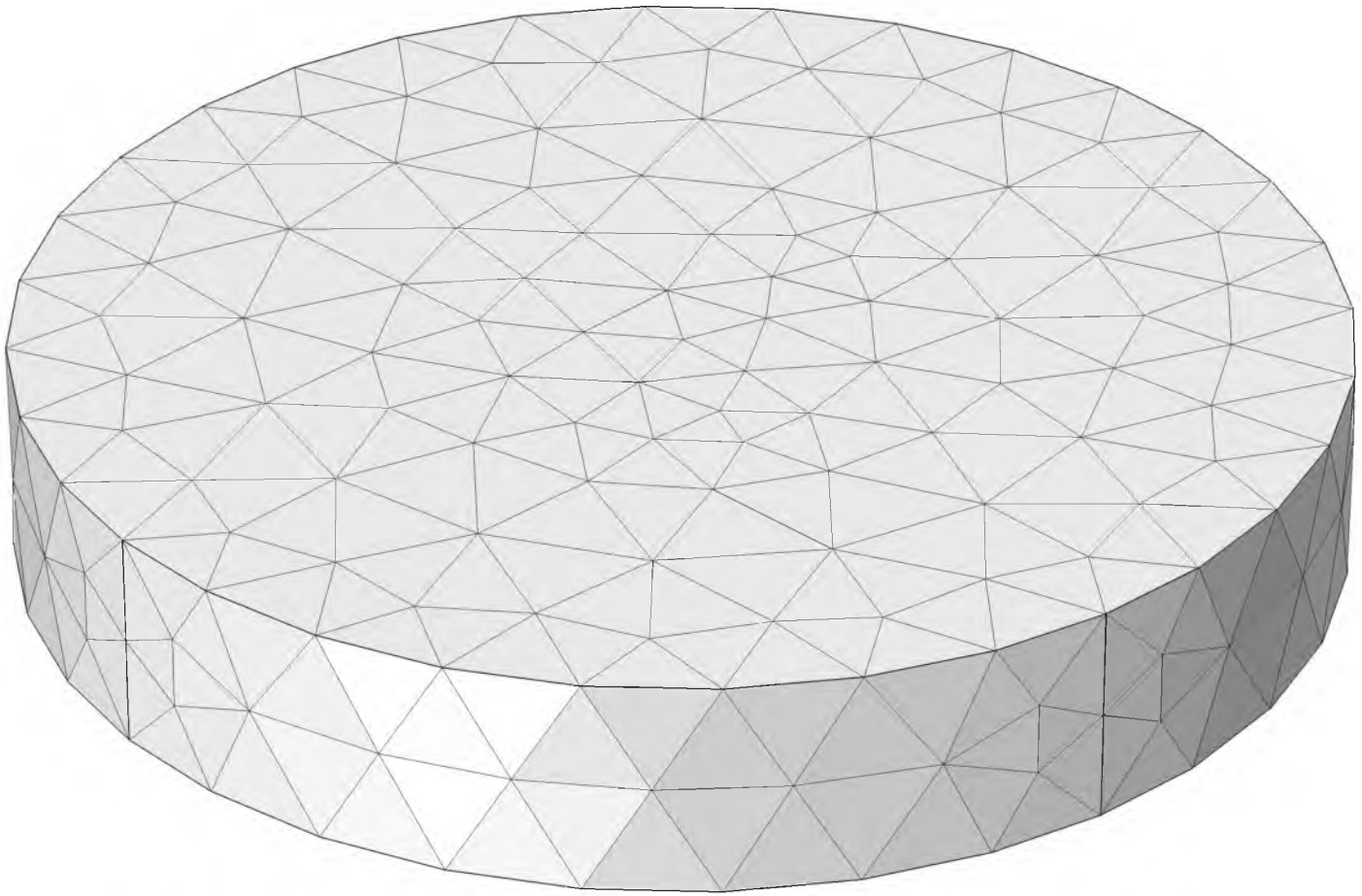

Figure 3-9. "Normal" element size of physics-controlled mesh in COMSOL Multiphysics

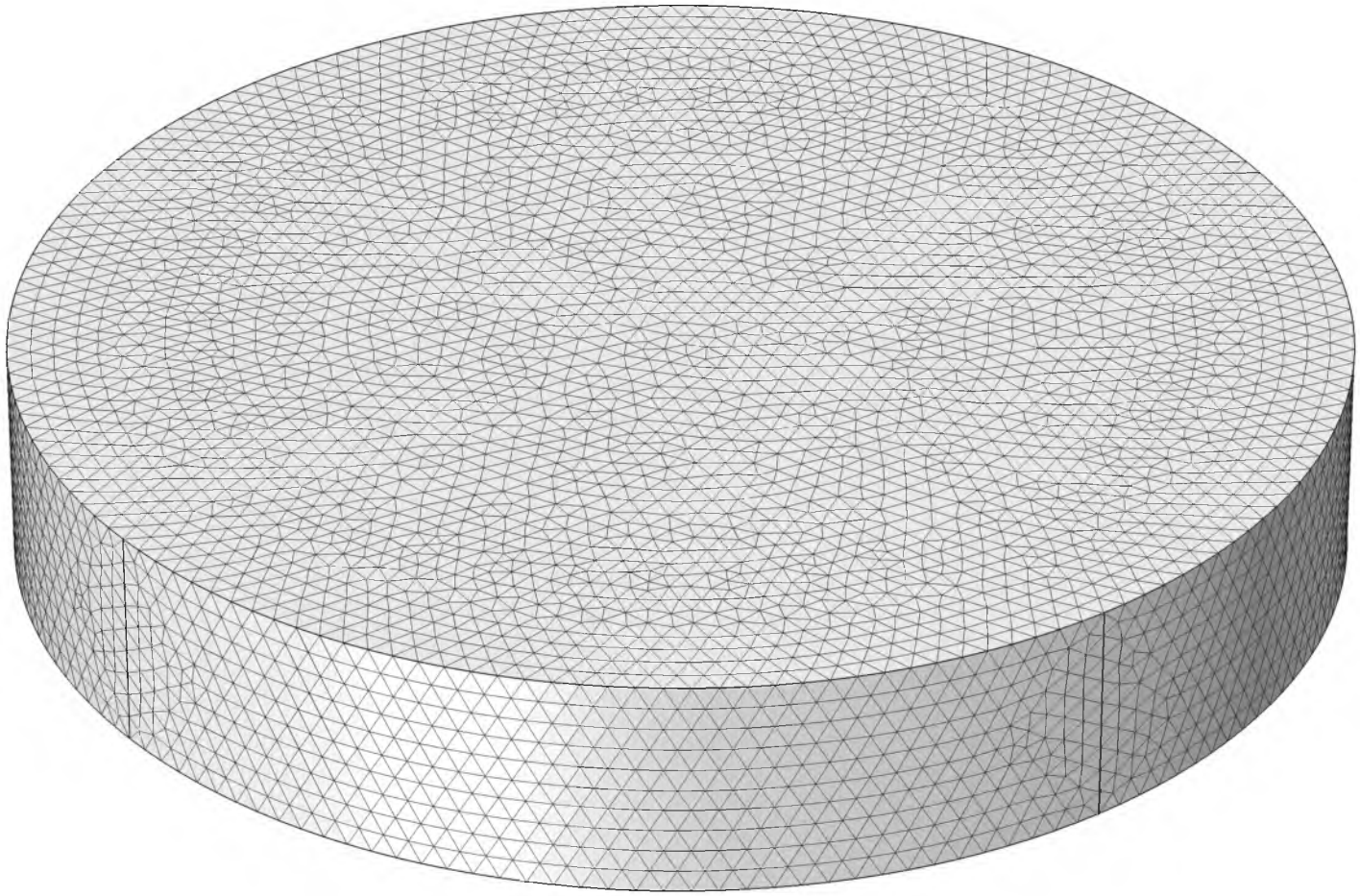

Figure 3-10. "Extremely fine" element size of physics-controlled mesh in COMSOL Multiphysics

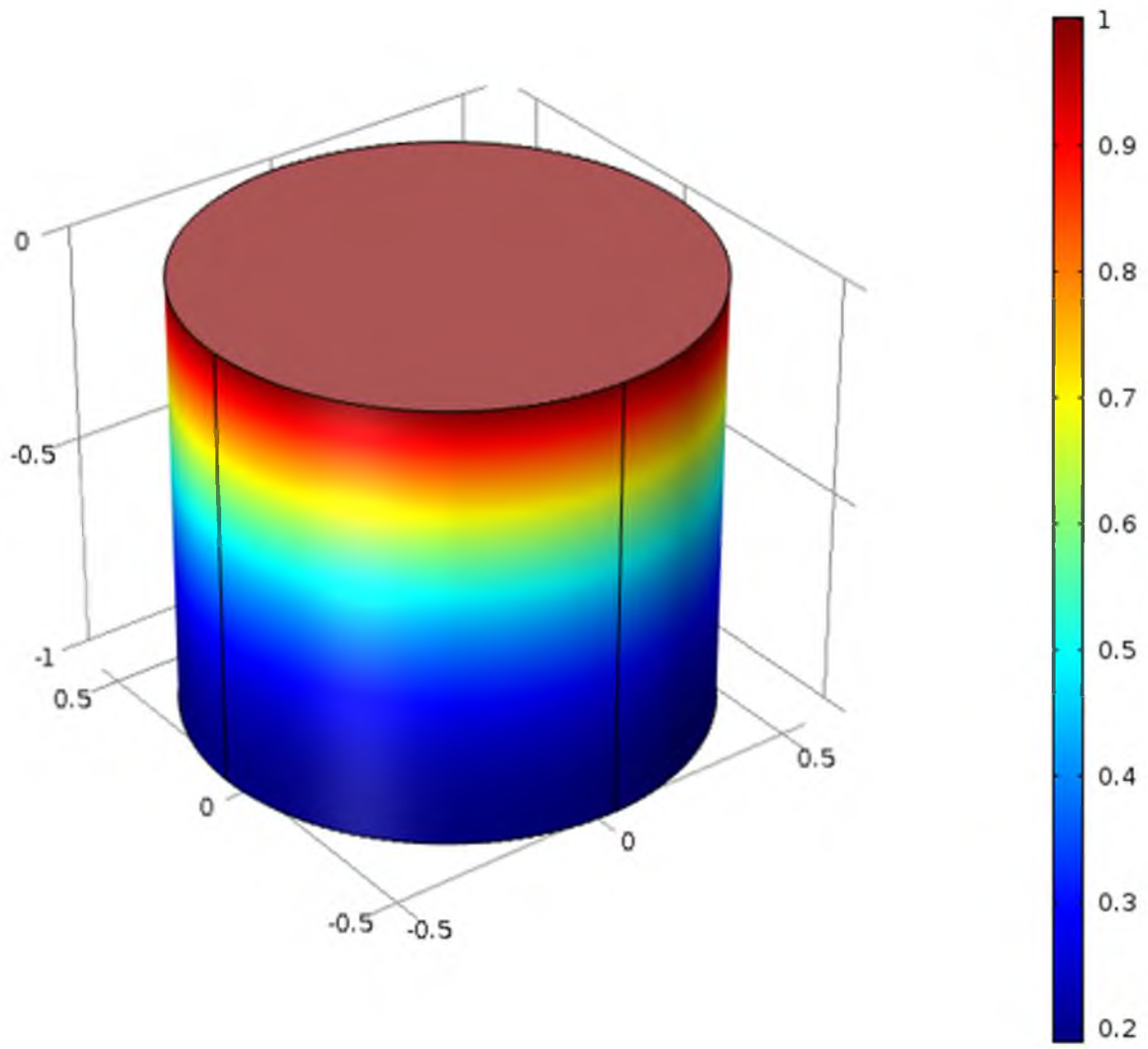

Figure 3-11. Relative radon concentration in air after 5 hours exposure

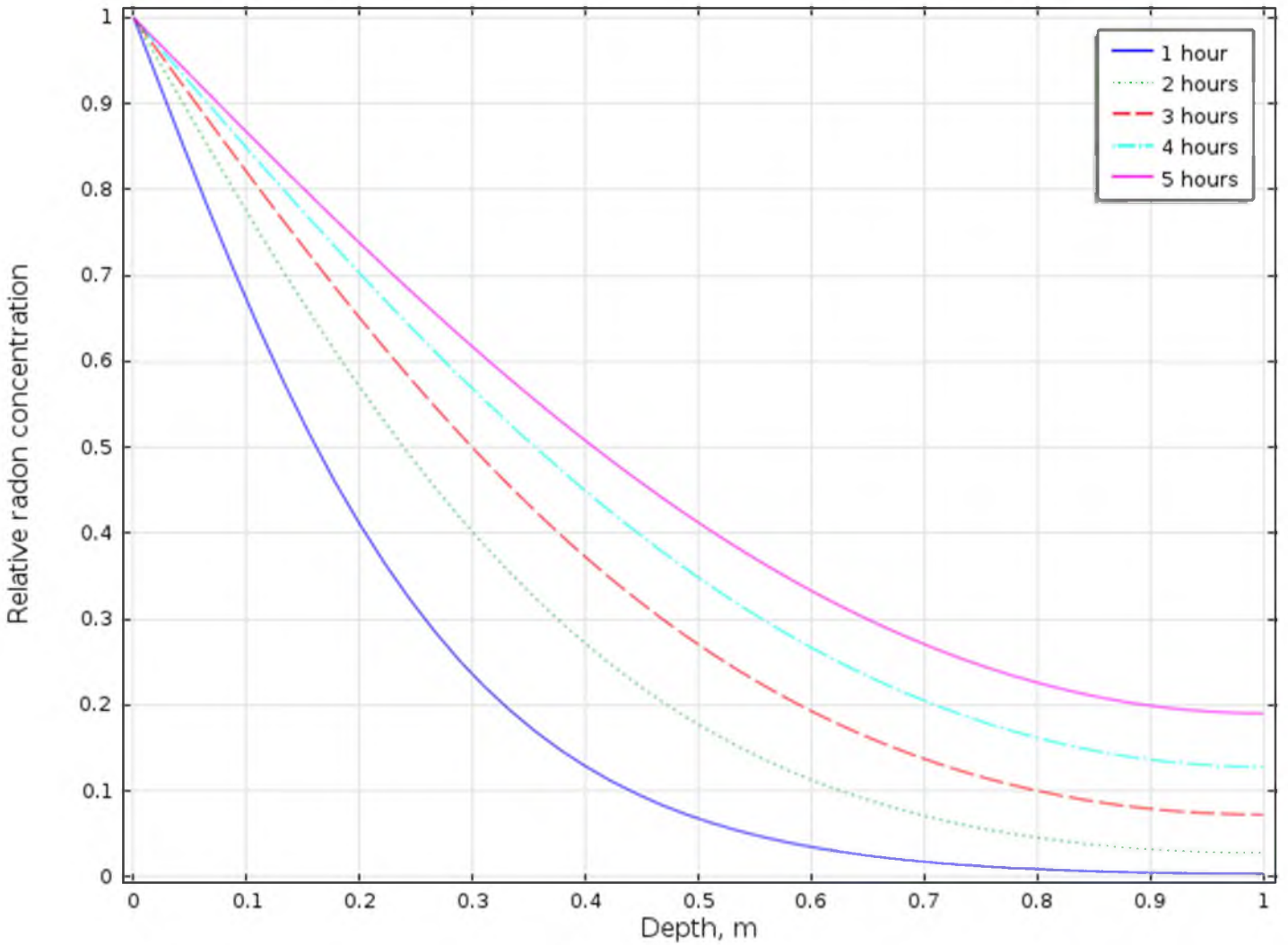

Figure 3-12. Relative radon concentration in air vs. cylinder depth

Table 3-5. Total radon activities in air cylinder for different time exposures

Time, hours	1	2	3	4	5
Total radon activity, Bq	41.07	59.00	72.79	84.65	94.97

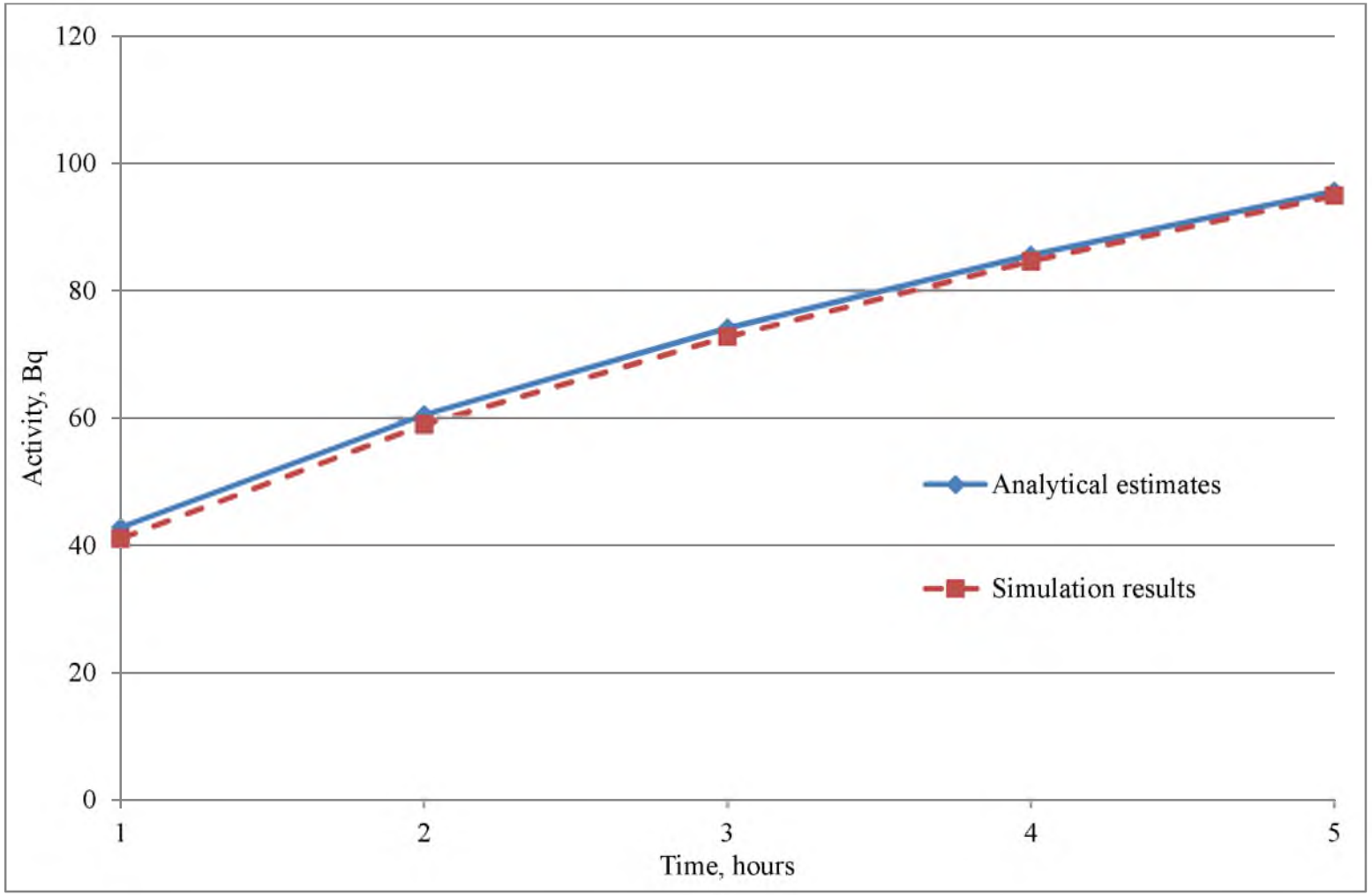

Figure 3-13. Analytical estimates and simulation results for total radon activity in air cylinder

Table 3-6. Simulation results of radon activities in water during different exposure times

Time, hours	12	24	36	48	60	72
A, 10^{-2} Bq	1.14	1.63	1.95	2.20	2.38	2.51

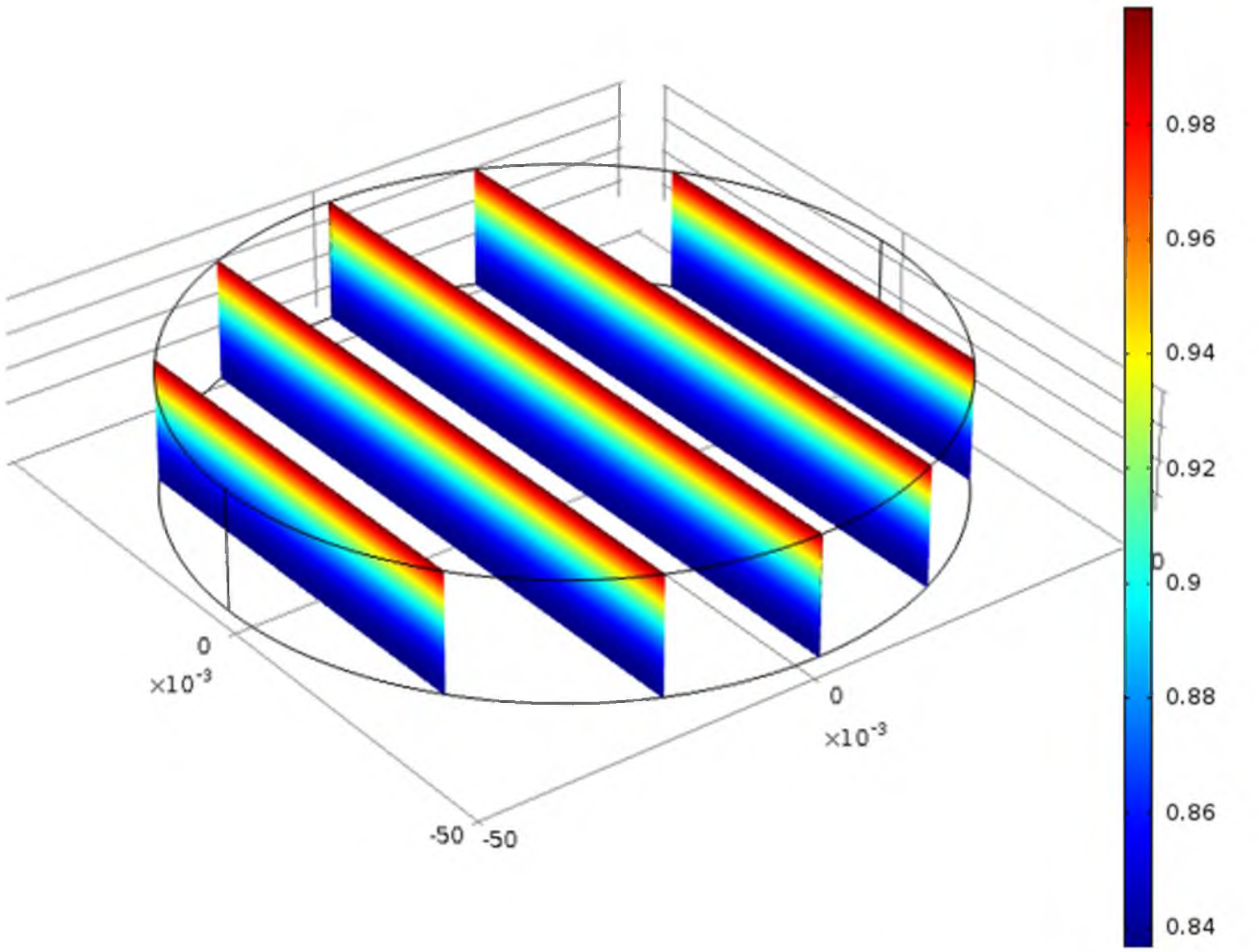

Figure 3-14. Relative radon concentration in water vs. cylinder depth after 72 hours exposure

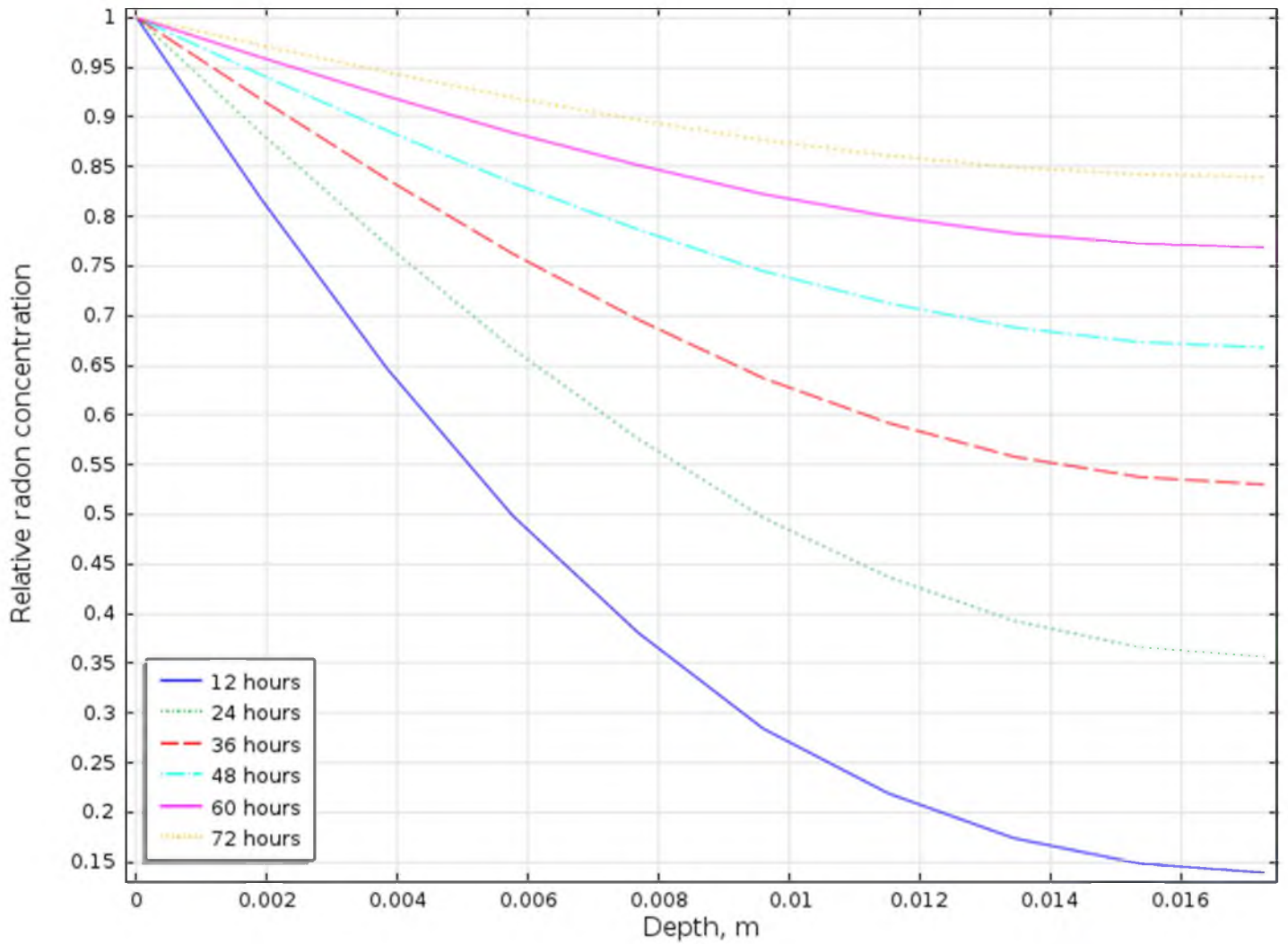

Figure 3-15. Relative radon concentration in water vs. cylinder depth

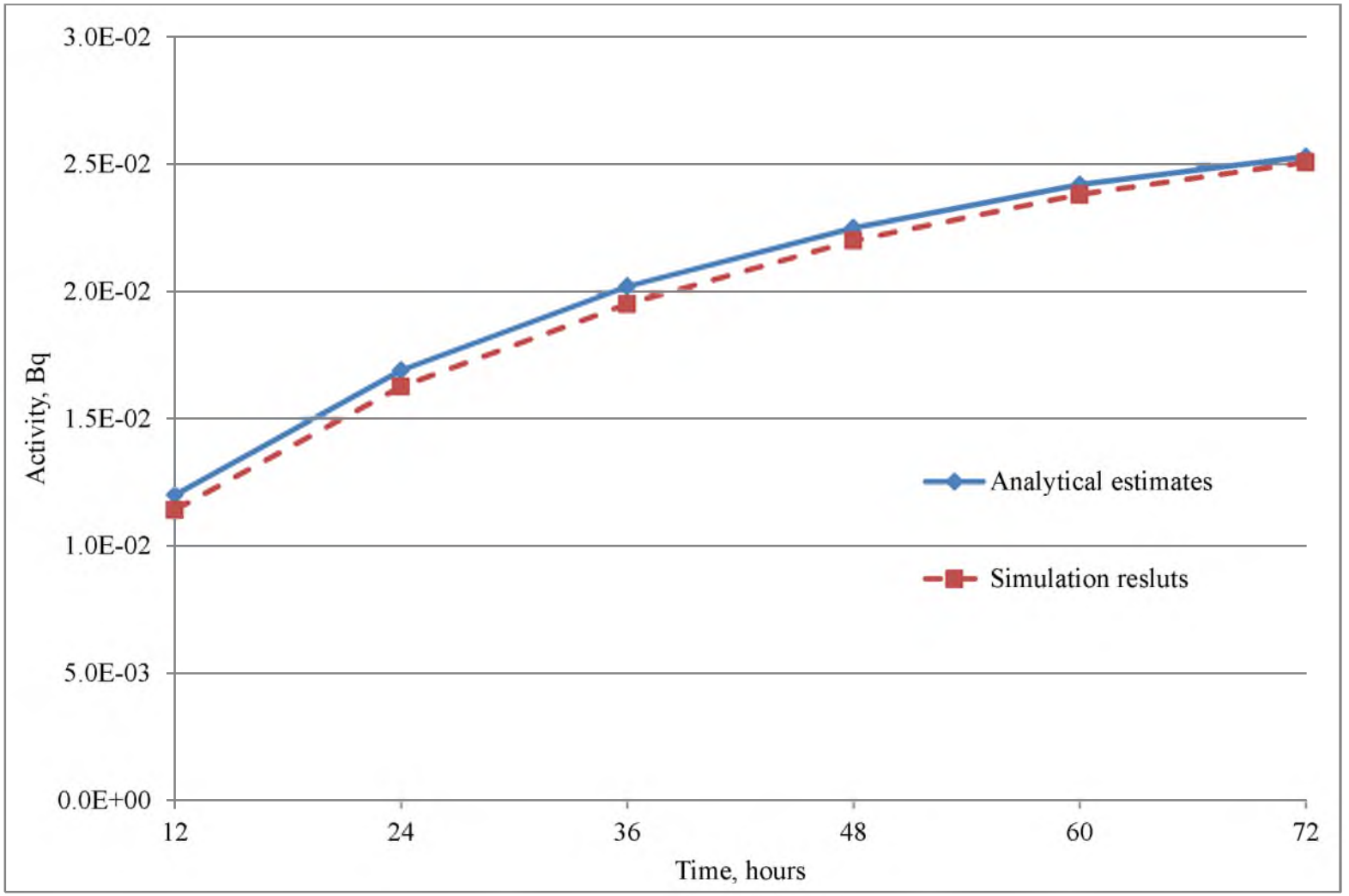

Figure 3-16. Analytical estimates and simulation results for total radon activity in water cylinder

Table 3-7. Simulation results of radon activities in soil during different exposure times

Time, minutes	10	20	30	40	50	60
A, 10^{-2} Bq	2.30	2.67	2.76	2.79	2.80	2.80

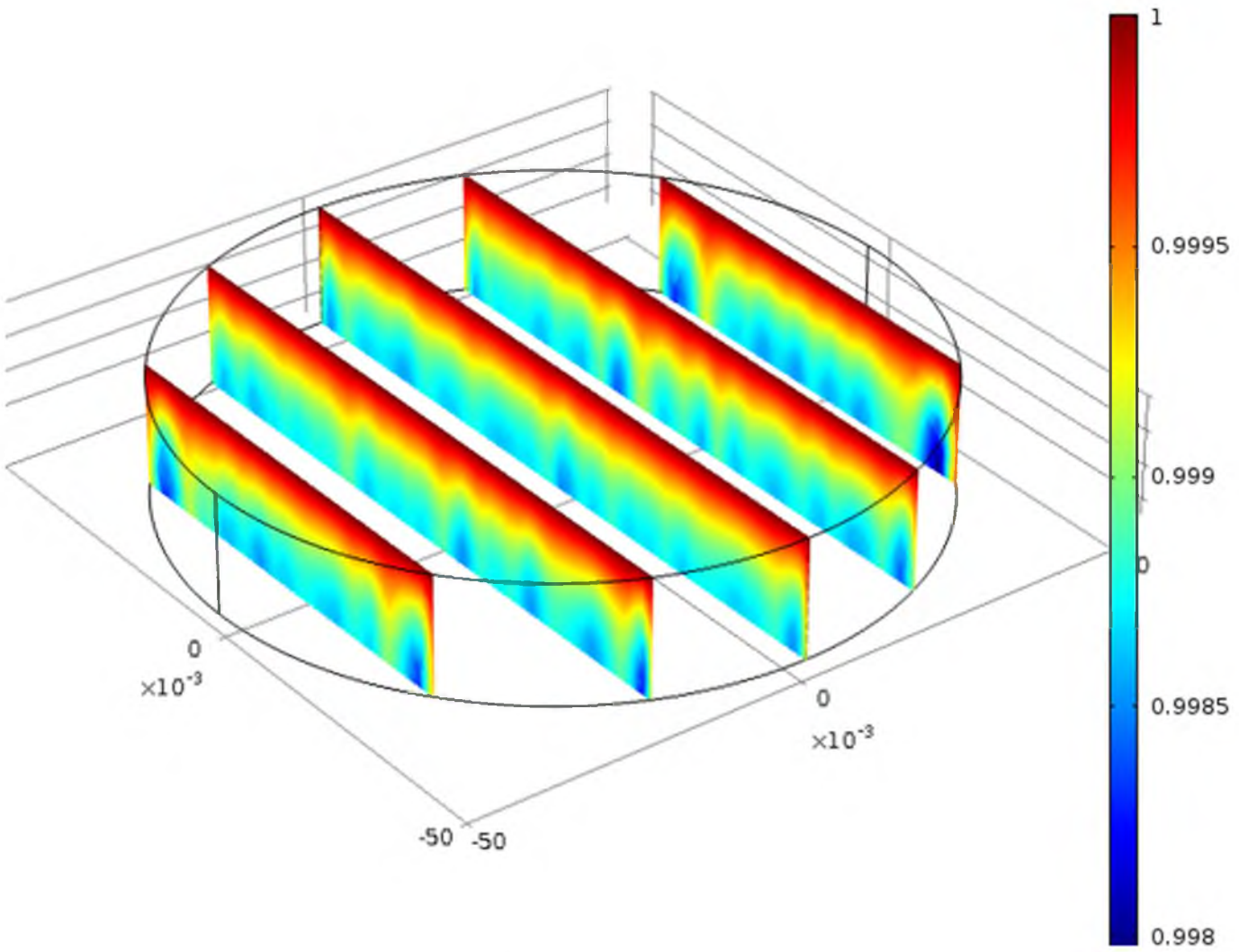

Figure 3-17. Relative radon concentration in soil vs. cylinder depth after 50 minutes exposure

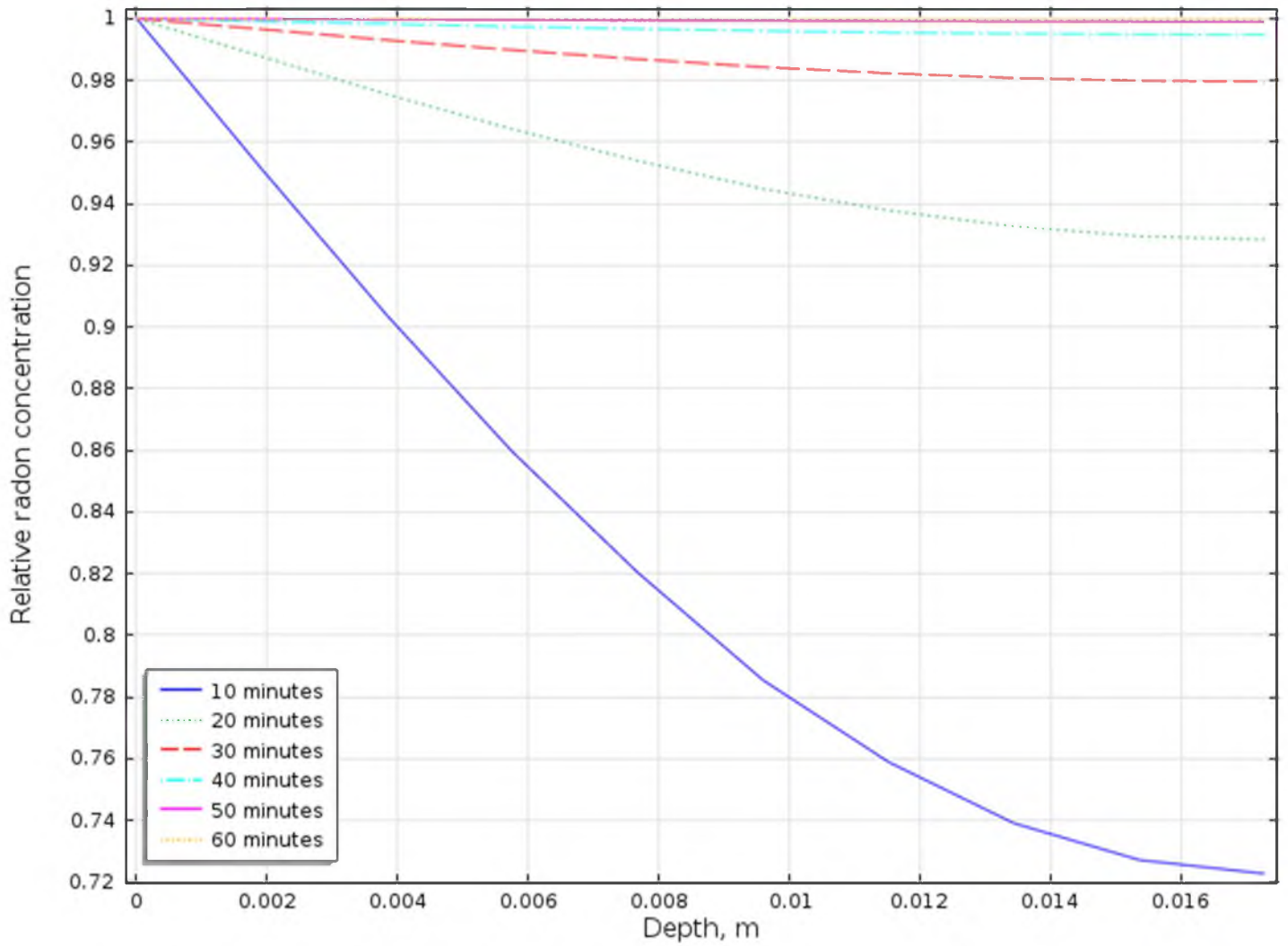

Figure 3-18. Relative radon concentration in soil vs. cylinder depth

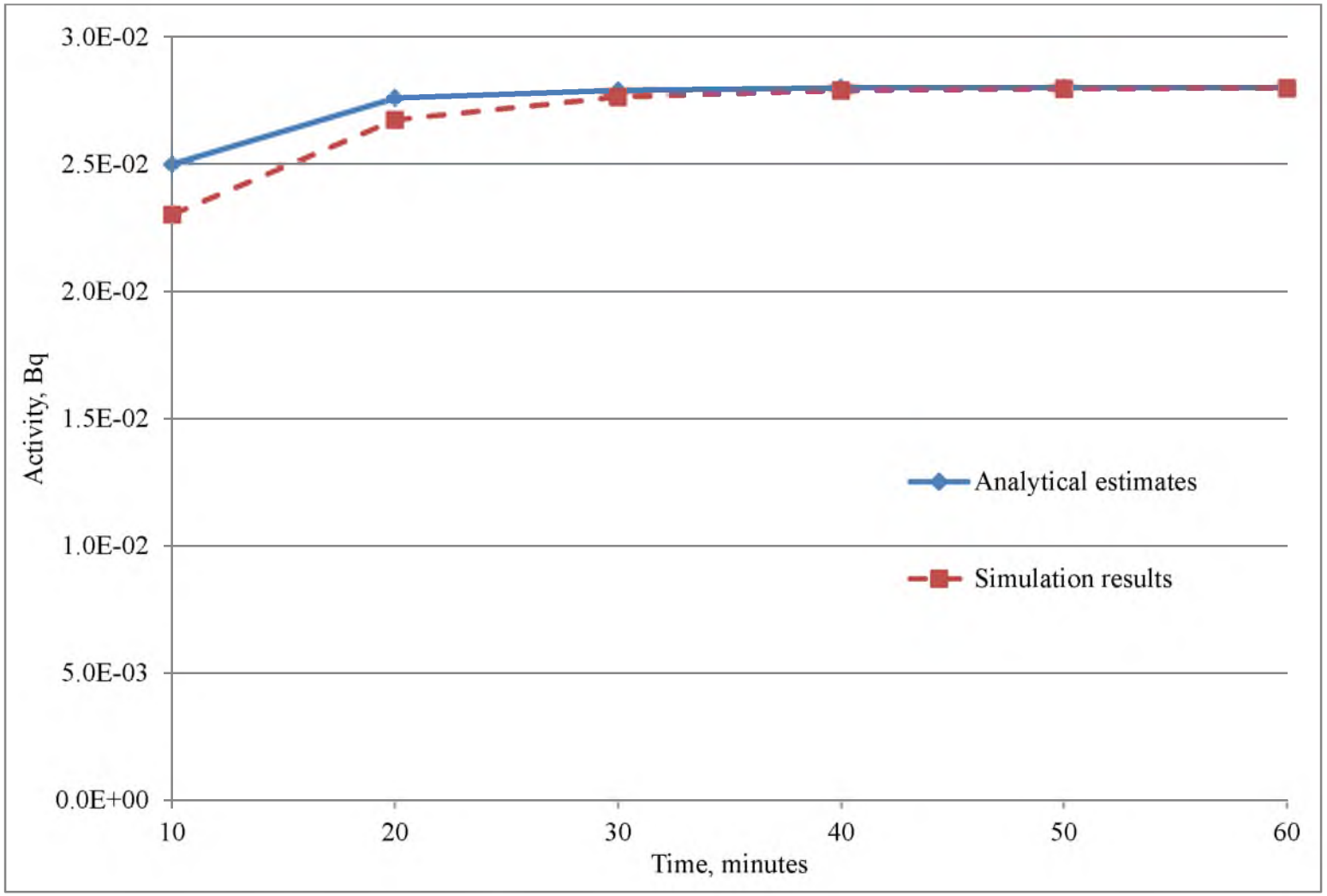

Figure 3-19. Analytical estimates and simulation results for total radon activity in soil cylinder

Table 3-8. Simulation results of radon activities in activated charcoal canister during different exposure times

Time, hours	12	24	36	48	60	72
Total radon activity, Bq	27.24	37.86	44.60	49.17	51.95	53.61

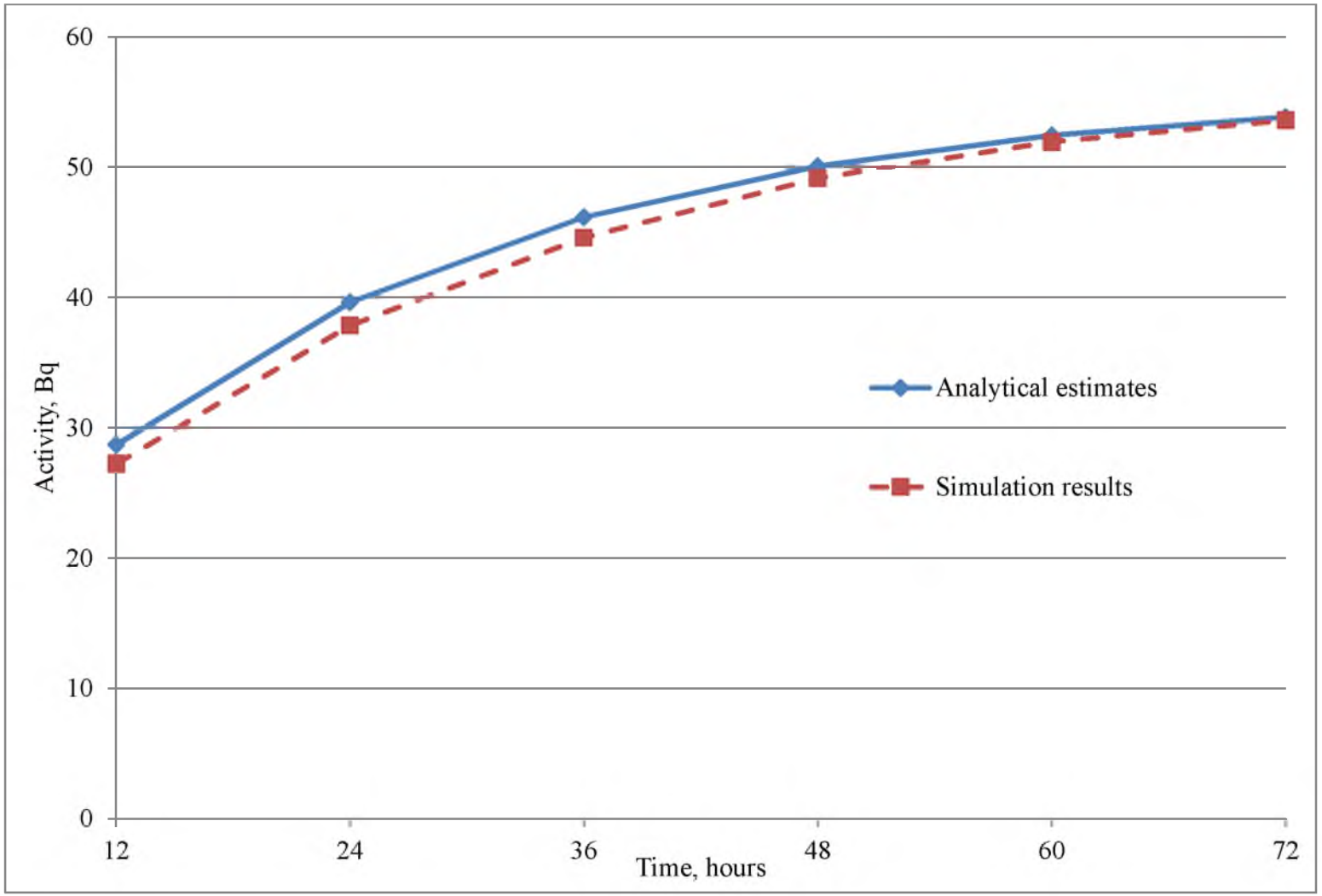

Figure 3-20. Analytical estimates and simulation results for total radon activity in activated charcoal

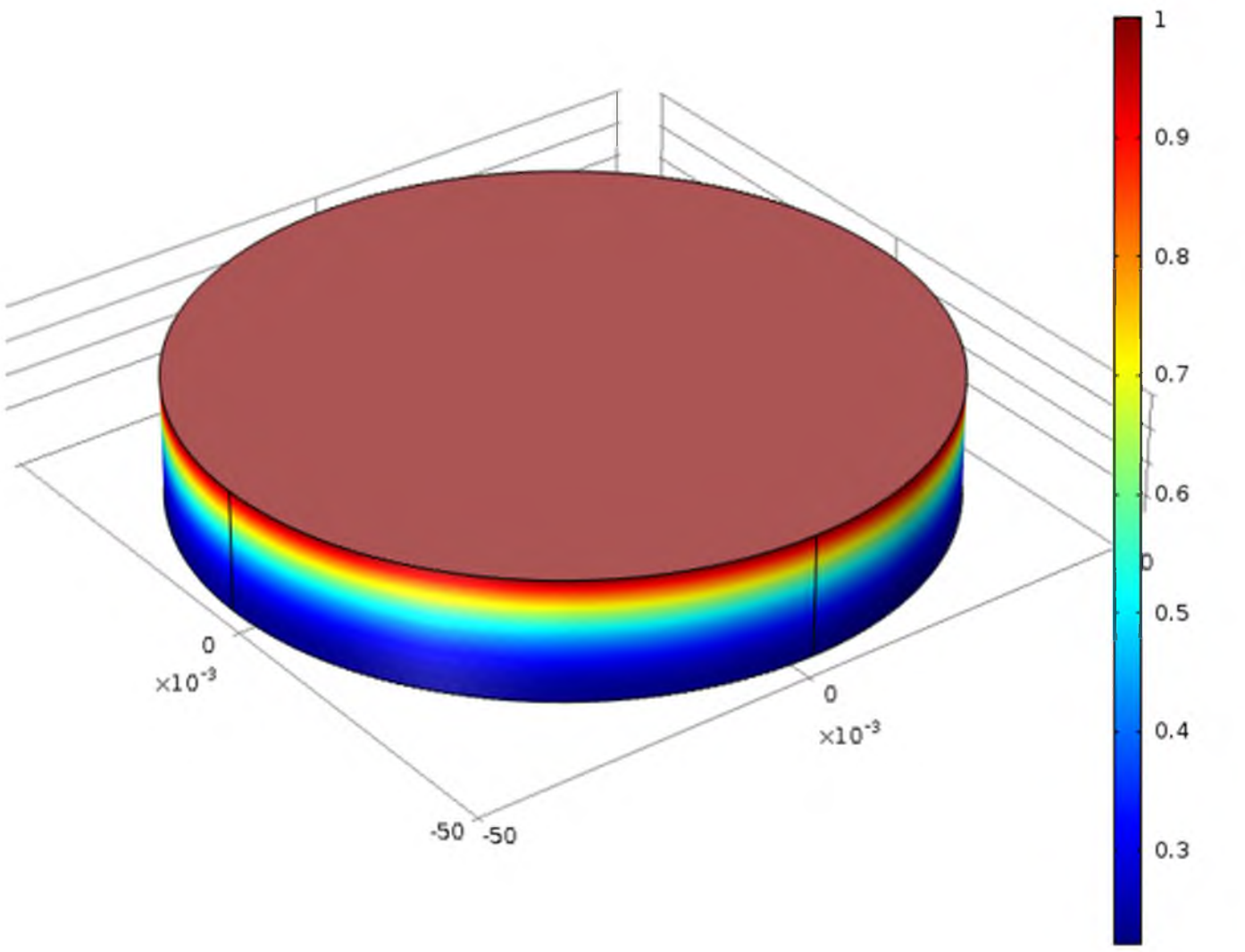

Figure 3-21. Relative radon concentration in activated charcoal vs. canister depth after 12 hours exposure

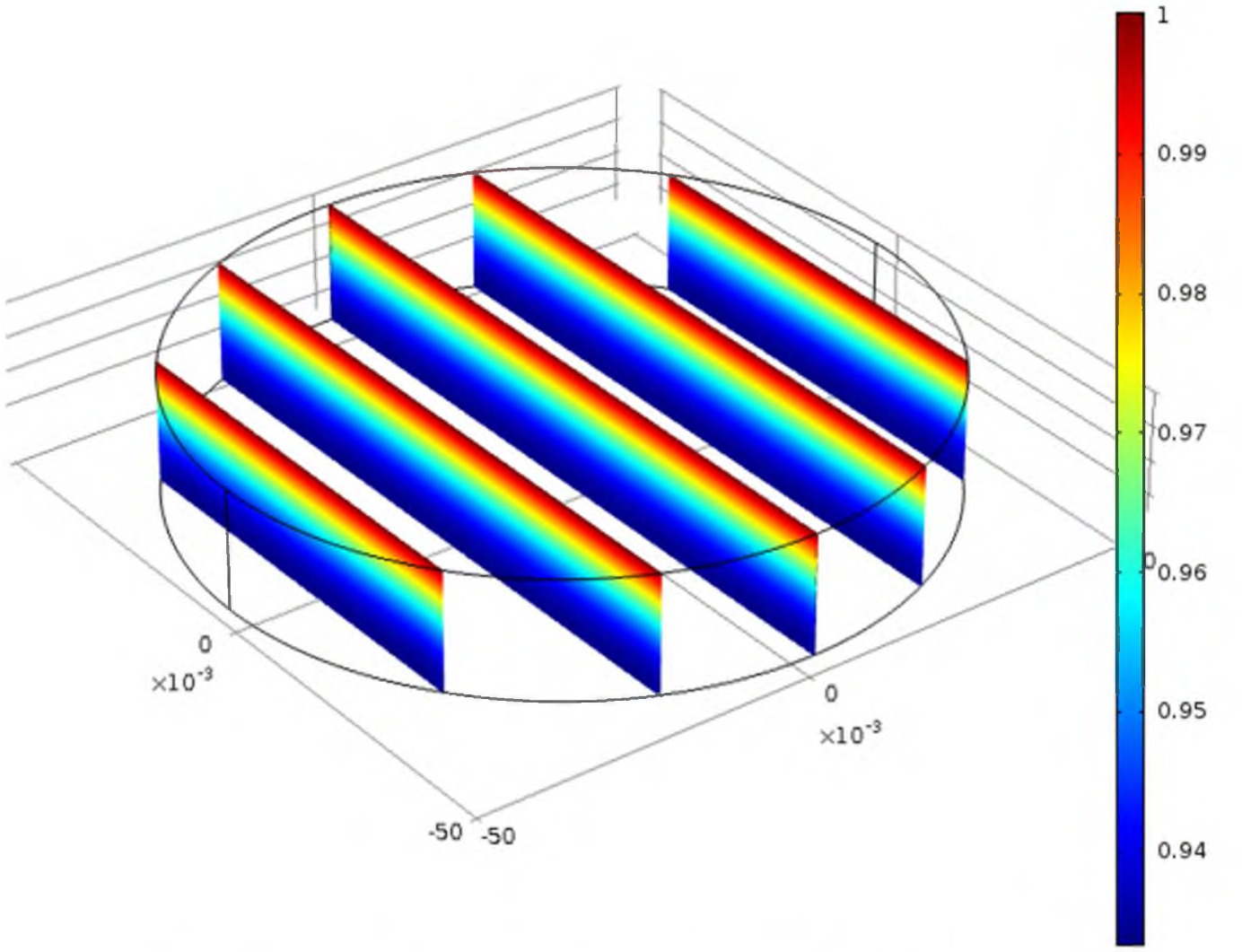

Figure 3-22. Relative radon concentration vs. canister depth after 72 hours exposure

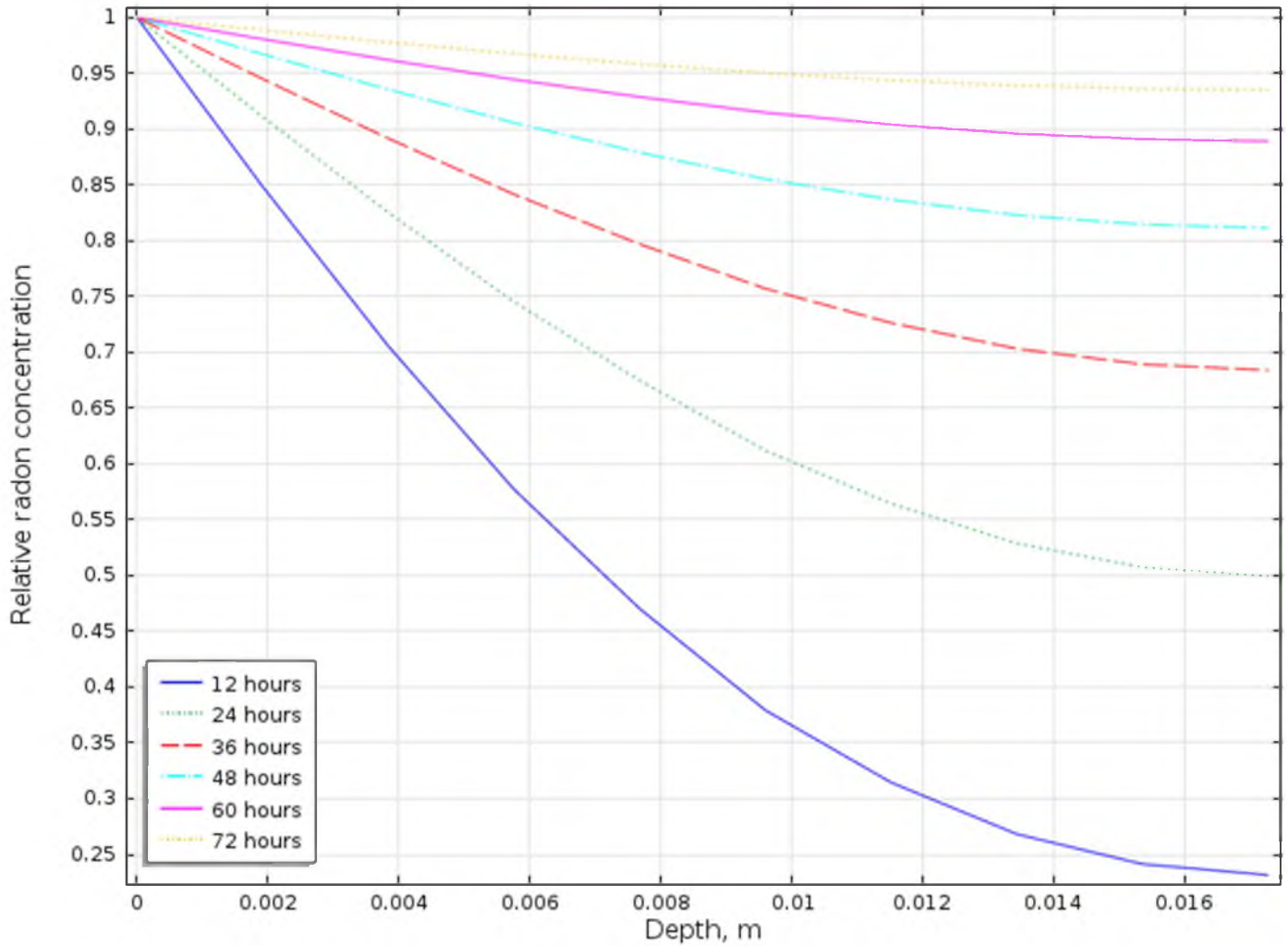

Figure 3-23. Relative radon concentration in activated charcoal vs. canister depth

CHAPTER 4

CHARCOAL AS RADON DETECTOR

4.1 Charcoal Characteristics

Charcoal is a black solid biomass that consists mostly of organic material. The main application of charcoal is using it for heating as fuel. The density of charcoal is about 0.5 g/cm^3. The most important feature of the charcoal in radon measurements is its porosity. Activated charcoal is usually used for such purposes. It is different from the usual charcoal because it went through an activation process. This can be done by carbonization, when gasses are used to open up the pores. Another method involves chemical activation, when phosphoric acid, sodium hydroxide, zinc chloride, and potassium hydroxide are used to open up the pores of the charcoal. Activated charcoal's surface area is dramatically increased during the activation process creating a network of tiny pores. As a result, the absorbing ability increases significantly.

4.2 Absorption of Radon by Charcoal

Activated charcoal adsorption of radon is used in charcoal detectors as it is described in section 2.3.7. Due to the high porosity of activated charcoal, radon is likely to penetrate much faster and much deeper inside compared to nonactivated charcoal. One of the objectives of this thesis is to estimate the radon diffusion coefficient for usual charcoal.

Activated charcoal absorption of radon also found an application in health physics [*6*]. The body burden radium may be inferred from measurements of radon concentration in the breath. Since radium transforms directly into radon, some of the radon dissolves in the body fluids and in adipose tissue, and the balance is exhaled. For analysis, radon from a measured volume of exhaled breath is adsorbed on activated charcoal. Then it is desorbed and transferred into an ionization chamber or scintillation cell for counting

4.3 One Data Point: Potential Use of Charcoal for Radon Measurements

A simple experiment was conducted to determine the absorbing ability of nonactivated charcoal. Five samples were prepared from a few briquettes of charcoal that were crushed into powder, mixed thoroughly and divided into five identical parts – samples with masses equal to 21.4 g. In addition, one activated charcoal sample was prepared from tablets that are usually used for food poisoning treatment. Mass of the activated charcoal sample is 9.27 g.

All samples were placed into 60 ml plastic bottles with a tight cap. Two high purity germanium (HPGe) detectors (Canberra GC2020 and Canberra GC4020, counting stations #4 and #8, respectively) were calibrated for the bottle geometry with Am-Eu calibration source, filled in the bottle to the same level as charcoal samples. Since the amount of activated charcoal sample is less than the amount of five other samples, two different calibrations were performed for counting station #4: one for five samples of masses 21.4 g which filled the bottle to approximately 3/4 top, and one for activated charcoal sample with mass of 9.27 g which filled only 1/3 of the whole bottle volume. Each sample was numbered and measured using HPGe detectors at the Utah Nuclear

Engineering Facility. The purpose of this measurement is to have values of initial activities of radon progeny for each sample. Counting time for all samples was 24 hours.

The next step was to place all the samples in the basement with higher radon concentration; the base-line measurement was performed with SafetySiren Pro 3 Radon Gas Detector showing the level of 2.6 pCi/l. As it was described in section 2.1.1, EPA defines 4 pCi/l as a safe radon concentration while mean indoor concentration in the United States is 1.5 pCi/l. This way, detected concentration of 2.6 pCi/l is above the average.

The samples were poured out of bottles on a paper and left to expose to radon during the following time intervals: #1 – 1 hour, #2 – 6 hours, #3 – 12 hours, #4 – 24 hours, and #5 together with activated charcoal sample – 54 hours. After each sample was exposed to radon for the corresponding time, it was sealed with wax to prevent radon leakage from the bottle.

Cylindrical shape was given to the charcoal samples in order to match the way of analytical estimates. The radius of the samples was measured with the ruler and had a value of 5.9 cm. Therefore, cross sectional surface area S of the cylindrical geometry equals approximately 110 cm^2. The thickness of the charcoal sample can be calculated from the mass, density and surface area. This way, $l = 0.39$ cm.

After exposure, each sample was allowed to stay for about 3 days to have about the half of radon decayed to produce its progeny. The main reason for this is the low relative intensity of emitting gamma rays by ^{222}Rn – only 0.076 [***12***]. Moreover, the ability of HPGe detectors to identify ^{222}Rn is very poor, as its gamma energy of 510 keV is close to annihilation peak with energy of 511 keV. The manufacturer specifies [***43***] full

width half max (FWHM) of Canberra GC2020 (counting station #4) to be 0.9 keV at gamma energy of 122 keV and 2.0 keV at 1.3 MeV. Resolution of Canberra GC4020 (counting station #8) is 1.1 keV at 122 keV and 2.0 keV at 1.3 MeV. This way, resolution of both HPGe detectors for ^{222}Rn gamma energy of 510 keV is more than 1 keV, and ^{222}Rn peak is undistinguishable from annihilation peak of 511 keV.

That is why it was chosen to let radon decay to produce progeny that can be detected with gamma spectrometry method. Activities of the isotopes that are detected are summarized in Table 4-1. The left column indicates sample's activities before exposure, the next contains activities after the exposure. Colors show correlations in activities between parent and daughter isotopes. Green fill indicates that the activity of the current isotope is in accordance with its parent isotopes or activities of the same isotope in other samples. Light green color shows that the current isotope's activity differs significantly from other samples but in accordance with its parent. Orange color indicates that the activity of the current isotope differs significantly from other samples but in accordance with all the measurements for the current sample. Red fill in a cell shows that the activity of the current isotope is not in accordance with its parent or other samples.

Although some data points are obviously off, it can be seen from the table that radon progeny concentrations slightly increased. Discrepancy between counting stations can be noticed. It can be explained by the different shielding used on detectors. Counting station #8 uses cylindrical copper shielding from CANBERRA, while station #4 has shielding constructed from lead bricks which does not cover the top side. The analysis of experimental data is described in section 4.4.

4.4 Experimental Data Analysis and Potential of Charcoal as Radon Detector

Since the waiting time after exposure for each sample was around 3 days before the samples were measured, radon and its short-lived progeny are obviously in equilibrium. This way, ^{222}Rn activity per gram for each sample can be estimated from average activities of ^{214}Bi and ^{214}Pb. Table 4-2 shows radon activities obtained from activities of ^{214}Bi and ^{214}Pb. White cells list the measured values as obtained at the station #8 values, while grey cells correspond to the values obtained from the station #4. Activities per gram should be multiplied by the mass of each sample in order to obtain total activities. Total activities of ^{214}Bi, ^{214}Pb and ^{222}Rn are listed in Table 4-3.

Radon activity increased after exposure for samples #2, #3, #4, and #5. Sample #1 decrease of activity can be explained by shot exposure time. More radon came out from the sample than diffused inside from the air, resulting in decrease of ^{214}Bi and ^{214}Pb activities. Since gamma rays from lead shielding contributed to measurements obtained with counting station #4, these data will not be considered in estimation of potential of nonactivated charcoal as radon detector.

In order to have judgments on nonactivated charcoal's ability to adsorb radon, its adsorption and diffusion coefficients are to be estimated. Before calculating the diffusion coefficient it must be shown how long it takes for the saturation of charcoal with radon to be reached in selected charcoal geometry. Since the maximum exposure time in this experiment is 54 hours, equation (3.33) that disregards radon decay can be used; however, calculations using equation (3.36) that considers radon decay are also performed to show that the difference between two equations for this experiment is

insignificant.

The next parameters and conditions are used for the calculation:

C_0 = 2.6 pCi/l = 96.2 Bq/m^3 – radon concentration in air measured with SafetySiren Pro 3 Radon Gas Detector;
m = 21.4 g – sample mass;
S = 110 cm^2 – surface of the cross section of the charcoal sample calculated through measured radius;
ρ = 0.5 g/cm^3 – charcoal density;
l = 0.39 cm – charcoal layer depth calculated through mass, surface area and density.

Adsorption coefficient does not contribute to the saturation time. In order to show when the saturation is reached, different diffusion coefficients are analyzed for both equations. Analytical estimates for total radon activities for different time intervals are given in Table 4-4.

Figure 4-1 illustrates how relative radon activity, normalized to maximum possible absorbed activity in the sample geometry, changes with exposure time for different diffusion coefficients. The plots show that for diffusion coefficients of order of 10^{-8} m^2/s, saturation in the sample geometry is reached in 1 hour; for diffusion coefficient of 10^{-9} m^2/s saturation is reached in about 12 hours; while for values of $D = 10^{-10}$ m^2/s and less, saturation is not reached even during the longest experiment exposure time interval of 54 hours.

It can be found from Table 4-3 that the gained activity for sample #3 is 10.7 pCi, and for sample #5 is 8.6 pCi. Taking into account uncertainties of 40% and more for the measurements, no conclusion can be made whether the saturation in the samples is reached or not.

In order to find diffusion coefficient values for experimental data, the equations (3.33) and (3.36) should be solved for 12 and 54 hours exposure cases. Since adsorption

coefficient for nonactivated charcoal is also unknown, the equations are solved for k ranging from 0 to activated charcoal value of 4. This way, initial data for sample #3:

$k = 0...4$ m^3/kg – charcoal adsorption coefficient;
$m = 21.4$ g – sample mass;
$S = 110$ cm^2 – surface of the cross section of the charcoal sample calculated through measured radius;
$\rho = 500$ kg/m^3 – charcoal density;
$l = 0.39$ cm – charcoal layer depth calculated through mass, surface area and density.
$C_0 = 2.6$ pCi/l = 96.2 Bq/m^3 – radon concentration in air measured with SafetySiren Pro 3 Radon Gas Detector;
$t = 12$ hours – sample #3 exposure time;
$A = 10.7$ pCi = 0.396 Bq – total absorbed radon activity.

To be estimated: D [m^2/s] – radon diffusion coefficient in nonactivated charcoal. Solutions for different values of k are given in Table 4-5.

The calculations can be stopped at this point because Cozmuta and van der Graaf [***44***] report the values for radon diffusion coefficient in concrete in the range 10^{-7} to 10^{-11} m^2/s. Since charcoal is more porous than concrete with lowest diffusion coefficient, its diffusion coefficient for radon should have a larger value than 10^{-11} m^2/s. The first three solutions in Table 4-5 satisfy this condition.

This way, radon adsorption coefficient in nonactivated charcoal varies from 0.2 to 0.4 m^3/kg and hence, 20 to 10 times less than the one of activated charcoal. Radon diffusion coefficient for nonactivated charcoal is in the range of 1.2×10^{-11} to 5.1×10^{-10} m^2/s. All values of diffusion coefficients obtained for different adsorption coefficients are plotted in Figure 4-2. Logarithmic dependence is shown in Figure 4-3.

The obtained values for nonactivated charcoal diffusion coefficient are less than the value for activated charcoal diffusion coefficient, since nonactivated charcoal has less porous structure, and radon moves slowly in it. Activated charcoal is better choice for any experiment that involves adsorption, including radon detection.

Table 4-5 and Figure 4-3 show that diffusion coefficient value for nonactivated charcoal is less than 10^{-9} m^2/s, while the diffusion coefficient for activated charcoal is 1.43×10^{-9} m^2/s. Therefore, nonactivated charcoal has less potential to be used in radon detection. Its structure is less porous which impede radon from being captured in pore volumes. This results in less absorption ability and lower diffusion coefficient value. Absorption ability of all analyzed media is shown in Figure 4-4. Geometry for each medium is the same – canister, described in the EPA Standard and Protocol. Here, adsorption coefficients for activated and nonactivated charcoals equal 4 m^3/kg and 0.2 m^3/kg, respectively. The graph illustrates that activated charcoal has the best absorption ability among all media analyzed. Total absorbed activity for nonactivated charcoal is more than one order of magnitude less, compared to activated charcoal. Finally, air, soil and water have poor radon absorption ability.

4.5 Comparison of Experimental Data with Numerical Simulations of Radon Diffusion in Nonactivated Charcoal

COMSOL Multiphysics simulations for nonactivated charcoal diffusion coefficients, obtained from experimental data, were performed to compare how total absorbed radon activities correlate with experimentally measured activities.

Activities, obtained from simulation shown in the right column of Table 4-6, are close to measured activities of 10.7 pCi and 8.6 pCi, shown in the left column. The table demonstrates also that activity values for adsorption coefficients of 0.2 m^3/kg are closer to actual gained activities of both samples.

Figure 4-5 shows the geometry used in the experiment and relative radon concentration change along the sample's depth during 12 hours exposure and diffusion coefficient $D = 4.3 \times 10^{-10}$ m^2/s, obtained with numerical simulation.

Table 4-1. Measurement data for all samples before and after exposure

Nuclide Name	1, pCi/g	1 exp., pCi/g	2, pCi/g	2 exp., pCi/g	3, p Ci/g	3 exp., pCi/g	4, pCi/g	4 exp., pCi/g	5, pCi/g	5 exp., pCi/g	Act. ch., pCi/g	Act. ch. exp., pCi/g
K-40		8.01E+00	4.22E+02	9.44E+01	4.58E+00	2.28E+00	7.51E+02		6.88E+00		7.94E+01	
Tl-207		1.50E+02		4.02E+02	1.03E+02	8.28E+01				1.02E+02		
Tl-208	1.68E-01	5.66E-01	1.72E+01	1.15E+01	2.99E-01	2.74E-01	6.63E+00	1.57E+01	9.38E-01	9.10E-01		1.80E+00
Pb-210	5.05E+01		2.90E+01	2.03E+01	4.05E+00		2.19E+01	2.33E+01		7.61E+01		
Pb-211			2.75E-01								2.08E+00	
Bi-212	5.85E+00	7.94E+01	4.30E+01	3.21E+01	1.14E+01	1.24E+00	5.45E+01	3.22E+01	6.68E+00	3.60E+00	1.26E+01	5.51E+00
Pb-212	1.40E+00	1.59E+00	3.75E+02	1.69E+02	1.99E+00	1.02E+00	1.47E+02	1.08E+01		1.51E+00	7.60E-01	
Bi-214	6.61E+00	3.14E+00	1.34E+01	2.27E+01	1.54E+00	3.30E+00	1.77E+01	1.73E+01	2.00E+00	2.70E+00	9.31E+00	1.11E+01
Pb-214	7.38E-01	1.44E+00	5.11E+00	7.66E+01	2.35E+00	1.45E+00	8.64E+00	2.44E+01	1.23E+00	1.27E+00	4.50E+01	1.86E+01
Rn-219	9.47E-01						1.09E+01	6.01E-01			7.73E-01	2.18E-01
Ra-223					1.37E+00		3.79E+00	3.21E+00		6.02E-01		
Ra-224	3.22E+00									9.64E-01		
Th-227	1.22E+00	5.55E-01	2.66E+01		7.20E-01	1.38E+00	3.22E+00	1.36E+01			1.53E+00	4.62E+00
Ac-228	2.83E+00	1.13E+00	1.88E+01	4.26E+01	3.76E+00	3.28E+00	2.03E+01	3.35E+01	2.21E+00	3.73E+00	1.89E-01	4.97E+00
Th-228	2.94E+00				8.80E+00					1.65E+01		
Th-230				7.59E+01				1.68E+01				9.96E-01
Pa-231			3.10E+01				3.85E+01					1.11E+00
Th-231	3.68E+00							6.70E+00				1.25E+01
Pa-234	5.18E-01		4.55E+00		1.80E+00		5.08E-01	1.09E+00		5.92E-01	3.99E-01	1.75E-01
Pa-234m	2.64E+01	1.36E+02			8.82E+01				3.22E+01	1.84E+02	1.27E+01	
Th-234	6.80E+00	9.52E+01	4.98E+00		4.42E+00		3.86E+01				1.11E+00	
U-234	1.35E+03		4.92E+00				1.69E+02		4.50E+02	2.77E+02		
U-235	1.14E+00	2.92E+00	6.01E+00				3.49E+00	5.19E-01	2.75E+00	1.39E-03	3.94E+00	

Table 4-2. ^{222}Rn and its progeny estimated activities per gram of each sample

Activity, pCi/g	S1, St. #8	S1e, St. #8	S2, St. #4	S2e, St. #4	S3, St. #8	S3e, St. #8	S4, St. #4	S4e, St. #4	S5, St. #8	S5e, St. #8	Act. ch., St. #4	Act. ch. e, St. #4
^{214}Bi	6.6	3.1	13	23	1.5	3.3	18	17	2	2.7	9.3	11
^{214}Pb	0.74	1.4	5.1	77	2.3	1.5	8.6	24	1.2	1.3	45	19
^{222}Rn	3.7	2.3	9	50	1.9	2.4	13	20	1.6	2	17	15

Table 4-3. Total activities for ^{222}Rn and its progeny in each sample

Total activity, pCi	S1, St. #8	S1e, St. #8	S2, St. #4	S2e, St. #4	S3, St. #8	S3e, St. #8	S4, St. #4	S4e, St. #4	S5, St. #8	S5e, St. #8	Act. ch., St. #4	Act. ch. e, St. #4
^{214}Bi	141	66.3	278	492	32.1	70.6	385	364	42.8	57.8	86.2	102
^{214}Pb	15.8	30.0	109	1647	49.2	32.1	184	514	25.7	27.8	417	176
^{222}Rn	78.4	48.1	158	1069	40.6	51.3	285	439	34.2	42.8	252	139

Table 4-4. Analytical prediction of total radon activities in Bq
for charcoal sample with mass of 21.4 g

Time	Equation (3.33)				Equation (3.36)			
D, m^2/s	10^{-9}	10^{-10}	10^{-11}	10^{-12}	10^{-9}	10^{-10}	10^{-11}	10^{-12}
1	1.130	0.358	0.113	0.036	1.127	0.357	0.113	0.036
6	2.013	0.877	0.277	0.088	1.994	0.864	0.273	0.086
12	2.062	1.233	0.392	0.124	2.040	1.197	0.381	0.120
24	2.063	1.652	0.555	0.175	2.042	1.565	0.523	0.165
54	2.063	1.992	0.832	0.263	2.042	1.827	0.732	0.231

Table 4-5. Diffusion coefficient values calculated for samples #3 and #5

Time	12 hours, sample #3		54 hours, sample #5	
	Equation (3.33)	Equation (3.36)	Equation (3.33)	Equation (3.36)
k, m^3/kg	D, m^2/s	D, m^2/s	D, m^2/s	D, m^2/s
$0 < k < \sim 0.2$	No solution	No solution	No solution	No solution
0.2	4.3E-10	5.1E-10	4.0E-11	5.6E-11
0.3	1.2E-10	1.2E-10	1.6E-11	2.1E-11
0.4	6.4E-11	6.8E-11	9.1E-12	1.2E-11
0.5	4.1E-11	4.3E-11	5.8E-12	7.6E-12
0.6	2.8E-11	3.0E-11	4.1E-12	5.3E-12
0.7	2.1E-11	2.2E-11	3.0E-12	3.9E-12
0.8	1.6E-11	1.7E-11	2.3E-12	3.0E-12
0.9	1.3E-11	1.3E-11	1.8E-12	2.3E-12
1.0	1.0E-11	1.1E-11	1.5E-12	1.9E-12
1.1	8.4E-12	8.9E-12	1.2E-12	1.6E-12
1.2	7.1E-12	7.5E-12	1.0E-12	1.3E-12

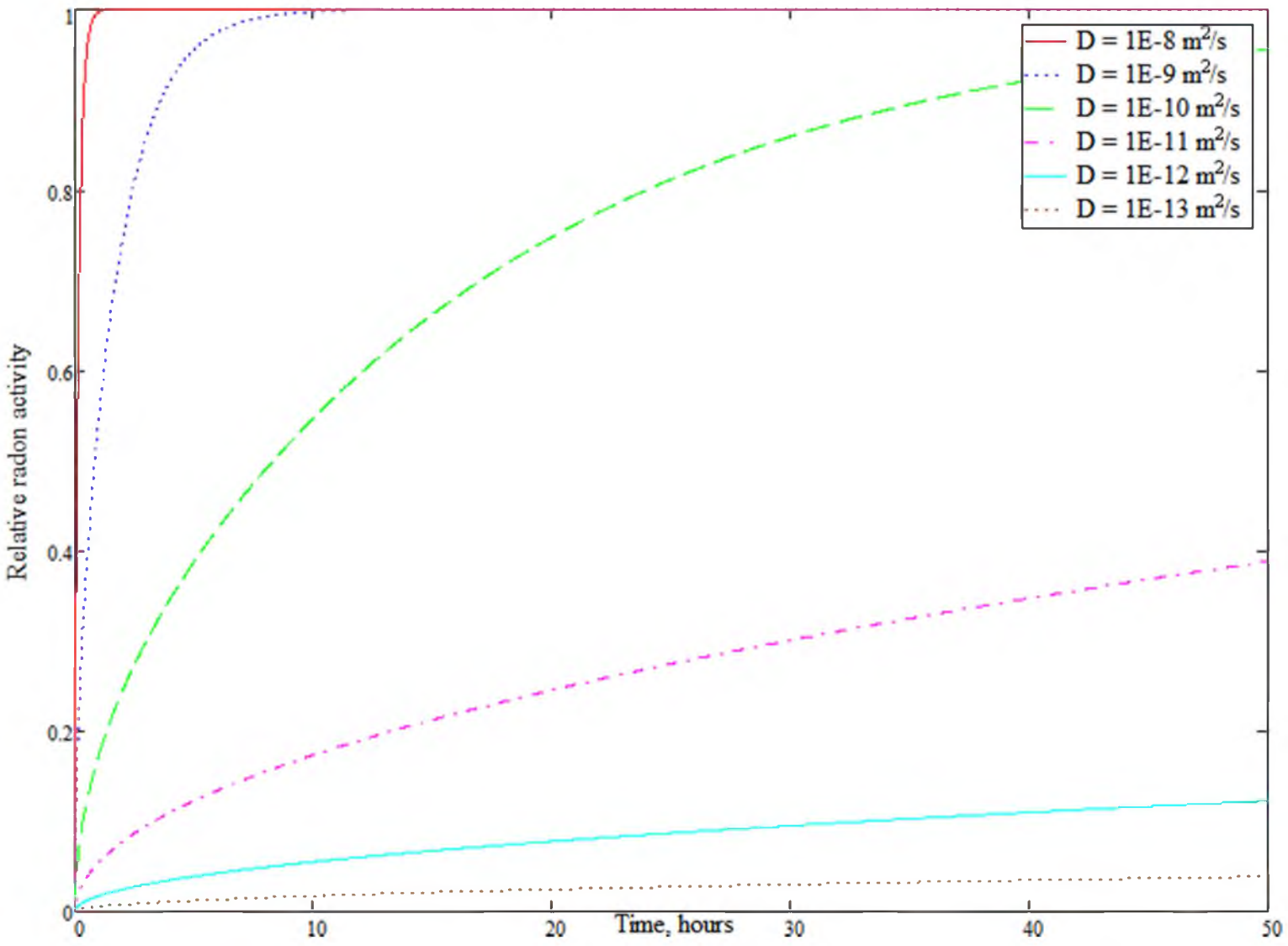

Figure 4-1. Relative radon activities in charcoal sample geometry for different diffusion coefficients vs. time

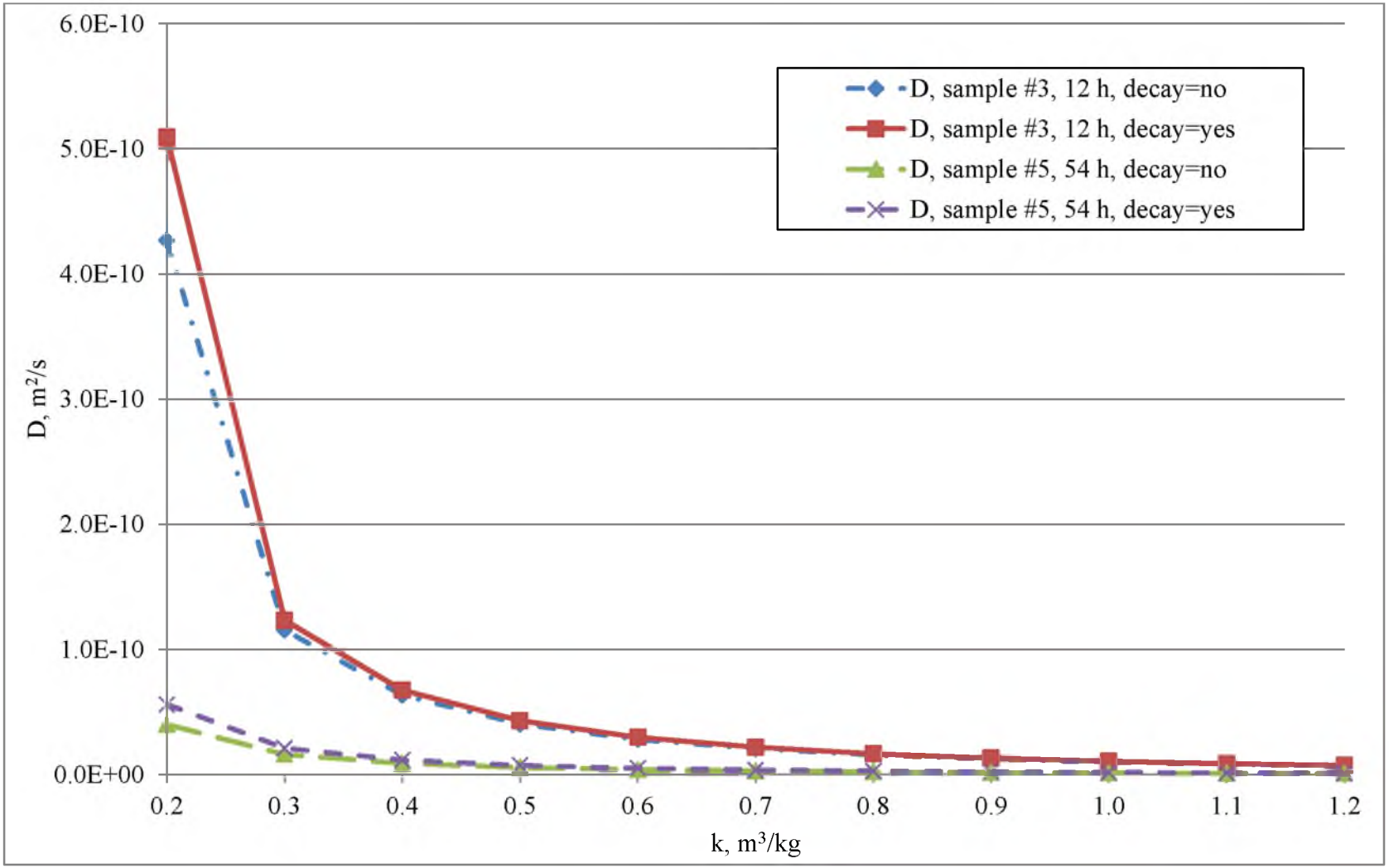

Figure 4-2. Radon diffusion coefficients in nonactivated charcoal vs. adsorption coefficient

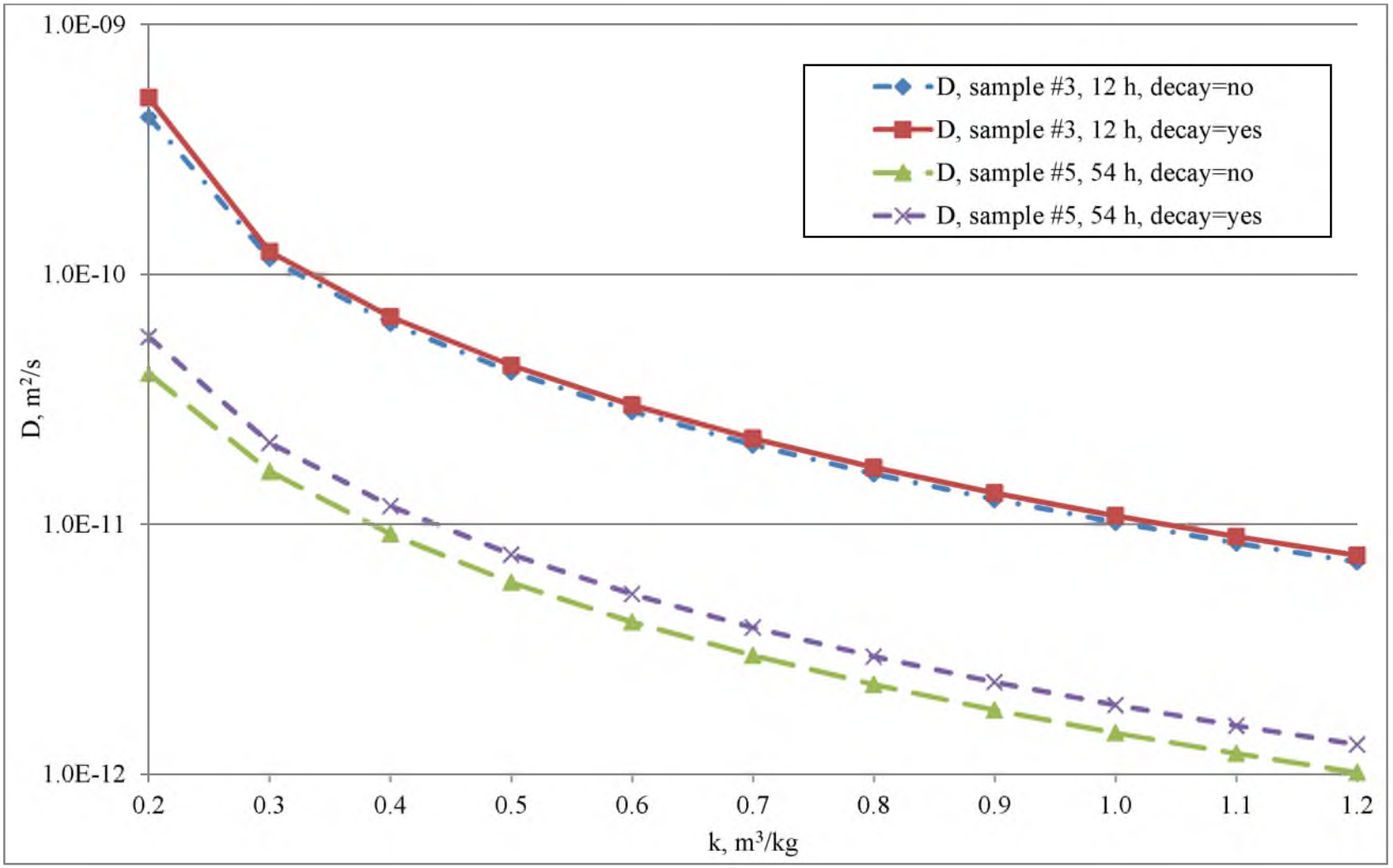

Figure 4-3. Radon diffusion coefficient in nonactivated charcoal vs. adsorption coefficient

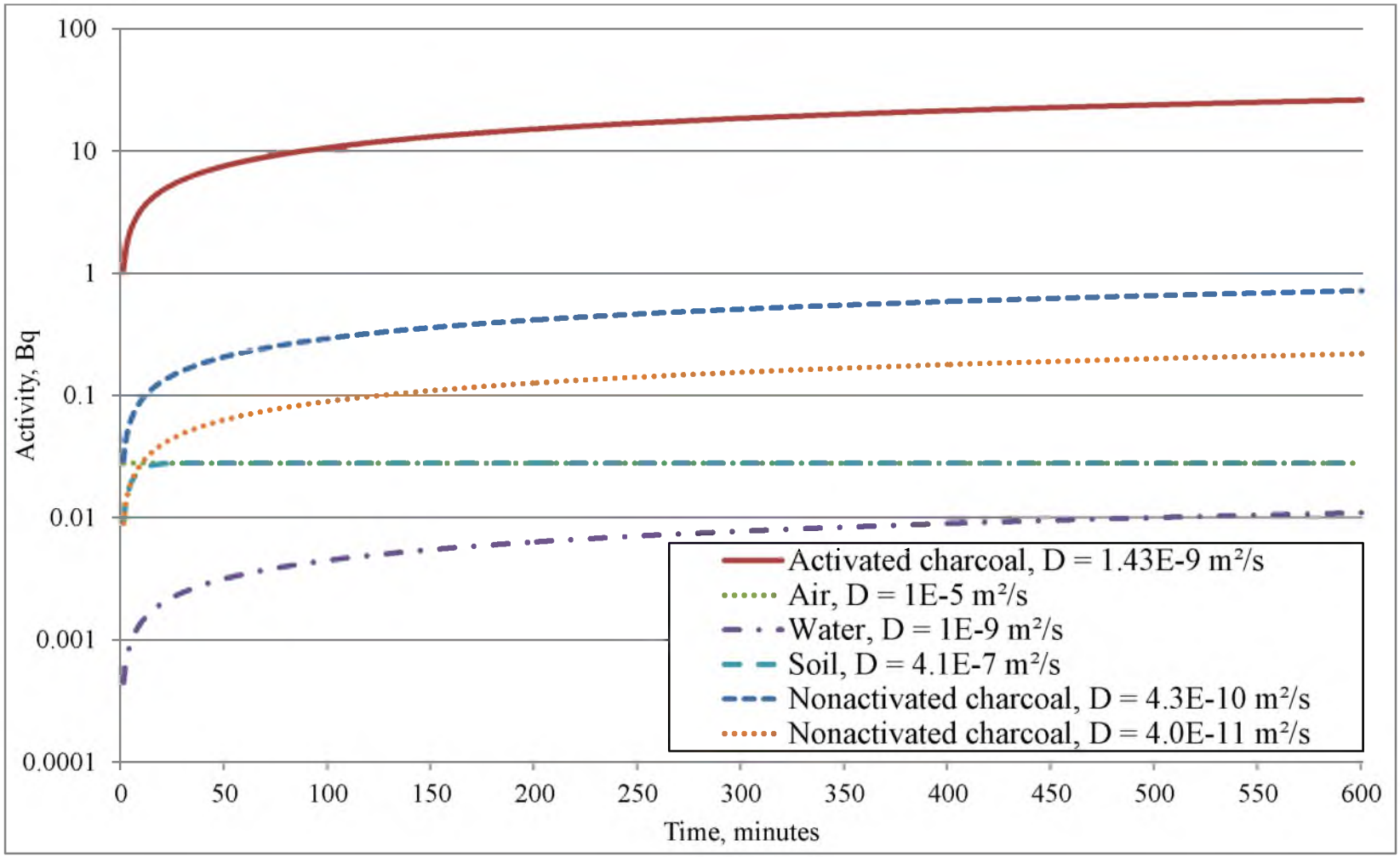

Figure 4-4. Comparison of various media's ability to absorb radon

Table 4-6. Activities for sample #3 and #5, obtained from simulations

Sample	D, m^2/s	k, m^3/kg	Activities, obtained from simulations, pCi
sample #3, 12 hours, 10.7 pCi	4.3E-10	0.2	10.3
	1.2E-10	0.3	11.1
	6.4E-11	0.4	11.8
sample #5, 54 hours, 8.6 pCi	4.0E-11	0.2	8.93
	1.6E-11	0.3	9.44
	9.1E-12	0.4	10.1

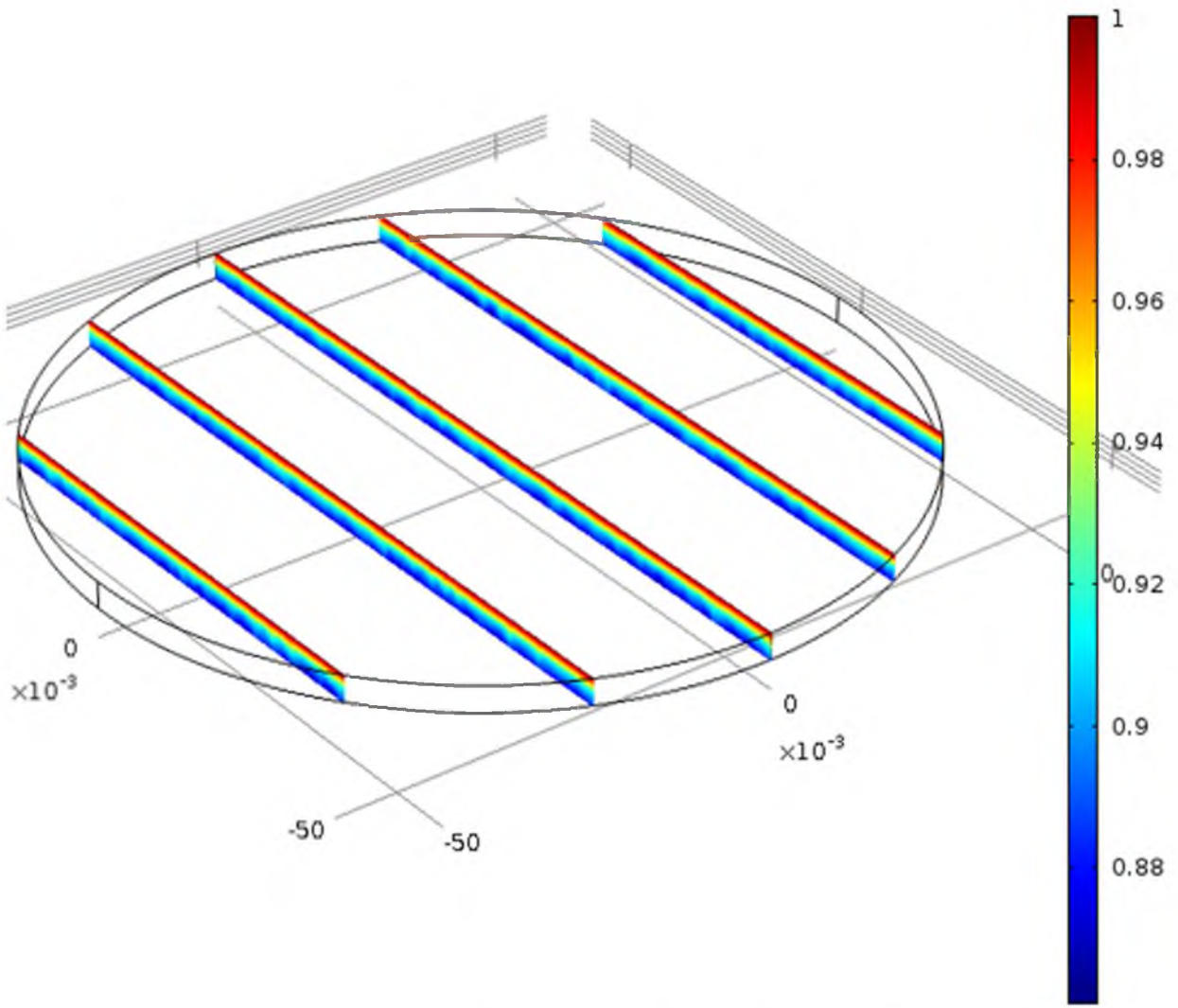

Figure 4-5. Relative radon concentration in the geometry of nonactivated charcoal sample #3 for D = 4.3E-10 m^2/s and t = 12 hours

CHAPTER 5

GEANT4 SIMULATIONS OF U-238 SERIES DECAY IN SOIL

5.1 Simulations of ^{238}U Decay in Soil

GEANT4 numerical code was used to simulate ^{238}U series decay in soil. The geometry adopted is 1 m^3 cylinder of 1 m length with radius of $\frac{1}{\sqrt{\pi}}$ m. Soil composition is chosen to consist of 45% minerals (sand and clay), 25% water, 25% air, and 5% organic material, where clay consists of 47% SiO_2, 39% of Al_2O_3, and 14% water. The model shows radioactive decay of ten ^{238}U atoms through the whole decay chain, shown in Figure 2-1 and includes all interaction of radiation with matter. The results of the simulation are illustrated in Figure 5-1.

Since the parent isotope is ^{238}U, the expected decay products for the first step are daughter isotope ^{234}Th and alpha-particle. Signature gamma rays can be emitted based on relative intensities and energies for each decaying isotope. During the next step ^{234}Th produces ^{234}Pa in beta-decay process. This way, the particles created, besides the daughter isotope itself, are electron, antineutrino and signature gamma rays. It must be noted that electrons can be produced also in the ionization process, when gamma ray has energy equal to or more than ionization potential of the atom that interacts with gamma.

Straight lines are tracks of antineutrinos. Since they almost do not interact with matter, their trajectory looks like a straight line. The lines that change direction represent

gamma ray tracks. Changing of their direction happens due to scattering.

To see electrons, alpha particles and uranium daughters, the picture should be zoomed, since their tracks are much shorter. demonstrates the zoomed view.

also shows all ^{238}U daughters up to ^{206}Pb and numerous alpha particles, electrons and gamma rays produced. It can be seen that recoil atoms move the least distance, compared to alphas. Electrons move farther, and gamma rays and antineutrinos are most penetrating. HepRep Data Browsing Application allows to rotate and zoom the picture, allowing to observe the processes closer, showing the points of interactions and angles of created particle trajectories. Label control function allows us to follow each particle energy during the interactions.

5.2 Simulations of ^{222}Rn Decay in Soil

The same geometry was used to simulate ^{222}Rn series decay in soil. Soil composition is also the same as for uranium series simulations. The model includes all interaction of radiation with matter. The results of GEANT4 simulation are illustrated in Figure 5-3.

The same conclusions can be made as for uranium series with the exception that there are less particles because the decay chain starts not from ^{238}U, but from ^{222}Rn. This way there are less daughters, alphas, electrons, gammas and antineutrinos produced. To better see electrons, alpha particles and radon daughters, the picture should be zoomed. Figure 5-4 illustrates the zoomed view.

GEANT4 model can be merged with diffusion theory to make simulations for radon propagation in any material, including charcoal. This approach can be used in predicting the potential of using nonactivated charcoals for radon measurements.

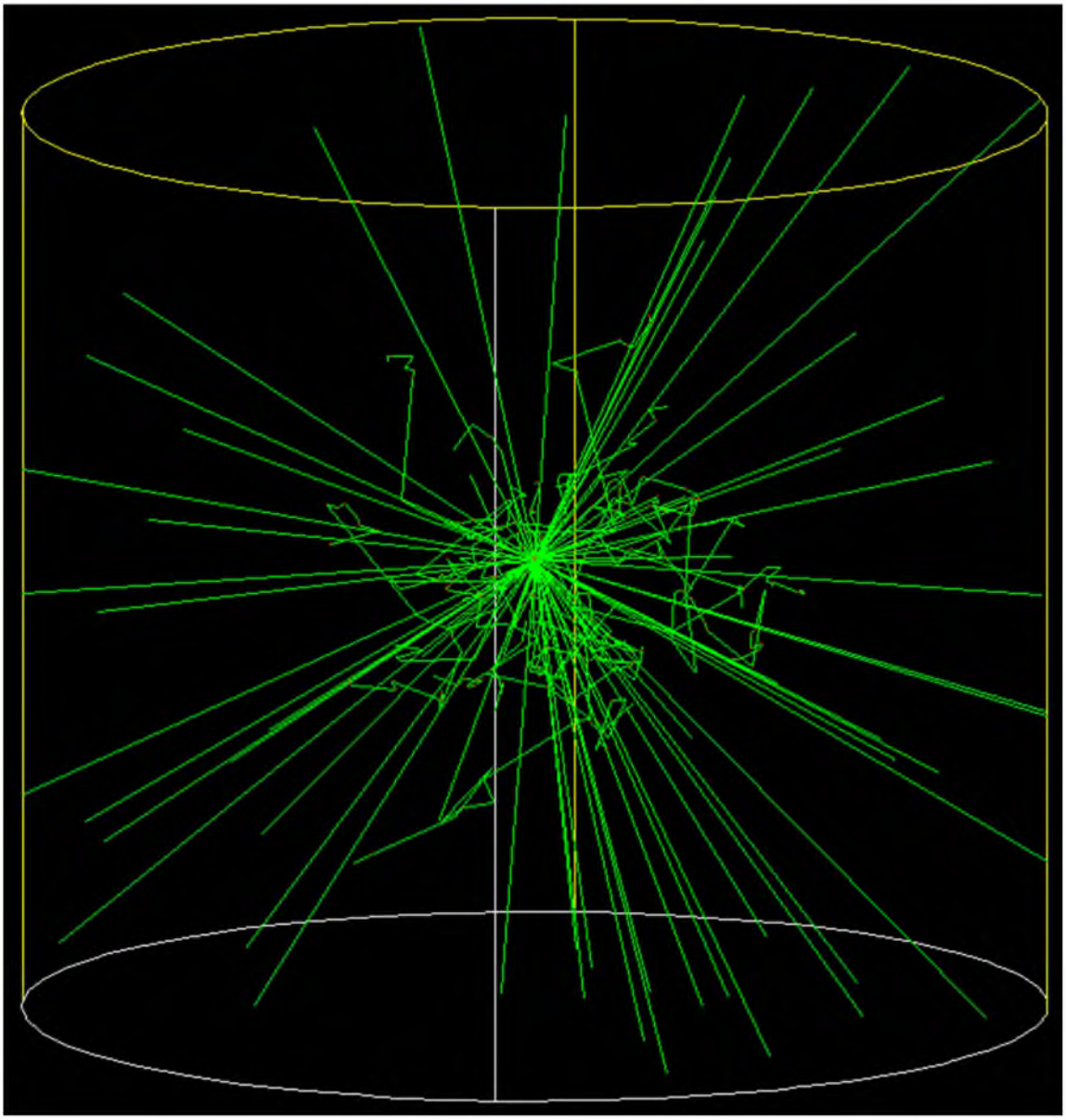

Figure 5-1. GEANT4 simulation of 10 ^{238}U atoms in soil cylinder

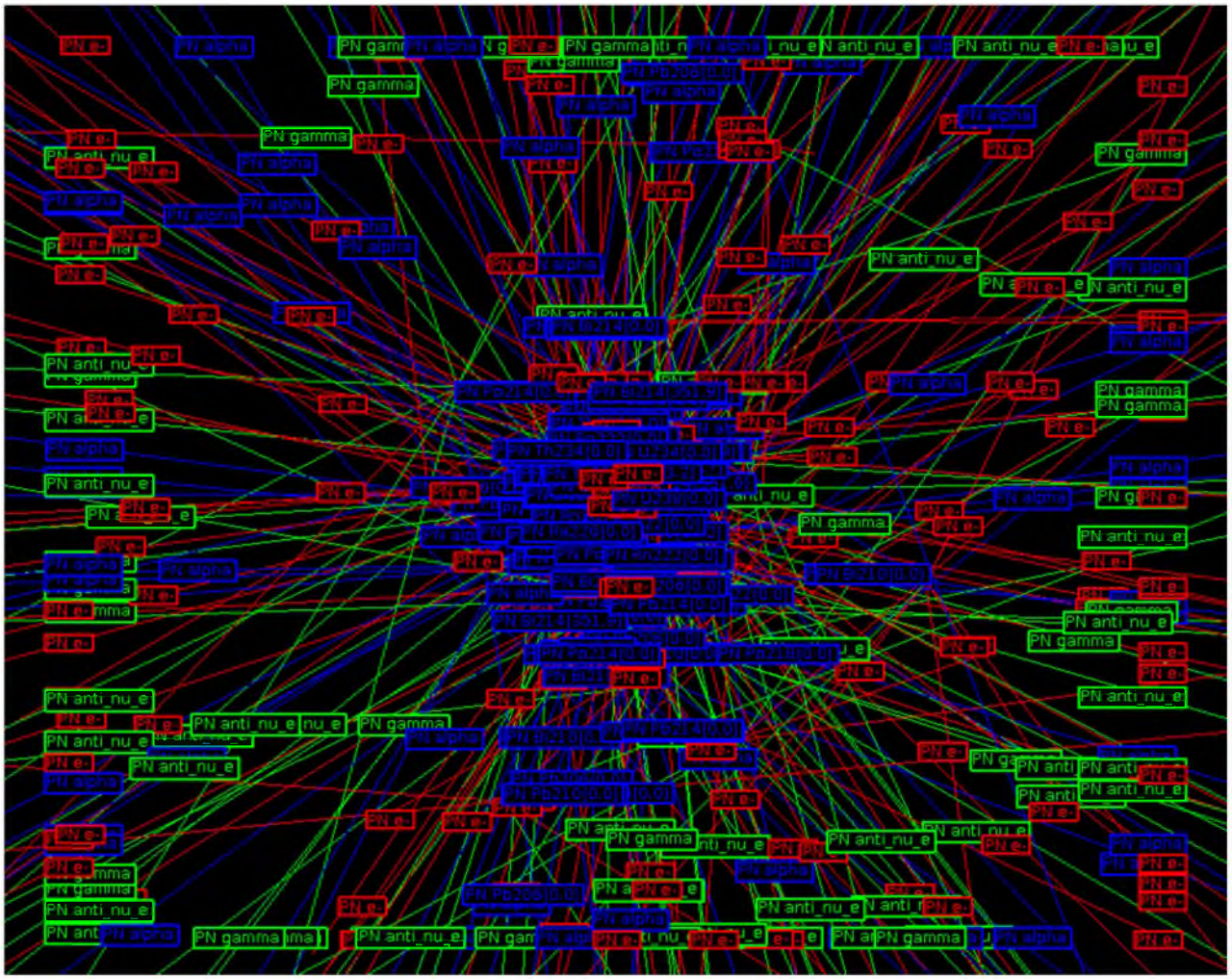

Figure 5-2. Closer look of 10 ^{238}U atoms decay in soil cylinder

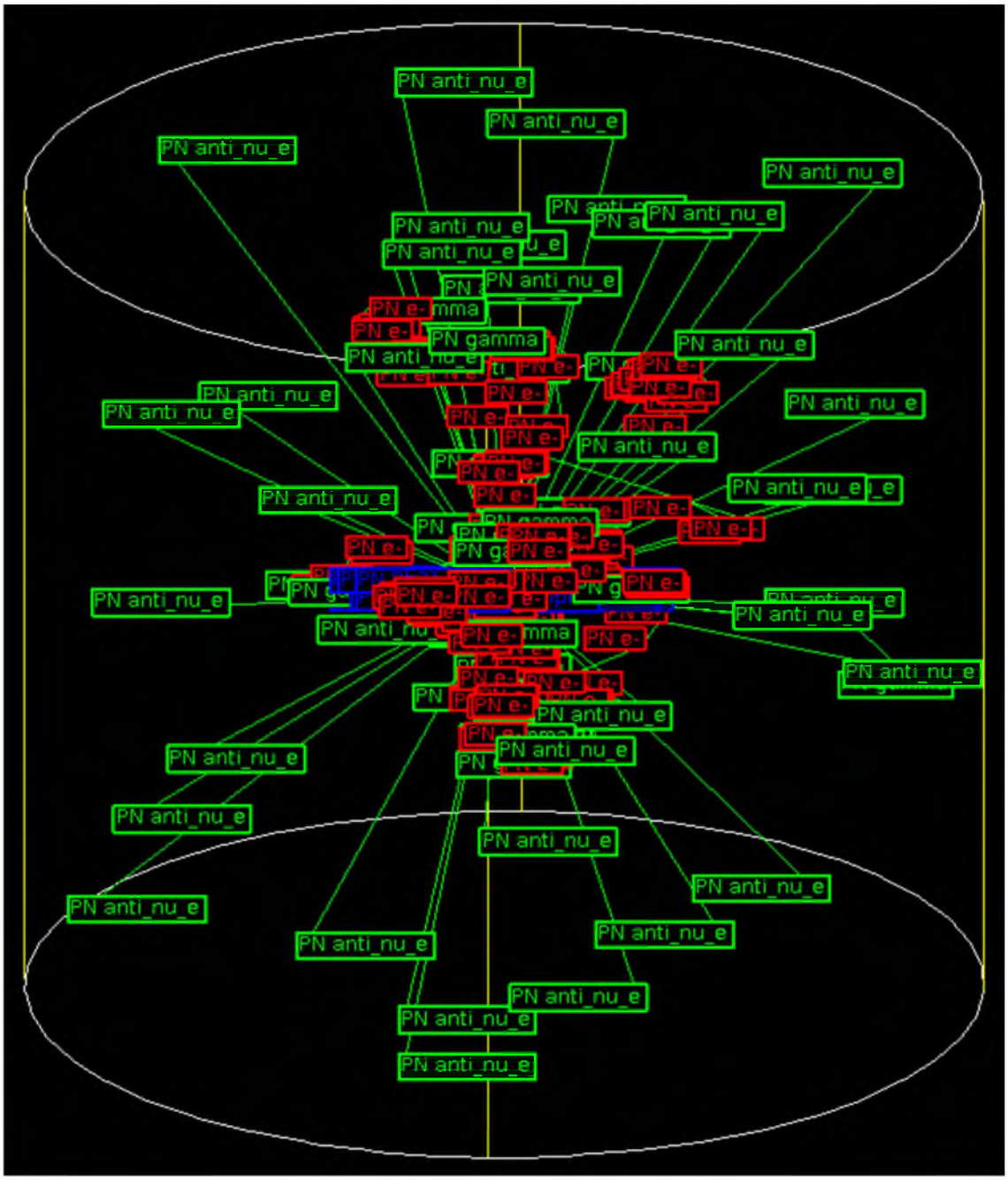

Figure 5-3. GEANT4 simulation of 10 ^{222}Rn atoms in soil cylinder

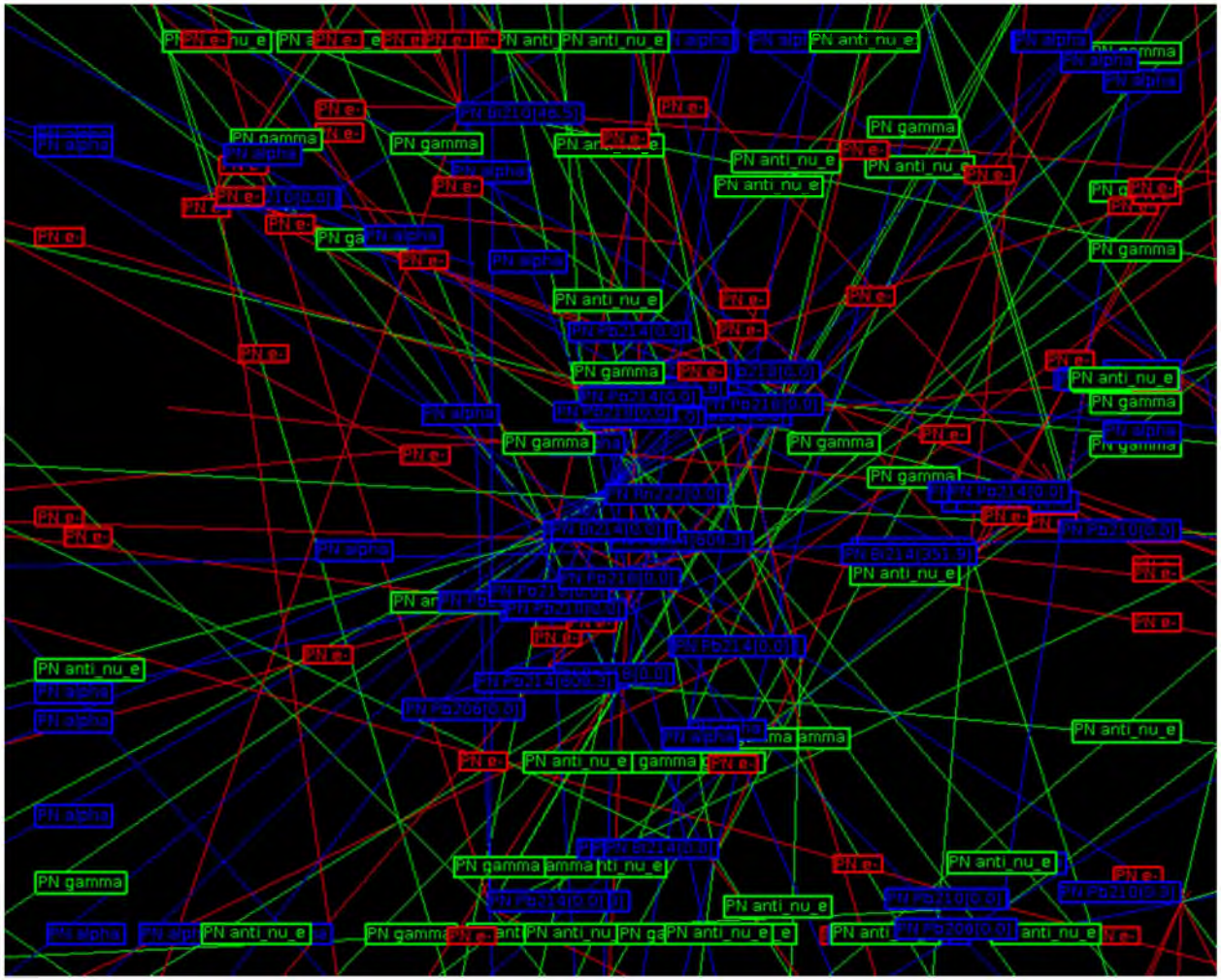

Figure 5-4. Closer look of 10 ^{222}Rn atoms decay in soil cylinder

CHAPTER 6

RADON AS EARTHQUAKE PREDICTOR

6.1 Earthquake Processes Overview

Earthquake processes according to Asada [*45*] include:

I. Buildup of elastic strain

II. Dilatancy and development of cracks

III. Influx of water and unstable deformation in the fault zone

IV. Fault rupture, or the earthquake

V. Sudden drop in stress followed by aftershocks

It was stated by the same author that concentration of radon in ground water does not change much under normal conditions. Radon emissions increase during stage II of an earthquake, and then levels off during stage III. During stage II, microcracks form in the rocks resulting in an increase in the surface area of the rocks. The increased surface area exposes more of the radon to water, which would cause a greater breakdown of the radioactive mineral. Radon emissions increase as the radon is washed out of the rock during stage II. As the water returns during stage III, radon emissions would level off because microcracks stop forming. The newly formed microcracks serve as pathways for more of the radon gas to escape to the surface; this results in higher radon emissions. Figure 6-1 illustrates these processes.

6.2 Radon Propagation in Soil

Radon gas generated in rocks from radium remains partly in the solid matrix, but some atoms can move to pore fluids and migrate away through interconnected pores, aquifer by the method of diffusion and fluid flow. It was reported by Teng [*46*] that in 1926, V.I. Spitsyn studied in detail the release of ^{222}Rn from natural minerals and found that the recoil energy of about 100 keV enables ^{222}Rn to travel through hundreds of crystalline lattice sites.

A GEANT4 simulation of radon transport in rock was made to estimate the track length of ^{222}Rn recoil atoms. Mean obtained value for the track length in silicon is 320 nm. This equals around 1200 silicon atoms per track. The simulation is shown in Figure 6-2. The input file for the simulation is shown in the Appendix.

In soil, radon migrates mostly with water that comes in contact with rocks. Taking into consideration diffusion coefficient of radon in water, radon can move only a distance of around 4 cm in completely still water within its half-life [*45*]. This way, radon migrates mostly due to moving groundwater and carbon dioxide and nitrogen that migrate upward. Therefore, radon that is formed in one place can move to other regions with considerable speed. The cracks and fissures in fault strands act as passages to the ground surface, helping radon to propagate. Figure 6-3 illustrates radon migration along the fracture zones. Eventually radon dissolves in the groundwater where it can be detected.

Simulations in COMSOL Multiphysics were performed in order to check how fast and how far radon can migrate by cracks and fissures in fault strands by diffusion only. In the first simulation a narrow cylinder with radius of 0.5 cm and length of 20 m was filled with air. Initial radon concentration was chosen to be 50 nCi/l or 500 eman. Boundary

conditions, used in the simulation, are the same as for all cylindrical geometries, described in section 3.4. Figure 6-4 illustrates results of the simulation.

It can be concluded that even during eight days or more than two half-lives of ^{222}Rn, its concentration at a distance of ten meters decreases significantly and equals only 1% of its initial value. Taking into account radioactive decay of radon, the concentration decreases approximately 400 times during eight days at distance of ten meters.

Since the underground depths where radon originates may have values much larger than 20 meters, another simulation was made with air cylinder with radius of 2.5 meters and length of 5 kilometers. Figure 6-5 shows this geometry and relative radon concentration changes close to the open end of the cylinder.

Relative radon concentrations were plotted against cylinder depth. It was chosen to limit the *x* axis of the graph with a depth of 30 meters, because the values of relative radon concentrations for deeper values are less than 10^{-10}. Figure 6-6 proves that radon cannot move by diffusion only at distances even of dozens of meters and it is obvious that nitrogen and carbon dioxide that move upward help radon atoms to migrate.

6.3 Examples of Radon Concentration Monitoring Prior to and After Earthquakes

Changes in radon concentration in groundwater was studied by Ulomov and Mavashev [*21*] in 1966. The concentration of radon in groundwater had been measured for several years prior to the Tashkent earthquake. The measurements showed increasing radon concentration starting around eight years prior the earthquake and immediately before the earthquake the concentration reached a maximum of three times the normal readings. The concentration recovered to a normal level after the earthquake. Figure 6-7

illustrates radon concentrations before and after the earthquake.

Another example of successfully predicted earthquakes, in China, was reported by Asada [*45*]. Long-term anomalies in radon concentration began two or three hours before the earthquakes and continued just before they occurred. The pattern of anomalous radon concentration varies: both positive and negative changes were recorded. Figure 6-8 illustrates radon concentration in groundwater and the timeline of the Songpan-Pingwu earthquakes.

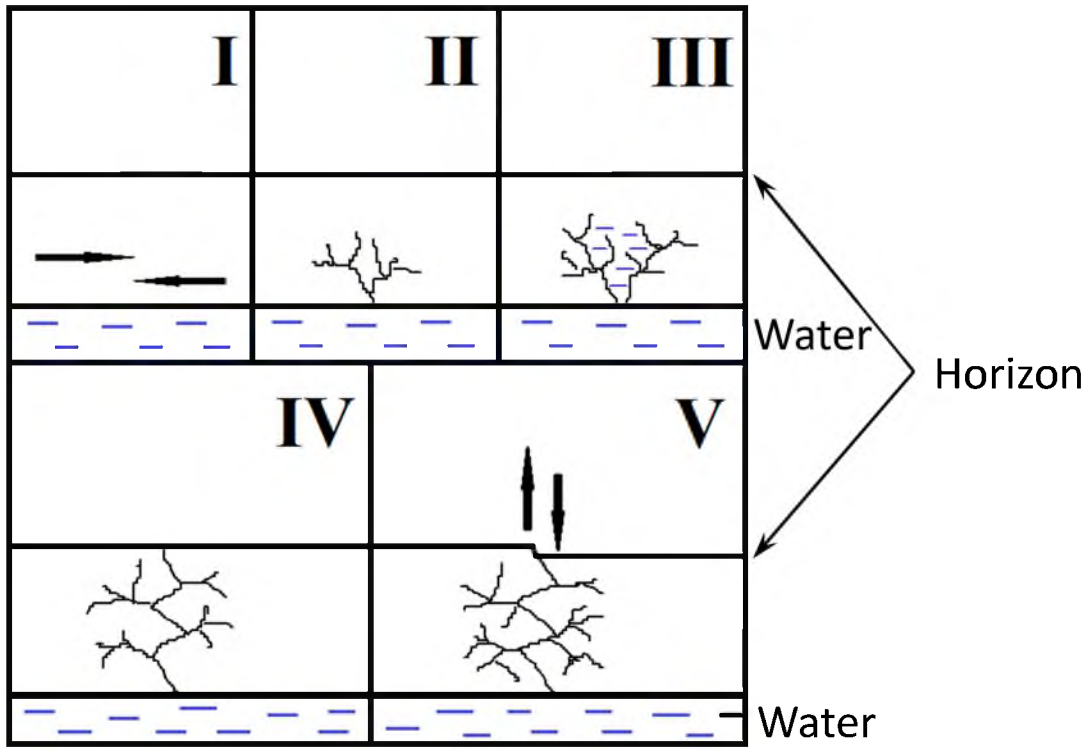

Figure 6-1. Five stages of an earthquake

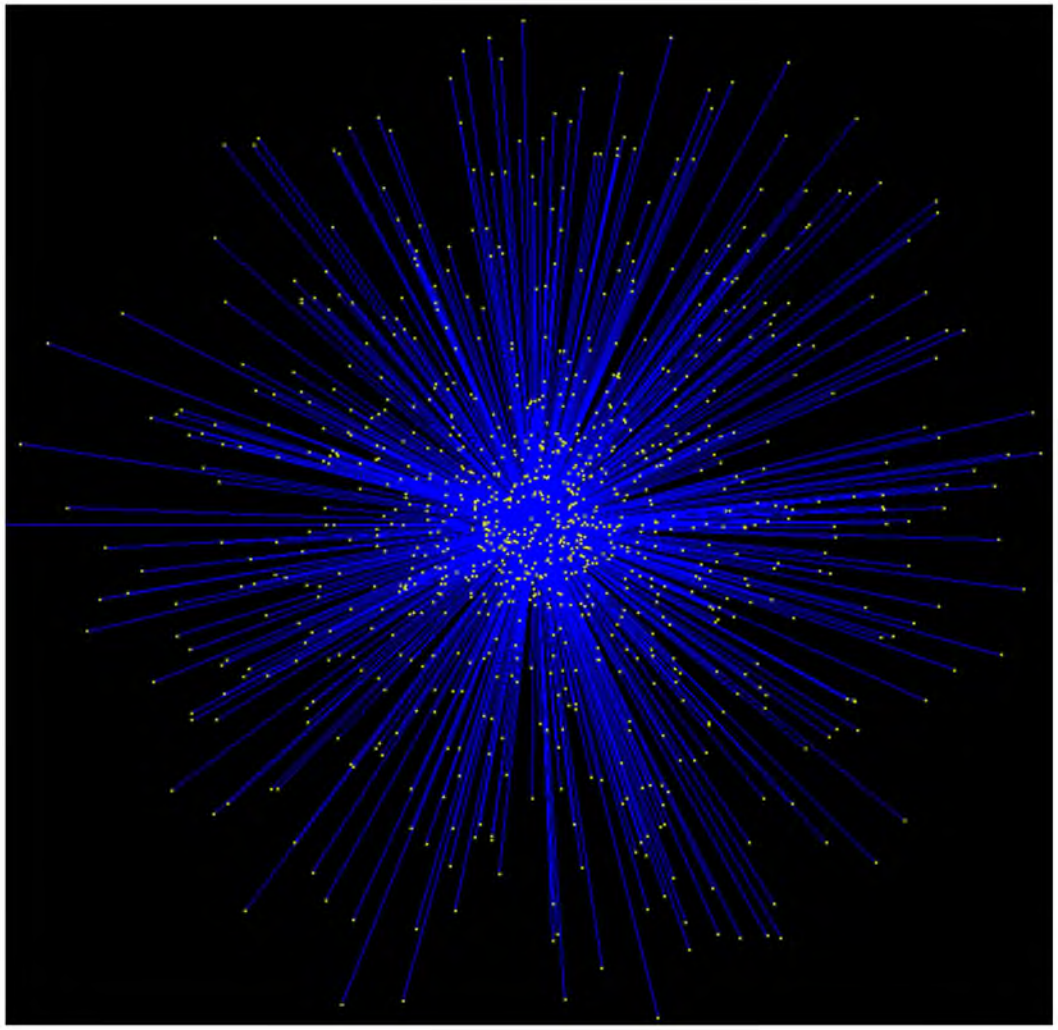

Figure 6-2. GEANT4 simulation of 100 keV 222Rn atoms in silicon

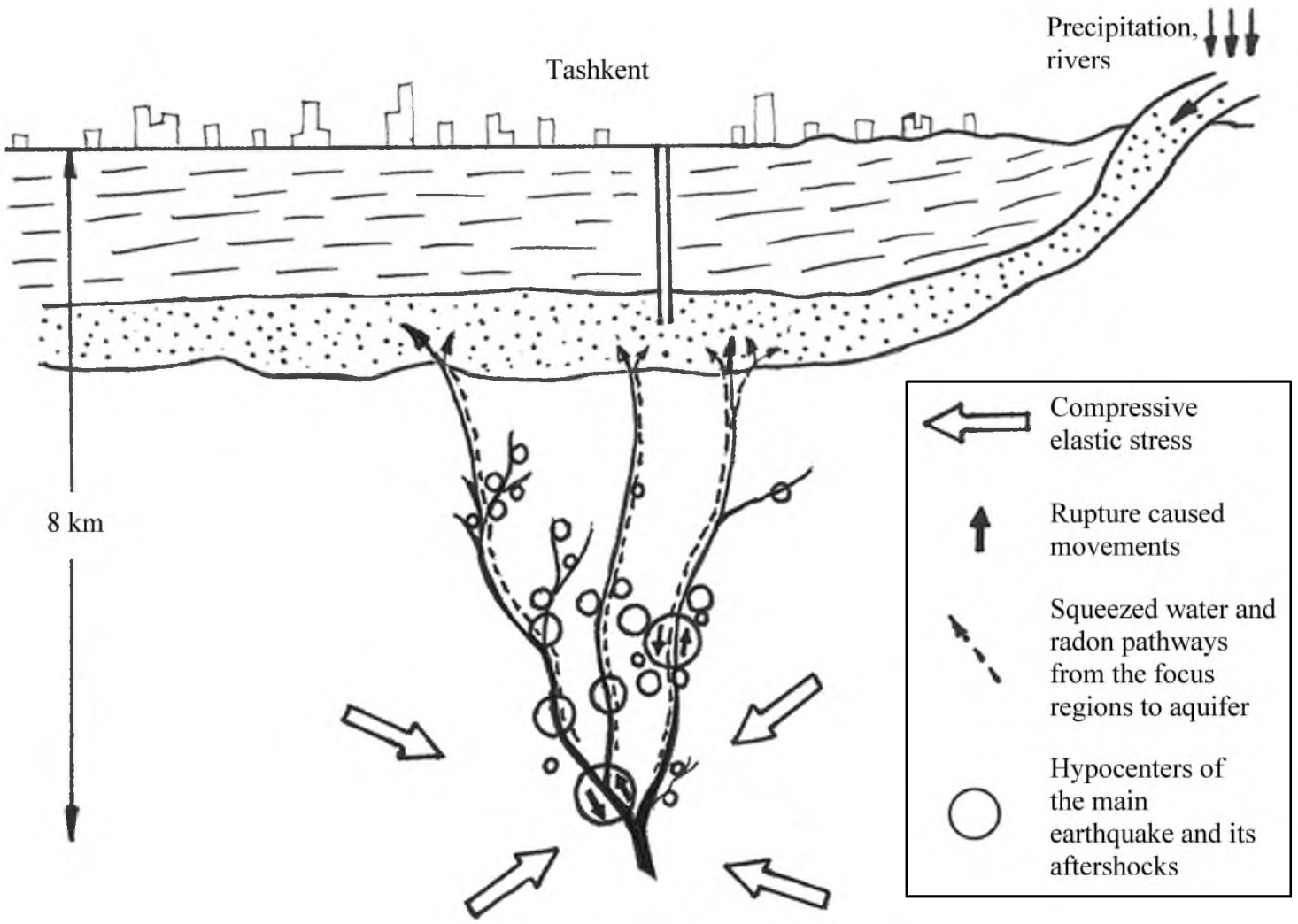

Figure 6-3. Schematic cross section of the radon release in the Tashkent groundwater basin, adapted from [*47*]

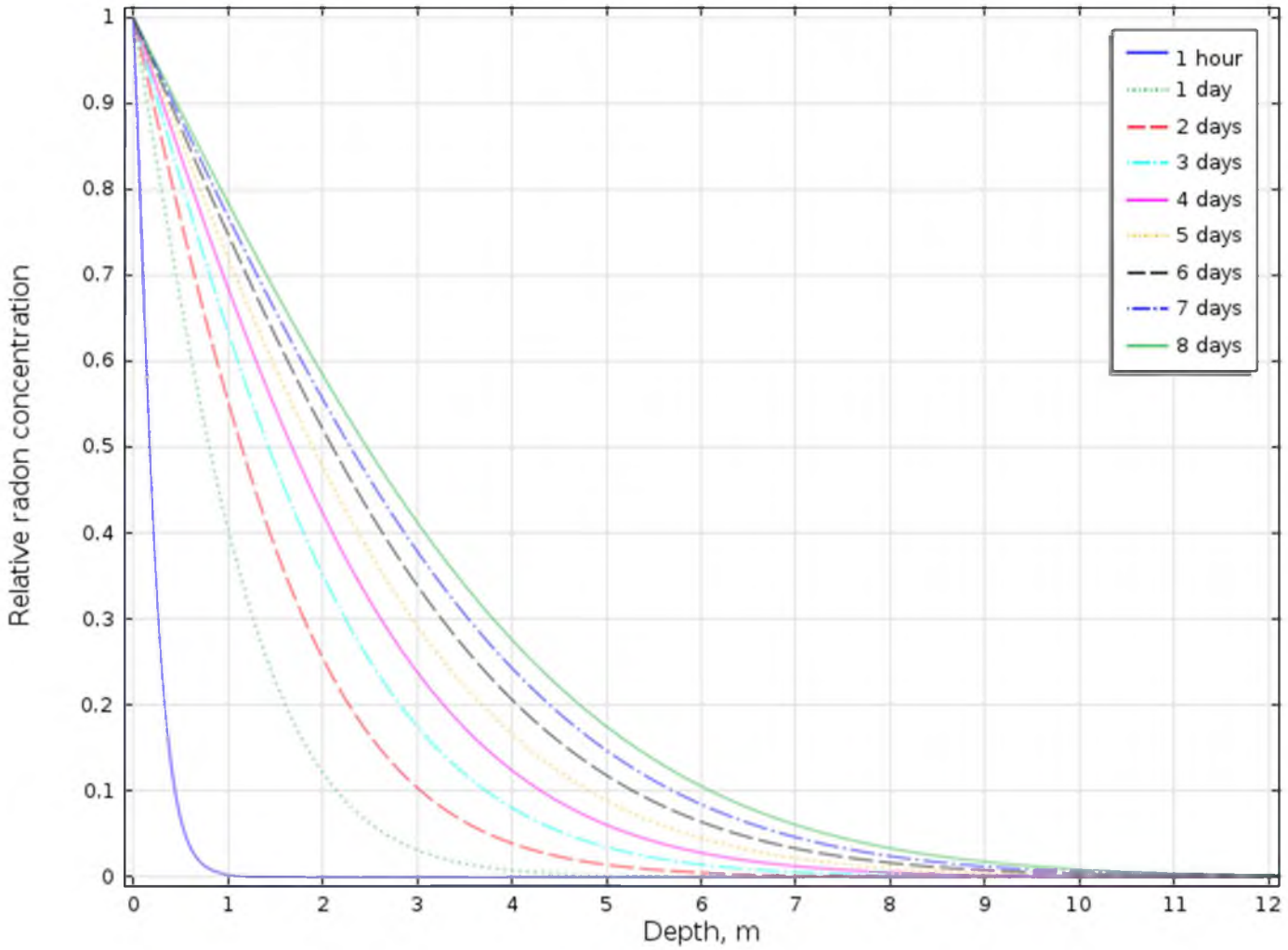

Figure 6-4. Relative radon concentration vs. fault depth obtained with numerical simulation

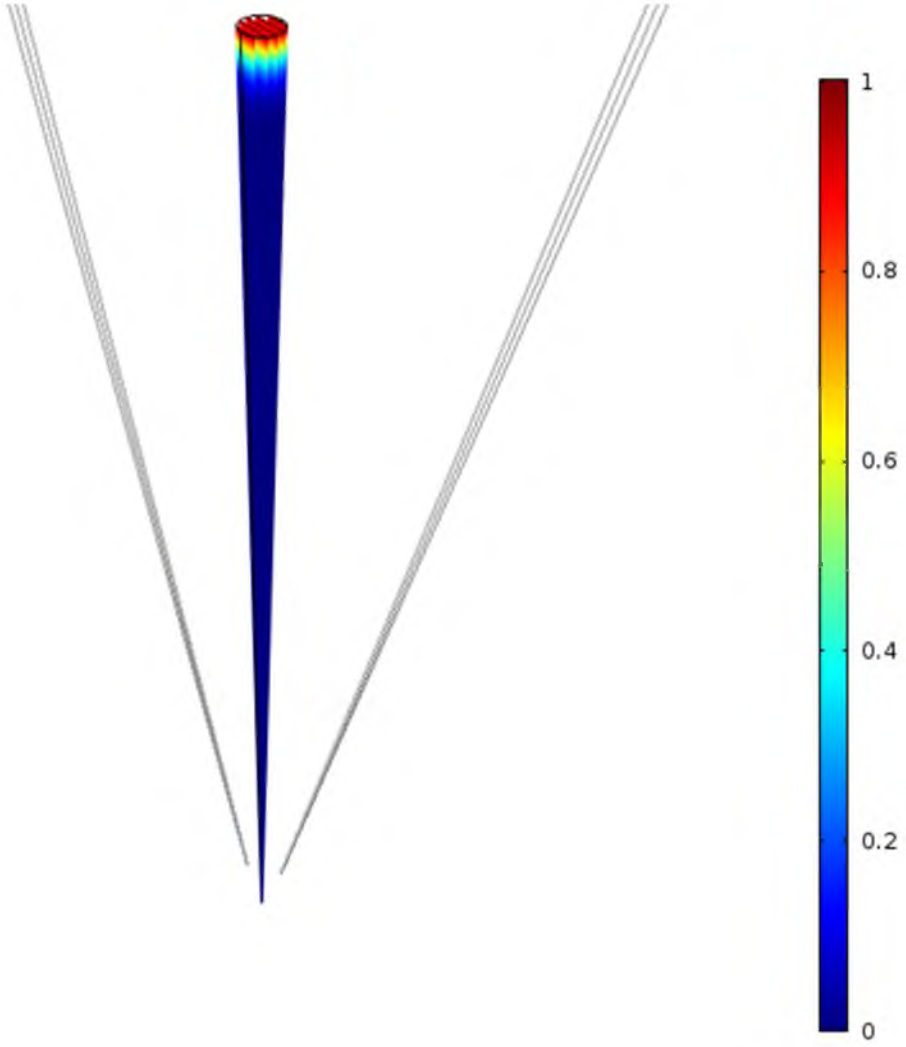

Figure 6-5. An air cylinder of 5 km length as a pathway for radon along the fault strand

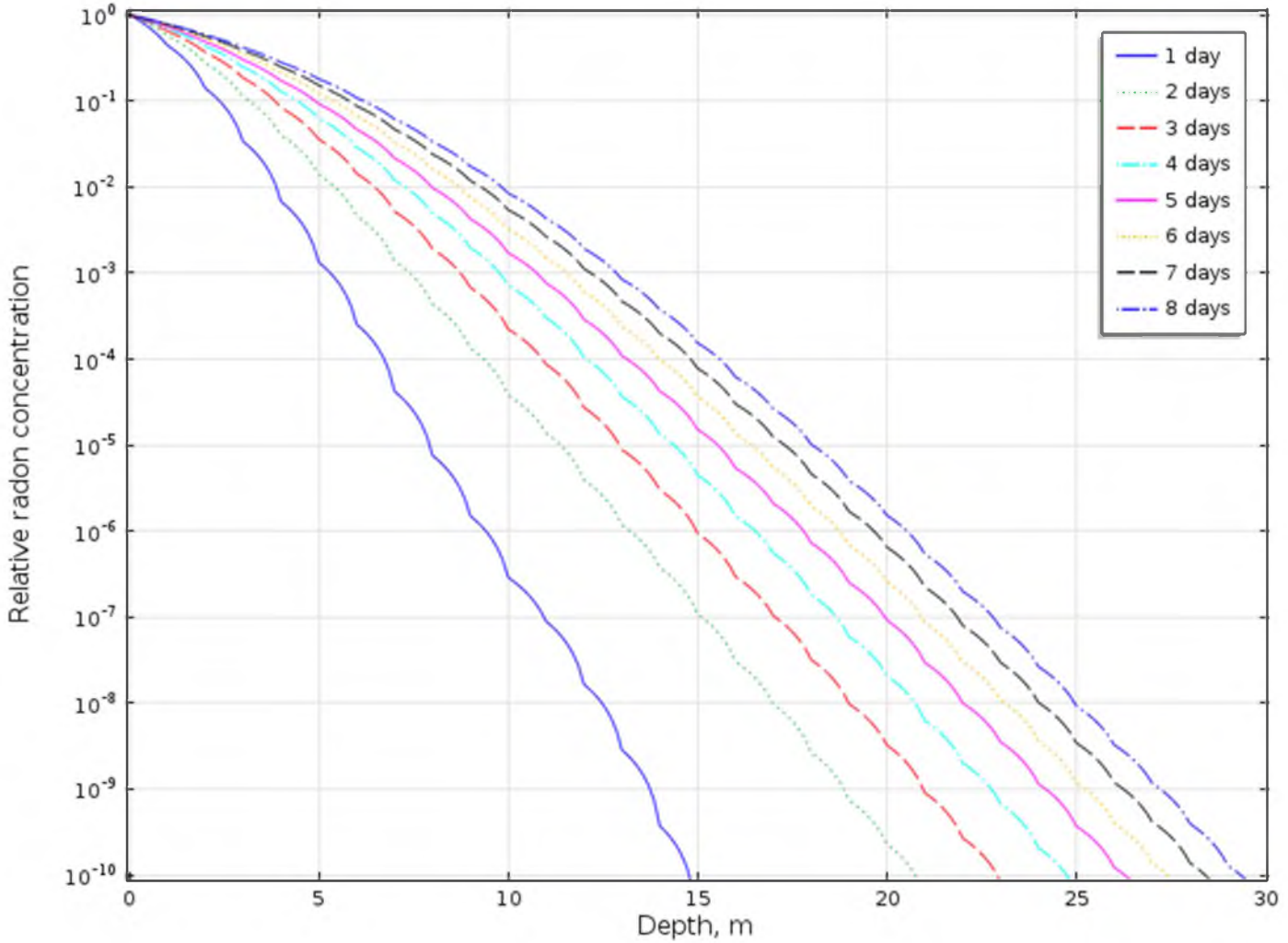

Figure 6-6. Relative radon concentration vs. fault depth obtained with numerical simulation

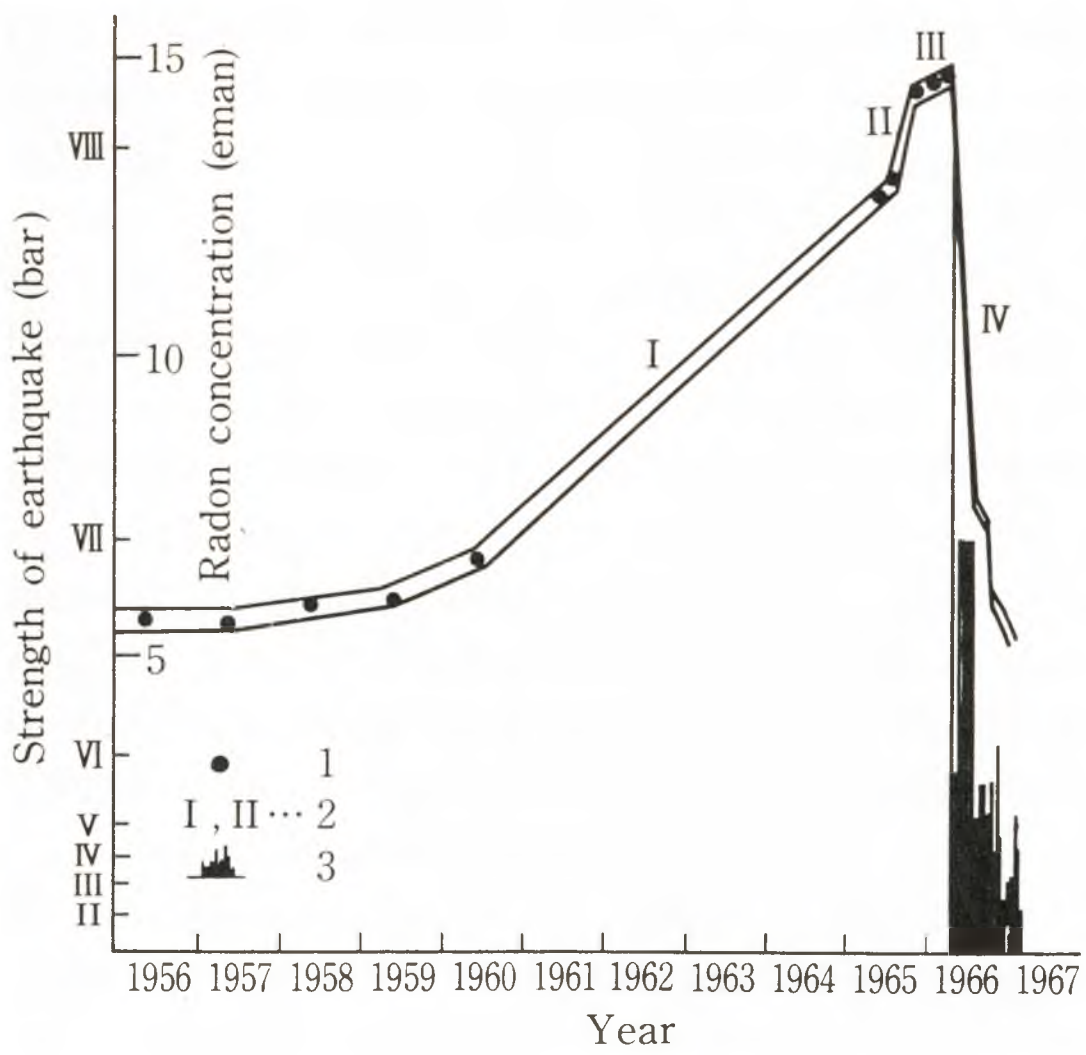

Figure 6-7. Radon concentration in groundwater prior to and after the 1966 Tashkent earthquake. Reprinted with permission of [*45*]

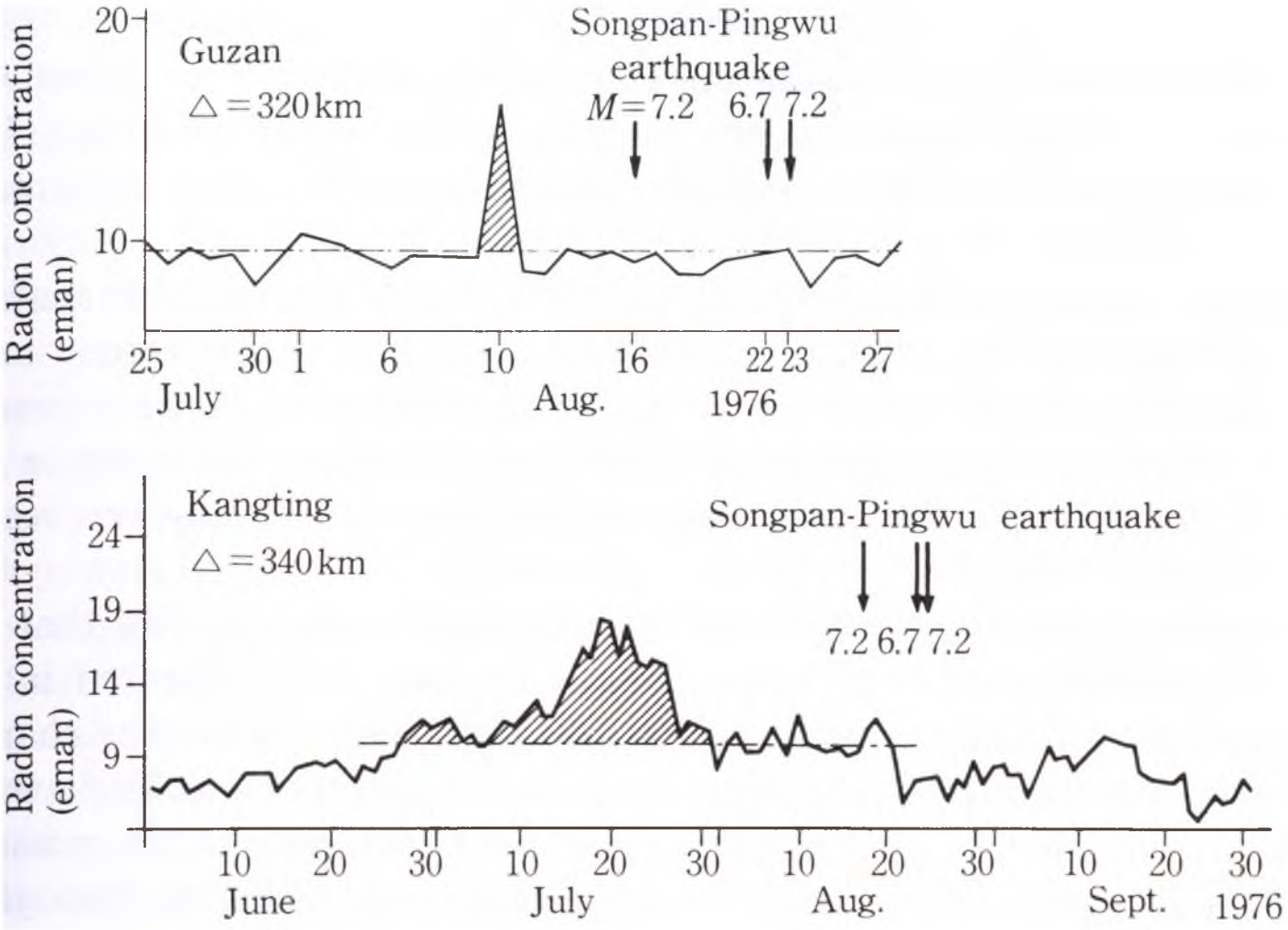

Figure 6-8. Radon concentrations in groundwater and the timeline of the Songpan-Pingwu earthquakes. Reprinted with permission of [*45*]

CHAPTER 7

CONCLUSION AND FUTURE WORK

7.1 Conclusion

The objectives of the thesis were to make analytical estimates of radon diffusion in various media and compare obtained values with numerical simulations; then to develop the experiment with nonactivated charcoal samples to measure radon absorption and calculate diffusion and adsorption coefficients for radon in nonactivated charcoal; followed by the analytical and experimental data, then to discuss potential of activated and nonactivated charcoals as radon detectors; in addition, to develop GEANT4 model to simulate ^{238}U series decay in soil and ^{222}Rn alone in soil and air and suggest the model of merging GEANT4 and diffusion theory in predicting potential of using nonactivated charcoals for radon measurements.

Analytical estimates of short-time and long-time radon diffusion in various media were obtained for charcoal, air, water and soil. Theoretical predictions were compared to numerical simulations of radon diffusion in the same media. The simulation values of total radon activities inside each material match quite well analytical estimates.

An experiment with nonactivated charcoal samples was performed. Its main objective was to measure radon absorption in nonactivated charcoal and estimate diffusion and adsorption coefficients. The analytical approach with disregarding and

considering radon decay was used to estimate these values. Radon adsorption coefficient in nonactivated charcoal varies from 0.2 to 0.4 m^3/kg and is 20 to 10 times less than the one of activated charcoal. Radon diffusion coefficient for nonactivated charcoal is in the range of 1.2×10^{-11} to 5.1×10^{-10} m^2/s in comparison to activated charcoal with adsorption coefficient of 4 m^3/kg and diffusion coefficient of 1.43×10^{-9} m^2/s. This way, potential to use nonactivated charcoal in radon detection is lower than the one of activated charcoal due to lower diffusion and adsorption coefficients values.

GEANT4 numerical code was used to simulate ^{238}U series decay in soil. Also, decay of ^{222}Rn alone was simulated in the same medium. Potential of using GEANT4 for radon diffusion is huge. The model can be extended by assigning time interval to each step and keeping numerous atoms in memory for simulating their migration in various media, based on diffusion coefficient value. Radon decay can be considered, based on probability for each time step.

Numerical simulations of radon propagation along the fault strand were made to estimate how fast and how far radon can migrate by diffusion only. Results show that migration at about ten meters during eight days decreases its concentration by 400 times.

Radon can be used as an earthquake predictor by measuring its concentration in groundwater or if possible along the faults. The known cases of successful correlations between radon concentration anomalies and earthquake are 1966 Tashkent and 1976 Songpan-Pingwu earthquakes. Thus, an idea of radon monitoring along the Wasatch Fault, using a system of activated/nonactivated charcoals, together with solid state radon detectors is suggested in the thesis. Also, the use of neutron activation analysis for soil samples, collected along and away from the Wasatch Fault, and looking for the trace

elements can result in correlation with earthquakes that have occurred in the past. This approach can be used for earthquake prediction in future.

7.2 Recommendation for Future Work

7.2.1 Analytical and Numerical Estimates of Radon Diffusion

Research in radon diffusion has great potential for future findings. Analytical estimates can be extended to be more complicated cases such as Knudsen diffusion which considers effects in small pores that can be used in estimates of radon emanation from bed rock. Numerical simulations in COMSOL Multiphysics can be extended to consider radon decay and adsorption coefficients for different material.

GEANT4 simulations have almost no limit in the model complexity. One of the far-reaching ideas to simulate in GEANT4 is a radon diffusion problem that will keep in memory numerous radon atoms during all steps. Each step can be assigned some time interval and consider radon decay, which can be based on probability. Geometries can be very complex, for example fault, filled with air and small rocks and porous soil with bigger rocks around it. Due to GEANT4's powerful visualization module, defining larger step time can show real-time radon emanation from the fault.

Another idea that can be useful for quick radon concentration assessment worldwide is to merge Google Earth with radon diffusion model. Such application may be treated with outdoor radon concentrations for different GPS coordinates and data on average wind speed and direction. Analytical estimates or simulation results of radon diffusion would result in the data that can be merged with Google Earth to display radon concentrations in three dimensions.

7.2.2 Use of Radon as Earthquake Predictor and Required Equipment

The most reliable method of using radon as earthquake predictor is a union of a few methods of measuring its concentrations continuously. This can include monitoring radon in water in a few deep wells in fault regions together with numerous solid state radon detectors installed in PVC pipes at approximately 1 m depth in soil.

Since it is very important to know about an earthquake at least a few days in advance, all the measurement data from all detectors must be obtained quite fast. Mobile and computer technologies, that are available today, can help to collect data from all measuring sites and process it immediately.

This approach can be applied to the Wasatch Fault region since the Utah Geological Survey [*48*] reports that a large Wasatch Fault earthquake occurs approximately every 350 years and the large most recent earthquake on the Wasatch Fault possibly happened around 385 years ago, considering the publishing date of the brochure.

Use of neutron activation analysis for soil samples, collected along and away from the Wasatch Fault, and looking for the trace elements in the samples can result in correlation with earthquakes that occurred in the past. This approach can be extended for earthquake prediction in future.

7.2.3 Potential of Charcoal as Radon Detector in Monitoring Tectonic Movements

Radon concentration measurements together with tectonic movements were studied by Šebela et al. [*49*]. The measurements were performed using Barasol probes and Radium 5 WP monitors. Measurement data was stored in the memory of the

detectors and then was transferred for evaluation every two months. The measurements showed that during horizontal movement radon pathways underground were partly closed, hindering radon migration and reducing its concentration in the cave air. Also, the compression process had opened some new routes for radon transport, thus facilitating radon migration and increasing its concentration in air.

Potential of activated charcoal detectors to use in monitoring tectonic movements can be estimated while used together with other radon detectors. However, since charcoal detectors are sensitive to humidity, their use can be limited in such places as caves.

APPENDIX

GEANT4 INPUT FILES

DetectorConstruction.cc input file for estimation of range of 100 keV ^{222}Rn atoms in silicon

```
#include "DetectorConstruction.hh"
#include "DetectorMessenger.hh"

#include "G4Material.hh"
#include "G4NistManager.hh"

#include "G4Box.hh"
#include "G4LogicalVolume.hh"
#include "G4PVPlacement.hh"
#include "G4PVReplica.hh"
#include "G4UniformMagField.hh"

#include "G4GeometryManager.hh"
#include "G4PhysicalVolumeStore.hh"
#include "G4LogicalVolumeStore.hh"
#include "G4SolidStore.hh"

#include "G4VisAttributes.hh"
#include "G4Colour.hh"

DetectorConstruction::DetectorConstruction()
:AbsorberMaterial(0),GapMaterial(0),defaultMaterial(0),
 solidWorld(0),logicWorld(0),physiWorld(0),
 solidCalor(0),logicCalor(0),physiCalor(0),
 solidLayer(0),logicLayer(0),physiLayer(0),
 solidAbsorber(0),logicAbsorber(0),physiAbsorber(0),
 solidGap (0),logicGap (0),physiGap (0),
 magField(0)
{
  // default parameter values of the calorimeter
  AbsorberThickness = 2.*um;
  GapThickness      =  0.*mm;
  NbOfLayers        = 1;
  CalorSizeYZ       = 5.*um;
  ComputeCalorParameters();

  // materials
  DefineMaterials();
  SetAbsorberMaterial("Silicon");
  SetGapMaterial("liquidArgon");
```

```
  // create commands for interactive definition of the calorimeter
  detectorMessenger = new DetectorMessenger(this);
}

DetectorConstruction::~DetectorConstruction()
{ delete detectorMessenger;}

G4VPhysicalVolume* DetectorConstruction::Construct()
{
  return ConstructCalorimeter();
}

void DetectorConstruction::DefineMaterials()
{
 //This function illustrates the possible ways to define materials

G4String symbol;             //a=mass of a mole;
G4double a, z, density;      //z=mean number of protons;
G4int iz, n;                 //iz=number of protons  in an isotope;
                             // n=number of nucleons in an isotope;

G4int ncomponents, natoms;
G4double abundance, fractionmass;

//
// define Elements
//

G4Element* Si = new G4Element("Silicon",symbol="Si" , z= 14., a= 28.09*g/mole);

//
// define simple materials
//

new G4Material("Aluminium", z=13., a=26.98*g/mole, density=2.700*g/cm3);
new G4Material("liquidArgon", z=18., a= 39.95*g/mole, density= 1.390*g/cm3);
new G4Material("Lead"     , z=82., a= 207.19*g/mole, density= 11.35*g/cm3);
new G4Material("Silicon"     , z=14., a= 28.09*g/mole, density= 2.329*g/cm3);
new G4Material("Iron"     , z=26., a= 55.845*g/mole, density= 7.874*g/cm3);

//
// define a material from elements.   case 1: chemical molecule
//


G4Material* SiO2 =
new G4Material("quartz",density= 2.200*g/cm3, ncomponents=2);
SiO2->AddElement(Si, natoms=1);
SiO2->AddElement(O , natoms=2);

//
// define a material from elements and/or others materials (mixture of
mixtures)
//

G4Material* Vacuum =
new G4Material("Galactic", z=1., a=1.01*g/mole,density= universe_mean_density,
                           kStateGas, 2.73*kelvin, 3.e-18*pascal);

G4Material* beam =
new G4Material("Beam", density= 1.e-5*g/cm3, ncomponents=1,
                       kStateGas, STP_Temperature, 2.e-2*bar);
```

```
beam->AddMaterial(Air, fractionmass=1.);

//
// or use G4-NIST materials data base
//
G4NistManager* man = G4NistManager::Instance();
man->FindOrBuildMaterial("G4_SODIUM_IODIDE");

// print table
//
G4cout << *(G4Material::GetMaterialTable()) << G4endl;

//default materials of the World
defaultMaterial  = Vacuum;
}

G4VPhysicalVolume* DetectorConstruction::ConstructCalorimeter()
{

  // Clean old geometry, if any
  //
  G4GeometryManager::GetInstance()->OpenGeometry();
  G4PhysicalVolumeStore::GetInstance()->Clean();
  G4LogicalVolumeStore::GetInstance()->Clean();
  G4SolidStore::GetInstance()->Clean();

  // complete the Calor parameters definition
  ComputeCalorParameters();

  //
  // World
  //
  solidWorld = new G4Box("World",                    //its name
                   WorldSizeX/2,WorldSizeYZ/2,WorldSizeYZ/2);     //its size

  logicWorld = new G4LogicalVolume(solidWorld,       //its solid
                                   defaultMaterial,  //its material
                                   "World");         //its name

  physiWorld = new G4PVPlacement(0,                  //no rotation
                            G4ThreeVector(),   //at (0,0,0)
                                 logicWorld,         //its logical volume

                                 "World",            //its name
                                 0,                  //its mother  volume
                                 false,              //no boolean operation
                                 0);                 //copy number

  //
  // Calorimeter
  //
  solidCalor=0; logicCalor=0; physiCalor=0;
  solidLayer=0; logicLayer=0; physiLayer=0;

  if (CalorThickness > 0.)
    { solidCalor = new G4Box("Calorimeter",          //its name
                     CalorThickness/2,CalorSizeYZ/2,CalorSizeYZ/2);//size

      logicCalor = new G4LogicalVolume(solidCalor,   //its solid
                                  defaultMaterial,   //its material
                                  "Calorimeter");    //its name
```

```
    physiCalor = new G4PVPlacement(0,               //no rotation
                                   G4ThreeVector(), //at (0,0,0)
                                   logicCalor,      //its logical volume
                                   "Calorimeter",   //its name
                                   logicWorld,      //its mother  volume
                                   false,           //no boolean operation
                                   0);              //copy number

//
// Layer
//
    solidLayer = new G4Box("Layer",                 //its name
                     LayerThickness/2,CalorSizeYZ/2,CalorSizeYZ/2); //size

    logicLayer = new G4LogicalVolume(solidLayer,    //its solid
                                     defaultMaterial,     //its material
                                     "Layer");      //its name
    if (NbOfLayers > 1)
      physiLayer = new G4PVReplica("Layer",         //its name
                                logicLayer,    //its logical volume
                                logicCalor,    //its mother
                                     kXAxis,          //axis of replication
                                     NbOfLayers,      //number of replica
                                     LayerThickness); //witdth of replica
    else
      physiLayer = new G4PVPlacement(0,             //no rotation
                                     G4ThreeVector(), //at (0,0,0)
                                     logicLayer,      //its logical volume

                                     "Layer",         //its name
                                     logicCalor,      //its mother  volume
                                     false,           //no boolean operation
                                     0);              //copy number
  }

//
// Absorber
//
solidAbsorber=0; logicAbsorber=0; physiAbsorber=0;

if (AbsorberThickness > 0.)
  { solidAbsorber = new G4Box("Absorber",           //its name
                        AbsorberThickness/2,CalorSizeYZ/2,CalorSizeYZ/2);

    logicAbsorber = new G4LogicalVolume(solidAbsorber,    //its solid
                                        AbsorberMaterial, //its material
                                        AbsorberMaterial->GetName()); //name

    physiAbsorber = new G4PVPlacement(0,                //no rotation
               G4ThreeVector(-GapThickness/2,0.,0.),  //its position
                                      logicAbsorber,     //its logical volume

                                      AbsorberMaterial->GetName(), //its name
                                      logicLayer,        //its mother
                                      false,             //no boulean operat
                                      0);                //copy number

  }

//
// Gap
//
```

```
  solidGap=0; logicGap=0; physiGap=0;

  if (GapThickness > 0.)
    { solidGap = new G4Box("Gap",
                      GapThickness/2,CalorSizeYZ/2,CalorSizeYZ/2);

      logicGap = new G4LogicalVolume(solidGap,
                               GapMaterial,
                               GapMaterial->GetName());

      physiGap = new G4PVPlacement(0,                       //no rotation
               G4ThreeVector(AbsorberThickness/2,0.,0.),    //its position
                                  logicGap,                 //its logical volume
                                  GapMaterial->GetName(), //its name
                                  logicLayer,               //its mother
                                  false,                    //no boulean operat
                                  0);                       //copy number
    }

  PrintCalorParameters();

  //
  // Visualization attributes
  //
  logicWorld->SetVisAttributes (G4VisAttributes::Invisible);

  G4VisAttributes* simpleBoxVisAtt= new G4VisAttributes(G4Colour(1.0,1.0,1.0));
  simpleBoxVisAtt->SetVisibility(true);
  logicCalor->SetVisAttributes(simpleBoxVisAtt);

 /*
  // Below are vis attributes that permits someone to test / play
  // with the interactive expansion / contraction geometry system of the
  // vis/OpenInventor driver :
 {G4VisAttributes* simpleBoxVisAtt= new G4VisAttributes(G4Colour(1.0,1.0,0.0));
  simpleBoxVisAtt->SetVisibility(true);
  delete logicCalor->GetVisAttributes();
  logicCalor->SetVisAttributes(simpleBoxVisAtt);}

 {G4VisAttributes* atb= new G4VisAttributes(G4Colour(1.0,0.0,0.0));
  logicLayer->SetVisAttributes(atb);}

 {G4VisAttributes* atb= new G4VisAttributes(G4Colour(0.0,1.0,0.0));
  atb->SetForceSolid(true);
  logicAbsorber->SetVisAttributes(atb);}

 {//Set opacity = 0.2 then transparency = 1 - 0.2 = 0.8
  G4VisAttributes* atb= new G4VisAttributes(G4Colour(0.0,0.0,1.0,0.2));
  atb->SetForceSolid(true);
  logicGap->SetVisAttributes(atb);}
  */

  //
  //always return the physical World
  //
  return physiWorld;
}

void DetectorConstruction::PrintCalorParameters()
{
  G4cout << "\n-------------------------------------------------------------"
         << "\n---> The calorimeter is " << NbOfLayers << " layers of: [ "
```

```
          << AbsorberThickness/mm << "mm of " << AbsorberMaterial->GetName()
          << " + "
          << GapThickness/mm << "mm of " << GapMaterial->GetName() << " ] "
          << "\n------------------------------------------------------------\n";
}

void DetectorConstruction::SetAbsorberMaterial(G4String materialChoice)
{
  // search the material by its name
  G4Material* pttoMaterial = G4Material::GetMaterial(materialChoice);
  if (pttoMaterial) AbsorberMaterial = pttoMaterial;
}

void DetectorConstruction::SetGapMaterial(G4String materialChoice)
{
  // search the material by its name
  G4Material* pttoMaterial = G4Material::GetMaterial(materialChoice);
  if (pttoMaterial) GapMaterial = pttoMaterial;
}

void DetectorConstruction::SetAbsorberThickness(G4double val)
{
  // change Absorber thickness and recompute the calorimeter parameters
  AbsorberThickness = val;
}

void DetectorConstruction::SetGapThickness(G4double val)
{
  // change Gap thickness and recompute the calorimeter parameters
  GapThickness = val;
}

void DetectorConstruction::SetCalorSizeYZ(G4double val)
{
  // change the transverse size and recompute the calorimeter parameters
  CalorSizeYZ = val;
}

void DetectorConstruction::SetNbOfLayers(G4int val)
{
  NbOfLayers = val;
}

#include "G4FieldManager.hh"
#include "G4TransportationManager.hh"

void DetectorConstruction::SetMagField(G4double fieldValue)
{
  //apply a global uniform magnetic field along Z axis
  G4FieldManager* fieldMgr
   = G4TransportationManager::GetTransportationManager()->GetFieldManager();

  if(magField) delete magField;         //delete the existing magn field

  if(fieldValue!=0.)                    // create a new one if non nul
  { magField = new G4UniformMagField(G4ThreeVector(0.,0.,fieldValue));
    fieldMgr->SetDetectorField(magField);
    fieldMgr->CreateChordFinder(magField);
  } else {
    magField = 0;
    fieldMgr->SetDetectorField(magField);
  }
```

```
}

#include "G4RunManager.hh"

void DetectorConstruction::UpdateGeometry()
{
  G4RunManager::GetRunManager()->DefineWorldVolume(ConstructCalorimeter());
}
```

DetectorConstruction.cc input file for simulating of ^{238}U and ^{222}Rn decay in soil

```
#include "exrdmDetectorConstruction.hh"

#include "exrdmDetectorMessenger.hh"

//#include "exrdmDetectorSD.hh"

#include "G4UImanager.hh"

#include "G4Material.hh"

#include "G4Tubs.hh"

#include "G4LogicalVolume.hh"

#include "G4PVPlacement.hh"

//#include "G4SDManager.hh"

#include "G4Region.hh"

#include "G4RegionStore.hh"

#include "exrdmMaterial.hh"

#include "G4VisAttributes.hh"

#include "G4Colour.hh"

#include "G4ios.hh"

#include <sstream>


exrdmDetectorConstruction::exrdmDetectorConstruction()

:solidWorld(0),  logicWorld(0),  physiWorld(0),

 solidTarget(0), logicTarget(0), physiTarget(0),

 solidDetector(0),logicDetector(0),physiDetector(0),

 TargetMater(0), DetectorMater(0),

 fWorldLength(0.)

{

  detectorMessenger = new exrdmDetectorMessenger(this);

  DefineMaterials();

  fDetectorThickness = 0.001* mm;
```

```
  fTargetRadius = 1/sqrt(pi)* m;
  fDetectorLength = 100. * cm;
  fTargetLength  = 100. * cm;
//--------- Sizes of the principal geometrical components (solids)  ---------
  fWorldLength = std::max(fTargetLength,fDetectorLength);
  fWorldRadius = fTargetRadius + fDetectorThickness;
}
exrdmDetectorConstruction::~exrdmDetectorConstruction()
{
  delete detectorMessenger;
}
void exrdmDetectorConstruction::DefineMaterials()
{

G4String symbol;             //a=mass of a mole;
G4double a, z, density;      //z=mean number of protons;
G4int iz, n;                 //iz=number of protons  in an isotope;
                             // n=number of nucleons in an isotope;

G4int ncomponents, natoms;
G4double abundance, fractionmass;
//--------- Material definition ---------

  materialsManager = new exrdmMaterial();
  //Germanium detector
  materialsManager->AddMaterial("Germanium","Ge",5.323*g/cm3,"");
  //CsI
  materialsManager->AddMaterial("CsI","Cs-I",4.51*g/cm3,"");
```

```
G4Element* H  = new G4Element("Hydrogen",symbol="H" , z= 1., a= 1.01*g/mole);
G4Element* C  = new G4Element("Carbon"  ,symbol="C" , z= 6., a= 12.01*g/mole);
G4Element* N  = new G4Element("Nitrogen",symbol="N" , z= 7., a= 14.01*g/mole);
G4Element* O  = new G4Element("Oxygen"  ,symbol="O" , z= 8., a= 16.00*g/mole);
G4Element* Si = new G4Element("Silicon",symbol="Si" , z= 14., a= 28.09*g/mole);

G4Material* Soil =
new G4Material("Soil", density= 1.6*g/cm3, ncomponents=5);
Soil->AddElement(H, fractionmass=0.15);
Soil->AddElement(O, fractionmass=0.40);
Soil->AddElement(Si, fractionmass=0.25);
Soil->AddElement(N, fractionmass=0.17);
Soil->AddElement(C, fractionmass=0.03);

  DefaultMater = materialsManager->GetMaterial("Soil");
  TargetMater  = materialsManager->GetMaterial("Soil");
  DetectorMater = materialsManager->GetMaterial("Soil");
}

G4VPhysicalVolume* exrdmDetectorConstruction::Construct()
{
//--------- Definitions of Solids, Logical Volumes, Physical Volumes ---------
  //--------- Sizes of the principal geometrical components (solids)  ---------

  fWorldLength = std::max(fTargetLength,fDetectorLength);
  fWorldRadius = fTargetRadius + fDetectorThickness;

  // World
solidWorld= new G4Tubs("world",0.,fWorldRadius,fWorldLength/2.,0.,twopi);
```

```
 logicWorld= new G4LogicalVolume( solidWorld, DefaultMater, "World", 0, 0, 0);


  //  Must place the World Physical volume unrotated at (0,0,0).
  //
  physiWorld = new G4PVPlacement(0,               // no rotation
                                 G4ThreeVector(), // at (0,0,0)
                                 logicWorld,      // its logical volume
                           "World",         // its name
                                 0,               // its mother  volume
                                 false,           // no boolean operations
                                 0);              // no field specific to
volume


  // Target
  G4ThreeVector positionTarget = G4ThreeVector(0,0,0);


  solidTarget = new
G4Tubs("target",0.,fTargetRadius,fTargetLength/2.,0.,twopi);
  logicTarget = new G4LogicalVolume(solidTarget,TargetMater,"Target",0,0,0);
  physiTarget = new G4PVPlacement(0,               // no rotation
                              positionTarget,  // at (x,y,z)
                              logicTarget,     // its logical volume

                              "Target",        // its name
                              logicWorld,      // its mother  volume
                              false,           // no boolean operations
                              0);              // no particular field


  // Detector
   G4ThreeVector positionDetector = G4ThreeVector(0,0,0);
```

```
  solidDetector = new
G4Tubs("detector",fTargetRadius,fWorldRadius,fDetectorLength/2.,0.,twopi);

  logicDetector = new G4LogicalVolume(solidDetector ,DetectorMater,
"Detector",0,0,0);

  physiDetector = new G4PVPlacement(0,              // no rotation

                            positionDetector, // at (x,y,z)

                            logicDetector,    // its logical volume


                            "Detector",       // its name

                            logicWorld,      // its mother  volume

                            false,           // no boolean operations

                            0);              // no particular field


  targetRegion = new G4Region("Target");

  detectorRegion   = new G4Region("Detector");

  targetRegion->AddRootLogicalVolume(logicTarget);

  detectorRegion->AddRootLogicalVolume(logicDetector);


  //--------- Visualization attributes -------------------------------

  logicWorld->SetVisAttributes(G4VisAttributes::Invisible);

  G4VisAttributes* TargetVisAtt= new G4VisAttributes(G4Colour(1.0,1.0,1.0));

  logicTarget ->SetVisAttributes(TargetVisAtt);

  G4VisAttributes* DetectorVisAtt= new G4VisAttributes(G4Colour(1.0,1.0,.0));

  logicDetector->SetVisAttributes(DetectorVisAtt);


  //------------ set the incident position ------

// get the pointer to the User Interface manager

  G4UImanager* UI = G4UImanager::GetUIpointer();

  //      UI->ApplyCommand("/run/verbose 1");

  //      UI->ApplyCommand("/event/verbose 2");

  //      UI->ApplyCommand("/tracking/verbose 1");
```

```
  G4double zpos = -fWorldLength/2.;

  G4String command = "/gps/pos/centre ";

  std::ostringstream os;

  os << zpos ;

  G4String xs = os.str();

  UI->ApplyCommand(command+"0. 0. "+xs+" mm");

  UI->ApplyCommand("/gps/pos/type Point");

  command = "/gps/position ";

  UI->ApplyCommand("/gps/particle proton");

  UI->ApplyCommand("/gps/direction 0 0 1");

  UI->ApplyCommand("/gps/energy 100 MeV");

  return physiWorld;

}

void exrdmDetectorConstruction::setTargetMaterial(G4String materialName)

{

  // search the material by its name

  G4Material* pttoMaterial = G4Material::GetMaterial(materialName);

  if (pttoMaterial)

     {TargetMater = pttoMaterial;

      if (logicTarget) logicTarget->SetMaterial(pttoMaterial);

      G4cout << "\n----> The target has been changed to " << fTargetLength/cm
<< " cm of "

             << materialName << G4endl;

     }

}

void exrdmDetectorConstruction::setDetectorMaterial(G4String materialName)

{

  // search the material by its name
```

```
  G4Material* pttoMaterial = G4Material::GetMaterial(materialName);

  if (pttoMaterial)

     {DetectorMater = pttoMaterial;

      if (logicDetector) logicDetector->SetMaterial(pttoMaterial);

      G4cout << "\n----> The Deetctor has been changed to" <<
fDetectorLength/cm << " cm of "

             << materialName << G4endl;

                                        }

                                      }
```

Macro file for simulating 10 ^{238}U atoms

```
/exrdm/phys/SelectPhysics Hadron

/run/initialize

/grdm/analogueMC 1

/grdm/verbose 0

/grdm/noVolumes

/grdm/selectVolume Target

/tracking/verbose 0

/gps/particle ion

/gps/ion 92 238 0 0

/gps/position 0 0 0

/gps/energy 0 keV

/run/beamOn 10
```

Macro file for simulating 10 ^{222}Rn atoms

```
/exrdm/phys/SelectPhysics Hadron

/run/initialize

/grdm/analogueMC 1

/grdm/verbose 0

/grdm/noVolumes

/grdm/selectVolume Target

/tracking/verbose 0

/gps/particle ion

/gps/ion 86 222 0 0

/gps/position 0 0 0

/gps/energy 0 keV

/run/beamOn 10
```

REFERENCES

[1] C. R. Cothern and J. E. Smith, "Environmental radon," *Environmental Science Research*, vol. 35, 1987.

[2] M. Wilkening, "Radon in the environment," *Studies in Environmental Science*, vol. 40, 1990.

[3] R. C. West, *CRC Hanbook of Chemistry and Physics*, 60th ed. Boca Raton, FL: CRC Press, 1979-1980, B-19.

[4] L. Stein, "Chemical properties of radon, and its decay products," *American Chemical Society*, pp. 240-251, 1987.

[5] H. F. Lucas, "Improved low-level alpha-scintillation counter for radon," *Rev. Sci. Instrum., 28*, pp. 680-683, 1957.

[6] H. Cember and T. E. Johnson, *Introduction to Health Psysics*, 4th ed. New York: The McGraw-Hill Companies, Inc, 2009.

[7] G. Saccomanno, G. Huth, O. Auerbach, et al. "Relationship of radioactive radon daughters and cigarette smoking in the genesis of lung cancer in uranium miners," *Cancer*, vol. 62, pp. 1402-1408, 1988.

[8] F. Lundin, J. Wagoner, V. Archer, and, "Radon daughter exposure and respiratory cancer quantitative and temporal aspects," *Report from the Epidemiological Study of U.S. Uranium Miners*. NIOSH and NIEHS, Joint Monograph No. 1. 1971.

[9] U.S. Public Health Service, "Toxological profile for radon," Agency for Toxic Substances and Disease Registry in collaboration with U.S. Environmental Protection Agency, December 1990.

[10] D. Probert and A. Lugg, "Indoor radon gas - a potential health hazard resulting from implementing energy-efficiency measures," *Applied Energy*, vol. 56, no. 2, pp. 93–

196, February 1997.

[11] M. Thoennessen and C. Fry, "Discovery of the astatine, radon, francium, and radium isotopes," *Atomic Data and Nuclear Data Tables*, pp. 12-20, 2012.

[12] Korea Atomic Energy Research Institute. (2000) http://atom.kaeri.re.kr/.

[13] Mueller Associates, Inc., SYSCON Corporation, Brookhaven National Laboratory; under the direction and authority of the United States Department of Energy, Office of Environmental Analysis, *Handbook of radon in buildings: detection, safety, and control*: Hemisphere Publishing Corporation, 1988.

[14] K. Q. Lao, *Controlling indoor radon: measurment, mitigation, and prevention*. New York: Van Nostrand Reinhold, 1990.

[15] National Council on Radiation Protection and Measurements, "Exposure of the Population of the United States and Canada from Natural Background Radiation," Bethesda, MD, NCRP Report No. 94 1987.

[16] C. E. Junge, *Air Chemistry and Radioactivity*. New York, NY: Academic Press, 1963.

[17] H. Israel, "Israel Program for Scientific Translations," *Atmospheric Electricity*, vol. 1, pp. 66-73 and pp. 193-194, 1970.

[18] J. Pradel and J. Bricard, "Electric charge and radioactivity of naturally occurring aerosols," *Aerosol Science*, pp. 91-104, 1966.

[19] A. Roffman, "Short-lived daughter ions of radon-222 in relation to some atmospheric processes," *J. Geophys. Rs.*, vol. 27, pp. 58-83, 1972.

[20] M. H. Wilkening, "Radon transport mechanisms below the earth's surface," in *The Natural Radiation Environment III*, Houston, TX, 1978, pp. 23-28, USDOE and University of Texas School of Public Health.

[21] B. Mavashev and V. Ulomov, "The precursor of a strong tectonic earthquake," *USSR Academy of Sciene Report*, vol. 176, 1967.

[22] A.C. George, "Instruments and methods for measuring indoor radon and radon progeny concentrations," *Indoor Radon*, pp. 87-101, 1986, Air Pollution Control

Association.

[23] G. Kim and J.-M. Lee, "A simple and rapid method for analyzing radon in coastal and ground waters using a radon-in-air monitor," *Journal of Environmental Radioactivity*, vol. 89, no. 3, pp. 219–228, 2006.

[24] N. Kávási et al., "Difficulties in the dose estimate of workers originated from radon and radon progeny in a manganese mine," *Radiation Measurements*, vol. 44, no. 3, pp. 300–305, March 2009.

[25] J. J. Gaware, B.K. Sahoo, B.K. Sapra, and Y.S. Mayya, "Indigenous development and networking of online radon monitors in the underground uranium mine," *Radiation Protection and Environment*, vol. 34, no. 1, pp. 37-40, 2011.

[26] H. F. Lucas, "A fast and accurate survey technique for both 222Rn and 226Ra," in *Natural Radiation Environment*, Chicago, 1964.

[27] J. Cetnar, "General solution of Bateman equations for nuclear transmutations," *Annals of Nuclear Energy*, vol. 33, no. 7, pp. 640-645, May 2006.

[28] H. M. Prichard, T. F. Gesell, and C. R. Meyer, "Liquid scintillation analyses for radium-226 and radon-222 in potable waters," *Liquid Scintillation Counting, Recent Applications and Development*, vol. 1, pp. 347-355, Physical Aspects.

[29] C. N. Grant, G. C. Lalor, M. K. Vutchkov, and M. Balcazar, "Radon mapping in soils in St. Elizabeth, Jamaica," *Journal of Radioanalytical and Nuclear Chemistry*, vol. 250, no. 3, pp. 295-302, 2001.

[30] Agency for Toxic Substances and Disease Registry, "Toxicological Profile for Radon," 1990, U.S. Public Health Service.

[31] DURRIDGE Company, RAD7 RADON DETECTOR User Manual, Revision 7.1.8., 2012.

[32] W. J. Speelman, Modelling and Measurement of Radon Diffusion Through Soil For Application On Mine Tailings Dams, 2004, MS Thesis, University of the Western Cape.

[33] P. Kotrappa, J. C. Dempsey, J. R. Kickey, and L. R. Stieff, "An electret passive environmental 222Rn monitor based on ionization measurements," *Health Physic*,

vol. 54, pp. 47-56, 1988.

[34] D. G. Brookins, *The Indoor Radon Problem*. New York: Columbia University Press, 1990.

[35] National Council on Radiation Protection and Measurements, "National Background Radiation in the United States," Bethesda, MD, NCRP Report No. 45 1975.

[36] National Council on Radiation Protection and Measurements, "Measurement of Radon and Radon Daughters in Air," Bethesda, MD, NCRP Report No. 97 1988.

[37] USGS, "Radon Migration In The Ground: A Supplementary Review," 1978.

[38] A. B. Tanner, "Radon migration in the ground," in *The Natural Radiation Environment, Symposium Proceedings*, Houston, TX, April 10-13, 1963, pp. 181-190.

[39] D. Urošević and V. Nikezić, "A theoretical study of radon measurement with activated charcoal," *Nuclear Instruments and Methods in Physics Research*, vol. A 406, pp. 486-498, 1998.

[40] Environmental Protection Agency, "Interim Indoor Radon and Radon Decay Product Measurement Protocols," 1986.

[41] Committee on Risk Assessment of Exposure to Radon in Drinking Water, "Risk Assessment of Radon in Drinking Water," Washington, D.C., 1999.

[42] C. Papachristodoulou, K. Ioannides, and S. Pavlides, "Radon diffusion coefficients in soils of varying moisture content," *Geophysical Research Abstracts*, vol. 11, 2009, EGU General Assembly.

[43] CANBERRA Industries. (2012) CANBERRA Industries. [Online]. http://www.canberra.com/products/detectors/germanium-detectors.asp

[44] I. Cozmuta and E.R. van der Graaf, "Methods for measuring diffusion coefficients of radon in building materials," *The Science of the Total Environment*, vol. 272, pp. 323-335, 2001.

[45] T. Asada, *Earthquake Prediction Techniques: Their Application in Japan*. Tokyo:

University of Tokyo Press, 1982.

[46] T.-L. Teng, "Some recent studies on groundwater radon content as an earthquake precursor," *Journal of Geophysical Research*, vol. 85, no. B6, pp. 3089-3099, 1980.

[47] V. I. Ulomov et al., *Tashkent Earthquake of April 26, 1966*. Tashkent: FAN UzSSR, 1971.

[48] Utah Geological Survey, "Public Information Series 40," 1996.

[49] S. Šebela, J. Vaupotič, B. Košťák, and J. Stemberk, "Direct measurement of present-day tectonic movement and associated radon flux in Postojna Cave, Slovenia," *Journal of Cave and Karst Studies*, vol. 72, no. 1, pp. 21–34, April 2010.